Iterative coupling of boundary and finite element methods.

Wael Mohammed Ali Elleithy

Civil Engineering

May 2000

Abstract

The present dissertation investigates the convergence Sequential Dirichlet-Neumann iterative finite elementary/boundary element coupling method. It also elaborates on the effect of several factors on solution convergence. It extends the Sequential Dirichlet-Neumann method to elasto-plasticity. The major contribution of this dissertation is the development of a new iterative domain decomposition coupling method. Unlike the existing iterative coupling methods, the new method is capable of handling cases where the natural boundary conditions are specified on the entire external boundary of the finite element sub-domains. The new method is most suited for problems involving infinite or semi-infinite regions. It is also extended to elasto-plasticity problems. Finally, the dissertation considers some practical applications, which include fracture mechanics, and deep and shallow tunnels.

ITERATIVE COUPLING OF BOUNDARY AND FINITE ELEMENT METHODS

BY

WAEL MOHAMED ALI ELLEITHY

A Dissertation Presented to the
DEANSHIP OF GRADUATE STUDIES

KING FAHD UNIVERSITY OF PETROLEUM & MINERALS

DHAHRAN, SAUDI ARABIA

In Partial Fulfillment of the
Requirements for the Degree of

DOCTOR OF PHILOSOPHY

In

CIVIL ENGINEERING

May, 2000

UMI Number: 9983985

Bell & Howell Information and Learning Company
300 North Zeeb Road
P.O. Box 1346
Ann Arbor, MI 48106-1346

KING FAHD UNIVERSITY OF PETROLEUM & MINERALS
DHAHRAN 31261, SAUDI ARABIA

DEANSHIP OF GRADUATE STUDIES

This dissertation, written by

Wael Mohamed Ali Elleithy

under the direction of his Dissertation Advisor and approved by his Dissertation Committee, has been presented to and accepted by the Dean of the Graduate Studies, in partial fulfillment of the requirements for the degree of

DOCTOR OF PHILOSOPHY IN CIVIL ENGINEERING

Dissertation Committee

Dr. Husain J. Al-Gahtani
Dissertation Advisor

Prof. Mohammed H. Baluch
Member

Dr. Hamdan N. Al-Ghamdi
Member

Dr. Naser A. Al-Shayea
Member

Dr. Mohammed A. El-Gebeily
Member

Prof. Hammad I. Al-Abdulwahhab
Department Chairman

Dr. Abdallah M. Al-Shehri
Dean of Graduate Studies

عمادة الدراسات العليا
DEANSHIP OF GRADUATE STUDIES

Date: 24/7/2000

I dedicate this dissertation to

my parents, *Mohamed Elleithy* and *F. Elleithy*, my son, ***Mohamed***,

and to those who do good deeds for the sake of ***Allah***

ACKNOWLEDGMENT

Thanks and praise be to Almighty ***Allah*** for his limitless help and guidance, and peace and prayers be upon his ***Prophet***.

I wish to express my sincere appreciation to King Fahd University of Petroleum & Minerals for support of this research. I have been most fortunate to have Dr. ***Husain J. Al-Gahtani*** as my dissertation committee chairman. Through his support and guidance, this work has been possible. I extend my thanks to my committee members, Prof. *Mohammed Baluch*, Dr. *Hamdan Al-Ghamdi*, Dr. *Naser Al-Shayea*, and Dr. *Mohamed El-Gebeily*.

I would like to thank all my friends; my sisters and brothers; especially *Khalid Elleithy*, for their support and encouragement.

My deep appreciation is extended to my father, *Mohamed Elleithy*, who sacrificed his time, effort, and education and devoted his support for me. My expression of thanks is due to my mother, *F. Elleithy*, who was incredibly patient and made unlimited sacrifices to raise me up.

TABLE OF CONTENTS

LIST OF TABLES vii
LIST OF FIGURES viii
DISSERTATION ABSTRACT xi
1. INTRODUCTION 1
1.1 OVERVIEW 1
1.2 OBJECTIVES 3
1.3 ORGANIZATION OF THE DISSERTATION 4
2. BACKGROUND ON BEM AND FEM 6
2.1 GENERAL 6
2.2 HISTORICAL REMARKS 6
2.3 THE VARIATIONAL FORMULATION FOR PLANE ELASTICITY 8
2.4 BEM FORMULATION IN ELASTOSTATICS 11
2.4.1 Fundamental Solutions 13
2.4.1.1 Kelvin's Solutions 13
2.4.1.2 Melan's Solution 15
2.4.2 Stresses at Internal Points 17
2.4.3 Boundary Integral Equations 18
2.4.4 Infinite and Semi-Infinite Regions 22
2.4.5 Numerical Implementation 24
2.5 BEM FORMULATION FOR POTENTIAL PROBLEMS 30
2.6 FINITE ELEMENT FORMULATION 31
2.7 COMPUTATIONAL STEPS OF THE FEM AND BEM 36
2.8 COMPARISON OF THE FEM AND BEM 39
2.9 COUPLING THE BEM AND FEM METHODS 43
3. BACKGROUND ON FEM/BEM COUPLING APPROACHES 45
3.1 GENERAL 45

3.2 FEM HOSTED APPROACH 46
3.3 BEM HOSTED APPROACH 51
3.4 ITERATIVE DOMAIN DECOMPOSITION METHODS 53
3.4.1 Parallel Schwarz Neumann-Neumann Method 55
3.4.2 Parallel Schwarz Dirichlet-Neumann Method 56
3.4.3 Sequential Schwarz Dirichlet-Neumann Method 57
3.5 SUMMARY 58
4. CONVERGENCE OF THE SEQUENTIAL DIRICHLET-NEUMANN ITERATIVE COUPLING METHOD 59
4.1 GENERAL 59
4.2 CONVERGENCE OF THE ITERATIVE METHOD 59
4.3 BENCHMARK EXAMPLES 66
4.3.1 Potential Flow Problem 66
4.3.2 Steel Cantilever Beam Subjected to Uniform Tension 73
4.4 SELECTION OF THE RELAXATION PARAMETER 84
5. OVERLAPPING ITERATIVE DOMAIN DECOMPOSITION METHOD FOR COUPLING THE FEM AND BEM 87
5.1 GENERAL 87
5.2 OVERLAPPING ITERATIVE COUPLING METHOD 88
5.3 CONVERGENCE CONDITIONS 92
5.4 INFINITE AND SEMI-INFINITE PROBLEMS 94
5.5 BENCHMARK EXAMPLES 98
5.5.1 Potential Flow Example 98
5.5.2 Elasticity Example 100
5.6 SELECTION OF THE COMMON REGION 100
6. EXTENSION OF THE ITERATIVE COUPLED FEM/BEM METHODS TO ELASTO-PLASTICITY 110
6.1 GENERAL 110
6.2 THE DIRICHLET-NEUMANN METHOD IN ELASTO-PLASTICITY 110

6.3 OVERLAPPING COUPLING METHOD IN ELASTO-PLASTICITY......... 116
7. APLLICATIONS 125
7.1 GENERAL 125
7.2 FRACTURE MECHANICS 125
7.2.1 LEFM Example 125
7.2.2 EPFM Example 127
7.3 TUNNEL PROBLEM 132
7.2.1 Deep Tunnel 132
7.3.1.1 Elastic Analysis 136
7.3.1.2 Effect of Non-homogeneity of the Surrounding Soil 140
7.3.1.3 Elasto-Plastic Stress Analysis 144
7.3.2 Shallow Tunnel 147
7.3.2.1 Elastic Analysis 147
7.3.2.2 Elasto-Plastic Stress Analysis 150
7.4 SUMMARY 155
8. SUMMARY, CONCLUSIONS AND RECOMMENDATIONS FOR FUTURE RESEARCH 156
8.1 SUMMARY 156
8.2 CONCLUSIONS 157
8.3 RECOMMENDATIONS FOR FUTURE RESEARCH 159
REFRENCES 161
VITA 168

LIST OF TABLES

Table		Page
4.1	Applicable Range and optimum values of α for Different Values of a_B/a_F and k_B/k_F	72
7.1	Stress Intensity Factors for the Cracked Plate	129
7.2	Remote Stress vs. Normalized Load-Point-Displacement for EPFM Example	133
7.3	CPU Time for EPFM Example	135
7.4	Number of Elements and CPU Time for Elastic Analysis of Deep Tunnel	139
7.5	Displacement at the Excavated Surface of Deep Tunnel	143
7.6	Displacements at the Excavated Surface of the Deep Tunnel for $E_1/E_2 \le 1$	145
7.7	Displacements at the Excavated Surface of the Deep Tunnel for $E_1/E_2 \ge 1$	145
7.8	Comparison of CPU Time for Elasto-Plastic Analysis of Deep Tunnel	148
7.9	Number of Elements and CPU Time for Elastic Analysis of Shallow Tunnel	153
7.10	Displacements at the excavated Surface of the Shallow Tunnel (Elastic Analysis)	153
7.11	Displacements at the Excavated Surface of the Shallow Tunnel (Elasto-Plastic Analysis)	154
7.12	Comparison of CPU Time for Elasto-Plastic Analysis of Shallow Tunnel	154

LIST OF FIGURES

Figure		Page
2.1	Geometrical Representation for the Boundary Element Domain	9
2.2	General Region $\Omega^* + \Gamma^*$ containing the body $\Omega + \Gamma$	14
2.3	Body $\Omega + \Gamma$ Located within the Semi-Infinite Plane $x_1 \geq 0$	16
2.4	Singular Point ζ on Γ surrounded by a semicircle	19
2.5	Body with Part of its Boundary Γ Coinciding with the Surface of the Semi-Infinite Plane	21
2.6	Infinite Region with Cavity	23
2.7	Semi-Infinite Region with or without Cavity	25
2.8	FEM versus BEM program	40
3.1	Domain Decomposition	47
4.1	Potential Flow Problem	67
4.2	Discretization for the Potential Flow Problem	69
4.3	Required Iterations vs. α for Different Values of k_B/k_F	70
4.4	Required Iterations vs. α for Different Values of a_B/a_F	71
4.5	Effect of Initial Guess on the Convergence of the Solution	74
4.6	Cantilever Beam Subjected to Uniform Loading	75
4.7	BEM/FEM Discretization (a) 3 Nodes at Interface (b) 5 Nodes at Interface (c) 9 Nodes at Interface	76
4.8	Effect of the Number of Nodes on the BEM/FEM Interface on α	77
4.9	Relative BEM to FEM Computational Sub-Domains	79
4.10	Effect of the Geometry of the Computational Sub-Domains on α	80
4.11	Effect of Material Properties of the Sub-Domains on α	81
4.12	Boundary Conditions	82
4.13	Effect of Boundary Conditions on α	83

4.14 Effect of the Initial Guess on α 85
5.1 Overlapping Domain Decomposition 89
5.2 Shallow Tunnel Modeled by the Coupled FEM/BEM 95
5.3 Domain Decomposition for Infinite and Semi-Infinite Problems 96
5.4 Potential Flow Example Using the New Overlapping Iterative Method. (Neumann Boundary Conditions are specified for the entire FEM sub-domain) 99
5.5 Circular Hole in an Infinite Elastic Domain Subjected to Uniform Pressure 101
5.6 Discretization of the Circular Hole Example 101
5.7 Radial Displacements for the Circular Hole Example 102
5.8 Potential Flow Example Using the New Overlapping Iterative Coupling Method 103
5.9 Maximum Allowable α vs. a_c/a_B for Different Values of k_B/k_F $(a_B/a_F=1)$ 104
5.10 Maximum Allowable α vs. a_c/a_B for Different Values of k_B/k_F $(a_B/a_F=3)$ 106
5.11 Maximum Allowable α vs. a_c/a_B for Different Values of k_B/k_F $(a_B/a_F=10)$ 107
5.12 Maximum Allowable α vs. a_c/a_B for Different Values of k_B/k_F $(a_B/a_F=1/3)$ 108
6.1 Structure of **EPFBE** Program 113
6.2 **EPFBE** Program Organization 117
6.3 **OVEPFBE** Program Organization 123
7.1 Plate with a Central Crack (LEFM Example) 126
7.2 FEM/BEM and FEM Discretization for LEFM Example 128
7.3 Geometry and Loading Condition for EPFM Example 130
7.4 Discretization for EPFM Example 131

7.5	Yielded Zones for EPFM Example	134
7.6	FEM and FEM/BEM Discretization for Deep Tunnel	137
7.7	Radial Displacements for Elastic Analysis of Deep Tunnel	141
7.8	Radial Stresses for Elastic Analysis of Deep Tunnel	142
7.9	Radial Displacements for Elasto-Plastic Analysis of Deep Tunnel	146
7.10	Geometry and Material Properties of the Shallow Tunnel	149
7.11	Discretization of the Shallow Tunnel	151

DISSERTATION ABSTRACT

Name of Student : Wael Mohamed Ali Elleithy

Title of Study : Iterative Coupling of Boundary and Finite Element Methods
Major Field : Civil Engineering
Date of Degree : May, 2000

The present dissertation investigates the convergence of the Sequential Dirichlet-Neumann iterative finite element/boundary element coupling method. It also elaborates on the effect of several factors on solution convergence. It extends the Sequential Dirichlet-Neumann method to elasto-plasticity. The major contribution of this dissertation is the development of a new iterative domain decomposition coupling method. Unlike the existing iterative coupling methods, the new method is capable of handling cases where the natural boundary conditions are specified on the entire external boundary of the finite element or boundary element sub-domains. The new method is most suited for problems involving infinite or semi-infinite regions. It is also extended to elasto-plasticity problems. Finally, the dissertation considers some practical applications, which include fracture mechanics, and deep and shallow tunnels.

DOCTOR OF PHILOSOPHY DEGREE

KING FAHD UNIVERSITY OF PETROLEUM AND MINERALS
Dhahran, Saudi Arabia

May, 2000

ملخص بحث

درجة الدكتوراه في الفلسفة

الاسم : وائل محمد علي الليثي

عنوان الرسالة : الإقران التكراري لطريقتي العناصر المحدودة والعناصر الحدية

التخصص : الهندسة المدنية

تاريخ الدرجة : مايو ٢٠٠٠

تعني هذه الرسالة بدراسة طريقة دريكلي – نومن المتتالية لإقران طريقتي العناصر المحدودة والعناصر الحدية. وكذلك توضح تأثير عوامل عدة على التقارب . تمدد أيضاً هذه الرسالة طريقة دريكلي – نومن المتتالية لدراسة المرونة – اللدونة. الإسهام الأكبر في هذه الرسالة هو إنشاء طريقة تكرارية جديدة لإقران طريقتي العناصر المحدودة والعناصر الحدية. هذه الطريقة ذات قدرة على التعامل مع الحالات والتي توصف فيها شروط حدية طبيعية على كامل محيط الحقل الممثل بطريقة العناصر المحدودة أو ذلك الممثل بطريقة العناصر الحدية على عكس طرق الإقران المتتالية الحالية. وتلائم هذه الطريقة الحالات التي تتميز بأن حقل المسألة ممتد لانهائياً. وكذلك مددت هذه الطريقة الجديدة لدراسة المرونة – اللدونة. وأخيرا تم دراسة بعض التطبيقات العملية مثل ميكانيكا الكسور والأنفاق العميقة والسطحية.

درجة الدكتوراه في الفلسفة

جامعة الملك فهد للبترول والمعادن

الظهران – المملكة العربية السعودية

صفر ١٤٢١هـ – مايو ٢٠٠٠م

CHAPTER 1

INTRODUCTION

1.1 OVERVIEW

The finite element method (FEM) is one of the most popular numerical techniques to solve a wide range of problems in applied science and engineering. The FEM has been applied successfully and has provided satisfactory results. In general, the FEM is used for large range of problems because it is a general-purpose method with mature technology. It is most efficient for finite domains in which material properties are nonhomogeneous, and for finite domains where nonlinear behavior occurs. In the general FEM, the region under consideration is discretized by finite elements, a variation of the unknown is assumed within each element, and the element response matrices are then found. Finally the element response matrices are assembled to obtain the response matrix of the problem domain. The final system of equations is solved, and the appropriate response quantities are determined as required.

Another numerical method that is becoming popular is the boundary element method (BEM). The BEM is most efficient for linear homogeneous problems with finite or infinite domains. Unlike the domain-type methods such as the FEM, the discretization process of the BEM is performed on the boundary only, which results in reducing the

dimension of the problem and simplifying the modeling considerably. Another important advantage of the BEM is its accuracy in predicting high gradients or stress concentrations. The BEM procedure consists of the transformation of the governing differential equations into equivalent integral equations relating only boundary values. The result is a set of linear algebraic equations that can be solved for the surface response. Thereafter, values inside the domain can be obtained from the boundary solution.

The two methods have their advantages and disadvantages. Each method performs better than the other for some problems or some parts of the same problem. Therefore, a combined analysis approach, which for example, models the nonlinear region around an underground opening using the FEM while using the BEM for the remaining infinite homogeneous region, would be both accurate and efficient.

Past efforts on coupling the FEM and BEM employ an entire equation for the whole domain, by combining the discretized equations for the FEM and BEM sub-domains. The approach for constructing the entire equation, however, is highly complicated when compared with that for each single equation. In order to overcome the stated inconvenience, iterative domain decomposition coupling methods, i.e., the Sequential Dirichlet-Neumann method, were developed. In these coupling methods there is no need to combine the coefficient matrices of the FEM and BEM sub-domains. A second advantage is that different formulation of the FEM and BEM can be adopted as base programs for coupling the computer codes only. Separate computation for

each sub-domain and successive renewal of the variables on the interface of both sub-domains, are performed to reach the final convergence. Unfortunately, the available iterative coupling methods are limited to linear elastic or potential problems with finite domains. The convergence of the iterative coupling methods is not fully addressed. Furthermore, there are some cases where these methods are not applicable. These include, i.e., tunnel problems where the natural (Neumann) boundary conditions are prescribed on the entire external boundary of the FEM sub-domain. Consequently, the usefulness of the existing iterative coupling methods becomes limited.

1.2 OBJECTIVES

The primary goal of the present study is to develop a hybrid FEM/BEM coupling method, which is capable of solving a wide range of problems, particularly those associated with infinite or semi-infinite domains in plane elasticity. The FEM sub-domain can be nonhomogeneous or nonlinear while the BEM sub-domain is linear elastic, infinite or semi-infinite. More specifically, the objectives of the present study are:

1. Investigate the convergence of the Sequential Dirichlet-Neumann iterative coupling method.
2. Develop a new iterative method that avoids the limitations existing in the available coupling methods.

3. Extend the Sequential Dirichlet-Neumann and the new iterative methods to elasto-plasticity.
4. Verify the reliability and the efficiency of the proposed method through some benchmark examples and practical applications.

1.3 ORGANIZATION OF THE DISSERTATION

The present chapter gives an overview and the objectives of this dissertation. The second chapter presents a brief background on the BEM and FEM. It gives some historical remarks on both methods. The chapter reviews the BEM formulation for elasticity and potential problems. It also gives the computational steps of the FEM and BEM and a comparison between the two methods.

Chapter 3 gives a critical review of the existing coupling methods. It also describes their limitations.

Chapter 4 establishes the convergence conditions of the Sequential Dirichlet-Neumann iterative coupling method. It also discusses the factors involved in the solution convergence.

Chapter 5 introduces a new overlapping iterative coupling method. The convergence of the method is investigated. Applications to problems involving infinite and semi-infinite regions are also illustrated.

Chapter 6 extends the Sequential Dirichlet-Neumann method and the new overlapping method, presented in Chapter 5, to elasto-plasticity.

Chapter 7 gives some practical applications to verify the efficiency of the iterative coupling methods. These include linear elastic and elasto-plastic fracture mechanics examples, and elastic/elasto-plastic analysis of deep and shallow tunnels. The solution using the coupled FEM/BEM is compared to the conventional FEM solution in terms of accuracy and CPU-time.

Finally, Chapter 8 summarizes the main conclusions and recommendations for future research.

CHAPTER 2

BACKGROUND ON BEM AND FEM

2.1 GENERAL

The FEM and the BEM are the most prominent numerical techniques to solve a wide range of problems in applied science and engineering. This chapter presents a brief background on both methods. Some historical remarks are given. For comparison purposes, a brief derivation of the BEM and FEM formulation in elasticity, using the weighted residual technique, is presented. The basic computational steps of the FEM and BEM are summarized. The chapter is concluded with a comparison between the FEM and BEM, which clearly indicates the advantages and disadvantages of each method and the merits behind their coupling.

2.2 HISTORICAL REMARKS

The modern development of the FEM began in the early 1940s in the field of structural engineering with the work of Hrenikoff [1], who introduced the so-called framework method, in which a plane elastic medium was represented as a collection of bars and beams. The use of piecewise-continuous functions defined over a sub-domain to approximate an unknown function can be found in the work of Courant [2],

who used an assemblage of triangular elements and the principle of minimum total potential energy to study the St. Venant torsion problem. Although certain key features can be found in the work of Hrenikoff [1] and Courant [2], the formal presentation of the FEM is attributed to Argyris and Kelsey [3] and Turner et al. [4]. The term "finite element", was first used by Clough in 1960 [73]. Since its inception, the literature on finite element applications has grown exponentially, and today there are numerous journals and conferences that are primarily devoted to the theory and application of the method.

The BEM, on the other hand, is not based on a differential problem description but rather on an integral problem formulation transformed to the boundary. The development of integral equation methods is due to the Soviet mathematicians, Muskhelishvili [5], Mikhlen [6], Smirnov [7] and Kupradze [8]. These methods, at first hardly recognized by engineers, were more introduced into applied physics. Under the names like "source method" or "indirect method", these techniques were applied in fluid mechanics and in potential theory. Very extensive investigations of the "indirect methods", were performed by Kellog [9], Jaswon [10], Symm [11] and Massonet [12], to mention a few. It is not easy to say who first formulated the "direct" BEM, although in another representation one can find it already in Kupradze's book [8]. But from the engineering point of view, the beginnings of the direct BEM applications in elastostatics have to be dated back to the papers of Rizzo [13] and Cruse and Rizzo [14]. The term "Boundary Elements", was first used by Brebbia [15] in 1978. The BEM is now firmly established as an important alternative

technique to the prevailing numerical methods of analysis. One of the most important applications is for the solution for a range of problems such as temperature diffusion, some types of fluid flow motion, flow in porous media, elastostatics, and many others that can be written as a function of potential. By now, the existing literature on the BEM is very extensive. For some specific applications, like problems characterized by infinite elastic regions, the BEM proved to be superior to other numerical techniques.

2.3 THE VARIATIONAL FORMULATION FOR PLANE ELASTICITY

Although there are different procedures for deriving the boundary integral and finite element equations, the weighted residual technique is considered here. In addition to its generality and applicability to any differential equation, regardless of the physical interpretation, the method has the advantage of relating the BEM to the FEM. In the following, the plane elasticity equations are first stated. Then the weighted residual technique is used to generate the variational statements for the FEM and the BEM.

Consider an isotropic, linear elastic solid of domain Ω enclosed by a boundary Γ as shown in Figure 2.1. The basic field equations for linear elastostatics are given as follows:

Equilibrium equations: $$\sigma_{ij,j} + b_i = 0 \qquad (2.1)$$

Kinematic relations: $$\varepsilon_{ij} = \frac{1}{2}(u_{i,j} + u_{j,i}) \qquad (2.2)$$

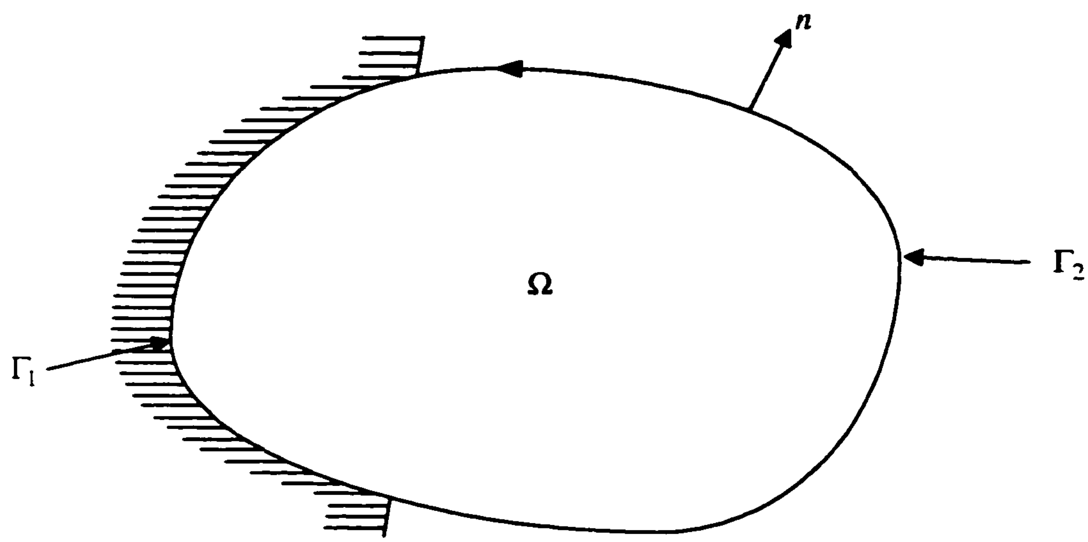

Figure 2.1: Geometrical Representation for the Boundary Element Domain

Constitutive equations: $$\sigma_{ij} = \frac{2\mu\nu}{1-2\nu}\varepsilon_{kk}\delta_{ij} + 2\mu\varepsilon_{ij} \tag{2.3}$$

where, the indicial notation and Cartesian reference frame are used. The quantities $u_i, \sigma_{ij}, \varepsilon_{ij}$ and b_i denote the components of the displacement vector, the symmetrical Cauchy stress tensor, the infinitesimal strain tensor, and the body forces, respectively. μ and ν are the shear modulus and Poisson's ratio, respectively. Using Equations (2.2) and (2.3) in (2.1), the equilibrium equations in terms of the displacement components can be obtained, i.e.,

$$\mu u_{i,jj} + \frac{\mu}{1-2\nu} u_{j,ji} = -b_i \tag{2.4}$$

Prescribed boundary conditions are given by:

$$u_i = \bar{u}_i \text{ on } \Gamma_1 \text{ and } t_i = \bar{t}_i \text{ on } \Gamma_2 \tag{2.5}$$

where t_i, is the traction at a point on the surface, and is given by:

$$t_i = \sigma_{ij} n_j \tag{2.6}$$

In Equation (2.6), n_j is the jth component of the unit normal to the surface Γ at the point of consideration. One can weigh Equation (2.4) by a displacement type function u_i^* and orthogonalize the product, i.e.,

$$\int_\Omega \left(L_{ij} u_j + b_i\right) u_i^* d\Omega = 0 \tag{2.7}$$

where, the operator L_{ij} on u_j is as given by the L.H.S. of Equation (2.4). Integrating Equation (2.7) by parts, one can obtain the weak variational form:

$$\begin{aligned}&-\int_{\Omega} u^{*}_{i,j}\left(\mu u_{i,j}+\frac{\mu}{(1-2\nu)}u_{j,i}\right)d\Omega \\ &+\int_{\Gamma} u^{*}_{i}\left(\mu u_{i,j}+\frac{\mu}{(1-2\nu)}u_{j,i}\right)n_j d\Gamma+\int_{\Omega} u^{*}_{i} b_i d\Omega=0\end{aligned} \tag{2.8}$$

Note that Equation (2.8) is the starting equation for the FEM.

Integrating Equation (2.8) by parts again yields the inverse variational form.

$$\int_{\Omega}\left(L_{ij}u^{*}_{j}\right)u_i d\Omega+\int_{\Gamma} u^{*}_{i} t_i d\Gamma-\int_{\Gamma} t^{*}_{i} u_i d\Gamma+\int_{\Omega} u^{*}_{i} b_i d\Omega=0 \tag{2.9}$$

where t^{*}_{i} are the tractions corresponding to the displacement type function u^{*}_{i}. Equation (2.9) is the starting equation for the BEM.

2.4 BEM FORMULATION IN ELASTOSTATICS

In this section, the theoretical foundation of the BEM in elasticity is presented. It should be noted that the ideas presented in this section are necessary preliminaries for the method. However, references [16-21] can be consulted for the detailed theory.

In Equation (2.9), u^{*}_{i} can be chosen such that:

$$L_{ij}u^{*}_{j}=-\delta(\zeta,x)e_i \tag{2.10}$$

where $\delta(\zeta,x)$ represents the Dirac delta function which has the well known properties:

$$\begin{aligned}&\delta(\zeta,x)=0 \quad \in \zeta \neq x\\&\delta(\zeta,x)=\infty \quad \in \zeta = x\\&\int_{\Omega} f(x)\delta(\zeta,x)d\Omega = f(\zeta)\end{aligned} \tag{2.11}$$

Notice that, ζ and x are the source and field points, respectively. The solution for Equation (2.10) is known as the fundamental solution. Using Equations (2.10) and (2.11) in (2.9), the following equation can be obtained:

$$u_i(\zeta)=\int_{\Gamma} u_i^{*}t_i d\Gamma - \int_{\Gamma} t_i^{*}u_i d\Gamma + \int_{\Omega} u_i^{*}b_i d\Omega \tag{2.12}$$

Equation (2.12) gives the displacements u_i at any point ζ inside the domain Ω in terms of the boundary values. The tractions and displacements can be written in the following form:

$$t_j^{*} = t_{ij}^{*}(\zeta,x)\, e_i \tag{2.13}$$

$$u_j^{*} = u_{ij}^{*}(\zeta,x)\, e_i \tag{2.14}$$

where, $u_{ij}^{*}(\zeta,x)$ and $t_{ij}^{*}(\zeta,x)$ represents the displacements and tractions in the j direction at the point x corresponding to a unit force applied at the source point ζ and acting in the e_i direction.

Equation (2.12) can now be written in the following form:

$$u_i(\zeta) = \int_{\Gamma} u_{ij}^{*}(\zeta,x)t_j(x)d\Gamma - \int_{\Gamma} t_{ij}^{*}(\zeta,x)u_j(x)d\Gamma + \int_{\Omega} u_{ij}^{*}(\zeta,x)b_j(x)d\Omega \qquad (2.15)$$

This equation is known as the Somigliana's identity, and it gives the value of the displacement at any point in terms of the boundary values u_j and t_j, the forces throughout the domain, and the known fundamental solution.

2.4.1 Fundamental Solutions

When using the integral Equation (2.15) to solve problems in solid mechanics, different fundamental solutions are needed to simulate certain problems properly. In general cases, the Kelvin's solution is used. In case of semi-infinite mediums, the more suitable fundamental solutions are the Mindlin's solution for 3D, or the Melan's solution for 2D. As the work is limited to two-dimensional cases, only the 2D Kelvin's solution and Melan's solution are given.

2.4.1.1 Kelvin's Solutions

In Figure 2.2, let us assume a domain Ω^* with boundary Γ^* that contains the domain Ω with boundary Γ under consideration. The elastic properties remain valid for both cases. For the Kelvin fundamental solution, Ω^* is assumed to be an infinite elastic plane, and consequently Γ^* is taken to infinity. The tensor expressions $u_{ij}^*(\zeta,x)$ and $t_{ij}^*(\zeta,x)$ for the two-dimensional plane strain problems are given by [22]:

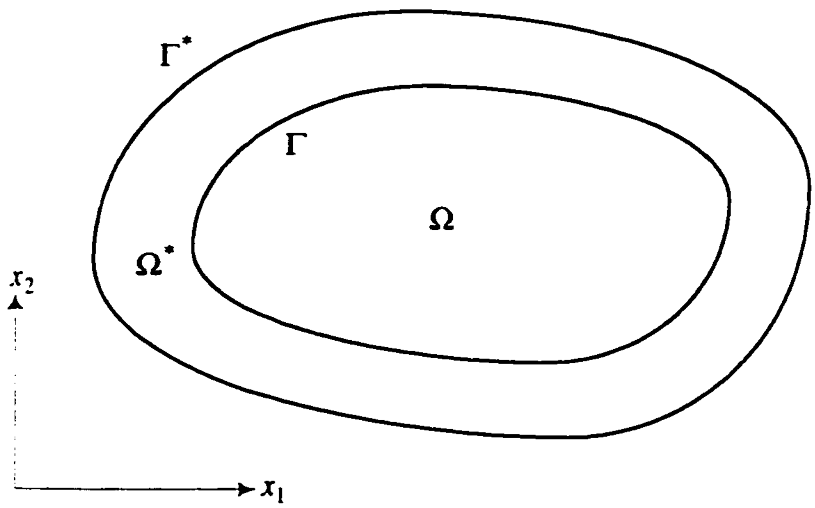

Figure 2.2: General Region $\Omega^* + \Gamma^*$ containing the body $\Omega + \Gamma$

$$u_{ij}^{*}(\zeta,x)=\frac{-1}{8\pi(1-\nu)G}\left[(3-4\nu)\ln(r)\delta_{ij}-r_{,i}r_{,j}\right] \tag{2.16}$$

$$t_{ij}^{*}(\zeta,x)=\frac{1}{4\pi(1-\nu)r}\left[\left[(1-2\nu)\delta_{ij}+2r_{,i}r_{,j}\right]\frac{\partial r}{\partial n}-(1-2\nu)(r_{,i}n_{j}-r_{,j}n_{i})\right] \tag{2.17}$$

For plane stress problems, ν is simply replaced by $\nu/(1+\nu)$. In these expressions,

$$r(\zeta,x)=\sqrt{r_i r_i} \text{ with } r_i=x_i(x)-x_i(\zeta) \tag{2.18}$$

represents the distance between the load point (ζ) and the field point (x), and the derivatives of $r(\zeta,x)$ with respect to the coordinates of x are denoted with:

$$r_{,i}=\frac{\partial r}{\partial x_i(x)} \tag{2.19}$$

2.4.1.2 Melan's Solution

Considering Figure 2.3, for semi-infinite problems the Kelvin region is subdivided by an infinite horizontal plane $\overline{\Gamma}$ and its lower part is considered as $\Omega^{*}+\Gamma^{*}$. Thus the region of interest becomes a semi-infinite medium with the plane part Γ^{*} being represented by the boundary surface $\overline{\Gamma}$. This lower half-plane is always assumed to contain the region $\Omega+\Gamma$ and the plane $x_1=0$ is taken to be the boundary surface $\overline{\Gamma}$.

The stress solution corresponding to a unit force acting in the half-plane was published by Melan [23] in 1932. During the first half century after its publication,

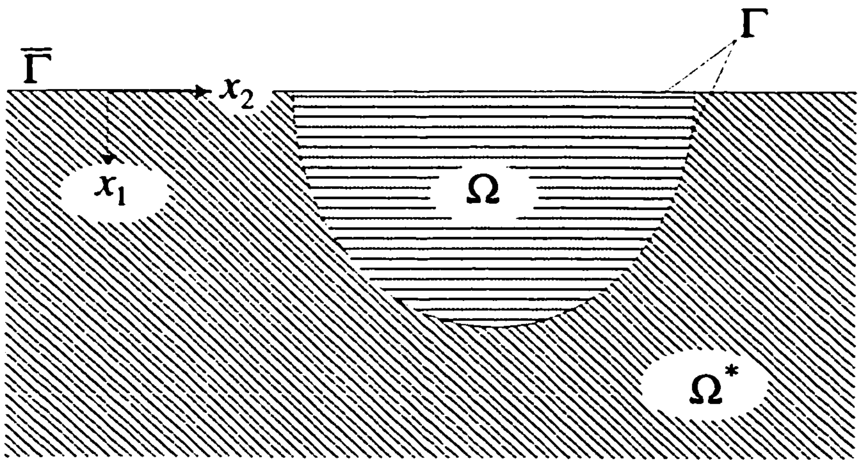

Figure 2.3: Body $\Omega + \Gamma$ Located within the Semi-Infinite Plane $x_1 \geq 0$

Melan's solution had been rarely used in calculations. It is mainly due to the development of boundary elements that Melan's solution has gained an important role in numerical analysis. Although Melan has found the stresses of his solution, he did not give the displacement expressions, which are necessary for the boundary element implementations. This work was accomplished by Telles and Brebbia [24] in 1981. They gave the expressions of Melan's solution. For a good background on this area, the reader may refer to [24-28].

The symbols and expressions proposed by Telles and Brebbia [24] are used throughout this investigation. Melan's solution, represented by $(\ )^m$, may be rearranged into two parts, a Kelvin's solution part represented by $(\ )^k$ and a complementary part $(\ )^c$. The complete forms of the complementary part $(\ )^c$ may be found in [24].

2.4.2 Stresses at Internal Points

Equation (2.15) is a continuous representation of displacements at any point $\zeta \in \Omega$. Consequently, the state of stress at this point can be obtained by combining the derivatives of Equations (2.15) with respect to ζ, to produce the strain tensor and then substituting the result into Hooke's law. The final expression becomes:

$$\sigma_{ij}(\zeta) = \int_{\Gamma} u^{*}_{ijk}(\zeta, x) t_k(x) d\Gamma - \int_{\Gamma} t^{*}_{ijk}(\zeta, x) u_k(x) d\Gamma + \int_{\Omega} u^{*}_{ijk}(\zeta, x) b_k(x) d\Omega \qquad (2.20)$$

For the Kelvin fundamental solution the new tensors u^{*}_{ijk} and t^{*}_{ijk} are given in reference [23]. Telles and Brebbia [24] have presented the complementary expressions for the tensors, corresponding to the half-plane fundamental solutions.

2.4.3 Boundary Integral Equations

In the preceding sections, the derivation of the Somigliana's identity has been presented without a need for the distinction between the different fundamental solutions employed. In this section, however, it is instructive to consider first the Kelvin solution, and then extend the complete formulation to semi-infinite type problems, where full advantage of the traction-free condition can be taken.

Considering the Kelvin case, Somigliana's identity is not satisfactory for obtaining solutions unless the boundary displacements and tractions are known throughout the boundary Γ. Therefore, it is interesting to examine the limiting form of Equation (2.15) as ζ goes to the boundary. Assuming first that the body can be represented as shown in Figure 2.4, with the point ζ as an internal point surrounded by part of a circle of radius ε. Equation (2.15) can be written in the following form:

$$
\begin{aligned}
u_j(\zeta) = & \int_{\Gamma-\Gamma_\varepsilon+\overline{\Gamma}_\varepsilon} u^{*}_{ij}(\zeta,x)t_j(x)d\Gamma - \int_{\Gamma-\Gamma_\varepsilon+\overline{\Gamma}_\varepsilon} t^{*}_{ij}(\zeta,x)u_j(x)d\Gamma \\
& + \int_{\Omega'} u^{*}_{ij}(\zeta,x)b_j(x)d\Omega
\end{aligned}
\tag{2.21}
$$

Taking the limit as $\varepsilon \rightarrow 0$, Equation (2.21) finally takes the form:

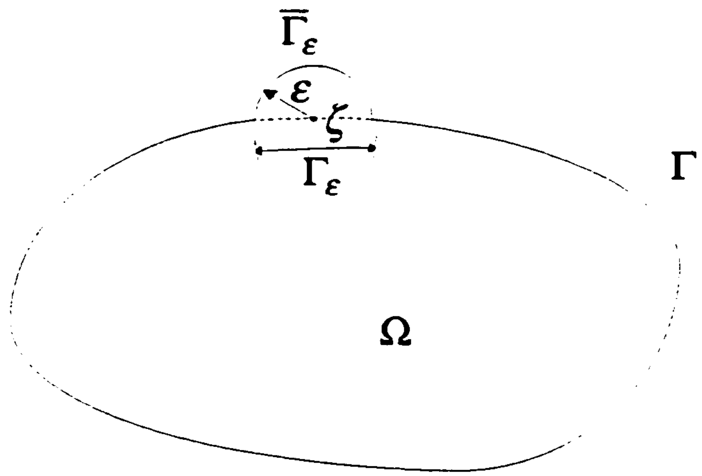

Figure 2.4: Singular Point ζ on Γ surrounded by a semicircle

$$c_{ij}(\zeta)u_j(\zeta)=\int_{\Gamma} u^*_{ij}(\zeta,x)t_j(x)d\Gamma-\int_{\Gamma} t^*_{ij}(\zeta,x)u_j(x)d\Gamma + \int_{\Omega} u^*_{ij}(\zeta,x)b_j(x)\,d\Omega \tag{2.22}$$

The integrals in Equation (2.22) present no special singularities and can be interpreted in the normal sense of integration. The coefficient $c_{ij}(\zeta)=\delta_{ij}/2$ if the tangent plane at ζ is continuous, but if this is not the case, closed form expressions for this coefficient have been presented in reference [29]. For practical applications, however, the coefficient c_{ij} can be indirectly computed by applying Equation (2.22) to represent rigid body movements as will be explained in Section 2.4.5.

Equation (2.22) is the starting equation for the BEM using the Kelvin fundamental solution. For semi-infinite domains, if the body that is being analyzed presents part of its boundary coinciding with the surface of the semi-infinite domain (Figure 2.5), the integral over this part which involves t^*_{ij} vanishes identically because of the traction-free condition included into the fundamental solution. Consequently, Somigliana's identity can be rewritten as follows:

$$u_j(\zeta)=\int_{\Gamma} u^*_{ij}(\zeta,x)t_j(x)d\Gamma-\int_{\Gamma'} t^*_{ij}(\zeta,x)u_j(x)d\Gamma+\int_{\Omega} u^*_{ij}(\zeta,x)b_j(x)d\Omega \tag{2.23}$$

where, Γ' represents the part of Γ in which $x_1>0$. The state of stress at an internal point is given by:

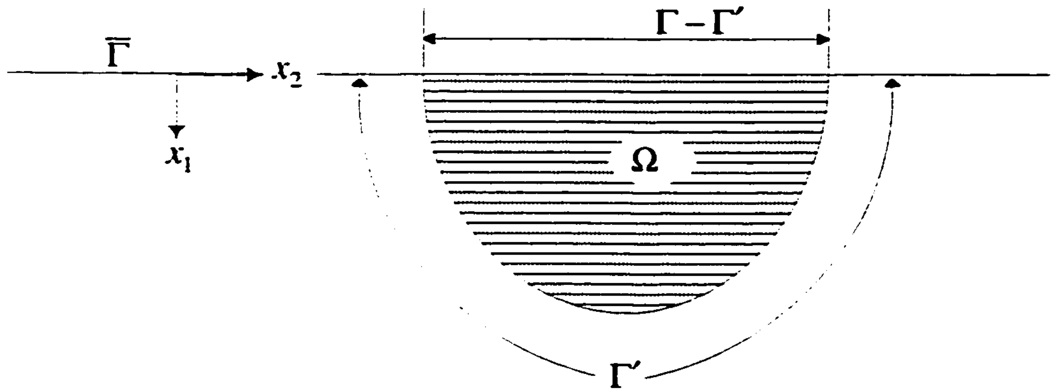

Figure 2.5: Body with Part of its Boundary Γ Coinciding with the Surface of the Semi-Infinite Plane

$$\sigma_{ij}(\zeta)=\int_{\Gamma} u^{*}_{ijk}(\zeta,x)t_k(x)d\Gamma-\int_{\Gamma} t^{*}_{ijk}(\zeta,x)u_k d\Gamma+\int_{\Omega} u^{*}_{ijk}(\zeta,x)b_k(x)d\Omega \tag{2.24}$$

2.4.4 Infinite and Semi-Infinite Regions

The extension of Equation (2.22) to infinite regular regions is not valid without further hypothesis on the functions involved. Such hypotheses are concerned with the behavior of the functions on an infinitely distant surface, and are referred to as regularity conditions [17]. Let q be the radius of a circle of surface Γ_q and centered at ζ, which encloses the cavity (or cavities) of the external problem as depicted in Figure 2.6. Equation (2.22) can be written for the region Γ and Γ_q as follows:

$$\begin{aligned} c_{ij}(\zeta)u_j(\zeta)=&\int_{\Gamma} u^{*}_{ij}(\zeta,x)t_j(x)\,d\Gamma+\int_{\Gamma_q} u^{*}_{ij}(\zeta,x)t_j(x)\,d\Gamma \\ &-\int_{\Gamma} t^{*}_{ij}(\zeta,x)u_j(x)d\Gamma-\int_{\Gamma_q} t^{*}_{ij}(\zeta,x)u_j(x)\,d\Gamma \end{aligned} \tag{2.25}$$

Clearly, if the limiting case $q\to\infty$ is considered, Equation (2.25) can be expressed in terms of the boundary integrals over Γ alone if:

$$\lim_{q\to\infty}\int_{\Gamma_q}\left(t^{*}_{ij}(\zeta,x)u_j(x)-u^{*}_{ij}(\zeta,x)t_j(x)\right)\,d\Gamma=0 \tag{2.26}$$

One can substitute $u_j(x)$ and $t_j(x)$ by the tensors corresponding to the fundamental solution, and indeed verify that Equation (2.26) is satisfied. This statement is also verified for semi-infinite problems where the semi-infinite fundamental solutions

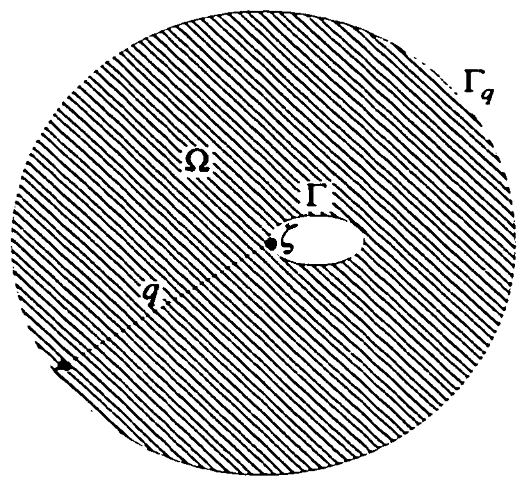

Figure 2.6: Infinite Region with Cavity

dictate the corresponding conditions. In conclusion, provided the regularity conditions are specified, infinite problems (Figure 2.6) can be represented by:

$$c_{ij}(\zeta)u_j(\zeta)=\int_\Gamma u^*_{ij}(\zeta,x)t_j(x)d\Gamma-\int_\Gamma t^*_{ij}(\zeta,x)u_j(x)d\Gamma \tag{2.27}$$

and also semi-infinite problems that may have a loaded boundary $\Gamma-\Gamma'$ (Figure 2.7) can be represented by:

$$c_{ij}(\zeta)u_j(\zeta)=\int_\Gamma u^*_{ij}(\zeta,x)t_j(x)\,d\Gamma-\int_{\Gamma'} t^*_{ij}(\zeta,x)u_j(x)\,d\Gamma \tag{2.28}$$

2.4.5 Numerical Implementation

In this section, a general numerical procedure for the solution of the BEM is described. In order to concentrate on the main aspects of the process, the different forms of boundary integral equation introduced in the previous sections will be represented in a unified manner as follows (body forces are omitted here for simplicity):

$$c_{ij}(\zeta)u_j(\zeta)+\int_\Gamma t^*_{ij}(\zeta,x)u_j d\Gamma=\int_\Gamma u^*_{ij}(\zeta,x)t_j(x)d\Gamma \tag{2.29}$$

where, depending on the fundamental solution employed (infinite or semi-infinite), the appropriate expression for $c_{ij}(\zeta)$ and the substitution of Γ by Γ' in the first integral are implied.

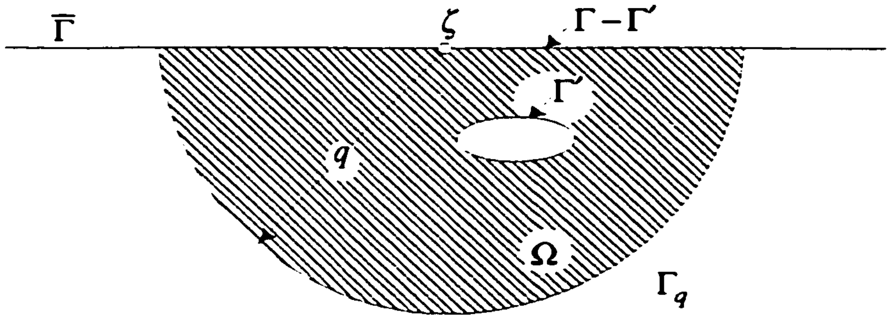

Figure 2.7: Semi-Infinite Region with or without Cavity

Instead of attempting closed form solutions to Equation (2.29), which is a difficult task and only attainable for simple geometry and boundary conditions, the BEM employs a numerical approach. The basic steps involved in this approach constitute the numerical essence of the technique. They are summarized as bellow:

1. The boundary Γ is discretized into a series of elements (NE is the number of elements), over which displacements and tractions are chosen to be piecewise interpolated between the element nodal points (N is the number of nodes).

2. Equation (2.29) is applied in a discretized form to each nodal point ζ of the boundary Γ and the integrals are computed (usually by a numerical quadrature scheme) over each boundary element. A system of $2N$ linear algebraic equations is therefore obtained, involving the set of $2N$ nodal tractions and $2N$ nodal displacements.

3. Boundary conditions are imposed, and consequently $2N$ nodal values (tractions or displacements) are prescribed. The system of $2N$ equations can therefore be solved by standard methods to obtain the remaining boundary data.

Values of displacements and stresses at any selected internal point can readily be computed by numerical quadrature using the appropriate Equations (2.15) and (2.20) or Equations (2.23) and (2.24) also in a discretized fashion.

For the discretization of Equation (2.29), the boundary, Γ, is approximated by using a series of elements. The Cartesian coordinates, $\boldsymbol{x}$, of points located within each

element Γ_j are expressed in terms of interpolation functions $\boldsymbol{\Psi}$ and the nodal coordinates $\boldsymbol{x}^m$ of the element, by the following matrix relation:

$$\boldsymbol{x} = \boldsymbol{\Psi}^T \boldsymbol{x}^m \tag{2.30-a}$$

where, $\boldsymbol{x}$ represents the x_1 and x_2 coordinates in two-dimensional problems. In a similar way, boundary displacements and tractions are approximated over each element through interpolation functions

$$\boldsymbol{u} = \varphi^T \boldsymbol{u}^n \tag{2.30-b}$$

$$\boldsymbol{t} = \varphi^T \boldsymbol{t}^n \tag{2.30-c}$$

where, $\boldsymbol{u}^n$ and $\boldsymbol{t}^n$ contain the nodal displacements and tractions, respectively. Note that the superscript m in Equation (2.30) refers to the number of boundary points required to define the geometry of each boundary element, whereas the superscript n in Equations (2.31) and (2.32) refers to the number of boundary nodes to which the nodal values of displacements and tractions are associated. These numbers may be different in general. Also note that the functions $\boldsymbol{\varphi}$ and ψ are expressed in the homogeneous system of coordinates (η).

It is now more convenient to work with matrices instead of the indicial notation. Let us define the following vectors and matrices:

$$u = \begin{Bmatrix} u_1 \\ u_2 \end{Bmatrix}, \qquad t = \begin{Bmatrix} t_1 \\ t_2 \end{Bmatrix} \tag{2.31-a}$$

$$u^* = \begin{bmatrix} u_{11}^* & u_{12}^* \\ u_{21}^* & u_{22}^* \end{bmatrix}, \qquad t^* = \begin{bmatrix} t_{11}^* & t_{12}^* \\ t_{21}^* & t_{22}^* \end{bmatrix} \tag{2.31-b}$$

where, u_{ij}^* and t_{ij}^* are the displacements and tractions in the j direction due to a unit force at a point under consideration, acting in the i direction.

Now Equation (2.29) can now be expressed in a matrix form as follows:

$$cu + \int_\Gamma t^* u \, d\Gamma = \int_\Gamma u^* t \, d\Gamma \tag{2.32}$$

Substituting Equations (2.30) into Equation (2.32), the following equation can be obtained:

$$cu + \sum_{j=1}^{NE} \left(\int_{\Gamma_j} t^* \varphi^T d\Gamma \right) u^n = \sum_{j=1}^{NE} \left(\int_{\Gamma_j} u^* \varphi^T d\Gamma \right) t^n \tag{2.33}$$

where, the summation from $j = 1$ to NE indicates the summation over the NE elements on the surface, and Γ_j is the surface of the j element. It is common to employ a numerical integration scheme in integrating Equation (2.33). Hence Equation (2.33) becomes:

$$cu + \sum_{j=1}^{NE} \left(\sum_{l=1}^{L} |J|_l \, w_l (t^* \varphi^T(\eta))_l \right) u^n = \sum_{j=1}^{NE} \left(\sum_{l=1}^{L} |J|_l \, w_l (u^* \varphi^T(\eta))_l \right) t^n \tag{2.34}$$

where, $|J|$ is the Jacobian transformation, and w_l are the numerical integration weighting coefficients. Note that Equation (2.34) gives a set of equations for node i which, can be written as:

$$c_i \boldsymbol{u}_i + \begin{bmatrix} \hat{\boldsymbol{h}}_{i1} & \hat{\boldsymbol{h}}_{i2} & \ldots & \hat{\boldsymbol{h}}_{ii} & \ldots & \hat{\boldsymbol{h}}_{iN} \end{bmatrix} \begin{Bmatrix} \boldsymbol{u}_1 \\ \boldsymbol{u}_2 \\ \vdots \\ \boldsymbol{u}_i \\ \vdots \\ \boldsymbol{u}_N \end{Bmatrix} = \begin{bmatrix} \boldsymbol{G}_{i1} & \boldsymbol{G}_{i2} & \ldots & \boldsymbol{G}_{ii} & \ldots & \boldsymbol{G}_{iN} \end{bmatrix} \begin{Bmatrix} \boldsymbol{t}_1 \\ \boldsymbol{t}_2 \\ \vdots \\ \boldsymbol{t}_i \\ \vdots \\ \boldsymbol{t}_N \end{Bmatrix}$$

(2.35)

where, $\hat{\boldsymbol{h}}_{ij}$ and $\boldsymbol{G}_{ij}$ are the interaction coefficients relating node i with all the nodes on the surface of the body. Note that, more than one element will contribute to $\hat{\boldsymbol{h}}_{ij}$ and $\boldsymbol{G}_{ij}$ sub-matrices.

A matrix equation such as Equation (2.35) can be written for each of the nodes under consideration as follows:

$$\begin{bmatrix} \boldsymbol{h}_{11} & \ldots & \hat{\boldsymbol{h}}_{1i} & \ldots & \hat{\boldsymbol{h}}_{1N} \\ \vdots & & \vdots & & \vdots \\ \hat{\boldsymbol{h}}_{i1} & & \boldsymbol{h}_{ii} & & \hat{\boldsymbol{h}}_{iN} \\ \vdots & & \vdots & & \vdots \\ \hat{\boldsymbol{h}}_{N1} & & \hat{\boldsymbol{h}}_{Ni} & & \boldsymbol{h}_{NN} \end{bmatrix} \begin{Bmatrix} \boldsymbol{u}_1 \\ \vdots \\ \boldsymbol{u}_i \\ \vdots \\ \boldsymbol{u}_N \end{Bmatrix} = \begin{bmatrix} \boldsymbol{G}_{11} & \ldots & \boldsymbol{G}_{1i} & \ldots & \boldsymbol{G}_{1N} \\ \vdots & & \vdots & & \vdots \\ \boldsymbol{G}_{i1} & & \boldsymbol{G}_{ii} & & \boldsymbol{G}_{iN} \\ \vdots & & \vdots & & \vdots \\ \boldsymbol{G}_{N1} & & \boldsymbol{G}_{Ni} & & \boldsymbol{G}_{NN} \end{bmatrix} \begin{Bmatrix} \boldsymbol{t}_1 \\ \vdots \\ \boldsymbol{t}_i \\ \vdots \\ \boldsymbol{t}_N \end{Bmatrix}$$

(2.36)

where, the sub-matrices $\boldsymbol{h}_{ii}$ on the diagonal are: $\boldsymbol{h}_{ii} = \hat{\boldsymbol{h}}_{ii} + \boldsymbol{c}_i$. Now, Equation (2.36) can be written as follows:

$$[H]\{u\} = [G]\{t\} \tag{2.37}$$

Note that the diagonal elements of $[\boldsymbol{H}]$ are based on the computation of singular integrals. However, a simpler, yet effective way, is by applying a rigid-body displacement to the body in any one direction; Equation (2.37) then becomes:

$$[H]\{I_l\} = 0 \tag{2.38}$$

where, $\{I_l\}$ is a vector defining a unit displacement in the direction l. Hence, the diagonals of $[\boldsymbol{H}]$ are simply:

$$\boldsymbol{H}_{ii} = -\sum_{i \neq j} \boldsymbol{H}_{ij} \tag{2.39}$$

which means that neither the $\boldsymbol{c}_i$ nor the $\boldsymbol{H}_{ii}$ coefficients need be determined explicitly.

2.5 BEM FORMULATION FOR POTENTIAL PROBLEMS

The application of the BEM for the solution of potential problems is considered in this section. Consider a problem governed by Laplace equation:

$$k\nabla^2 u = 0 \text{ in } \Omega \tag{2.40}$$

where, k is the material property and u is the potential. The boundary conditions are such that:

$$
\begin{aligned}
u &= \bar{u} \quad on\ \Gamma_1 \\
t &= \bar{t} \quad on\ \Gamma_2
\end{aligned}
\tag{2.41}
$$

where, t is the flux vector, given by:

$$
t = \partial u / \partial n \tag{2.42}
$$

One can weigh Equation (2.40) by a weighting function u^*. Integrating by parts twice yields the inverse formulation:

$$
\int_{\Omega} \left(K\nabla^2 u^* \right) u d\Omega + \int_{\Gamma} u^* t d\Gamma - \int_{\Gamma} t^* u = 0 \tag{2.43}
$$

This is the starting equation for the application of the BEM for potential problems and is equivalent to Equation (2.9). To avoid unnecessary repetition, one can follow the same procedures as in the previous section to finally obtain the BEM equations given by Equations (2.37). For a detailed formulation of the BEM for potential problems references [16-21] can be consulted.

2.6 FINITE ELEMENT FORMULATION

Although the common procedure for deriving the FEM equations in solid mechanics is based on energy principles, the weighted residual technique is used here for the

reasons explained earlier. It should be noted, however, that both procedures mathematically yield the same FEM model, but differs in their algebraic form.

The domain Ω of the original problem is divided into sub-domains Ω^e, $e = 1,\dots,N$, and construct the weak varaitional form by applying Equations (2.8) over element Ω^e, i.e.,

$$\begin{aligned}
&-\int_{\Omega^e} u^*_{i,j}\left(\mu u_{i,j} + \frac{\mu}{(1-2\nu)}u_{j,i}\right)d\Omega \\
&+\int_{\Gamma^e} u^*_i\left(\mu u_{i,j} + \frac{\mu}{(1-2\nu)}u_{j,i}\right)n_j d\Gamma + \int_{\Omega^e} u^*_i b_i d\Omega = 0
\end{aligned} \tag{2.44}$$

Equation (2.44) can be written as:

$$\begin{aligned}
B^{11}(u^*_1, u_1) + B^{12}(u^*_1, u_2) = l^1(u^*_1) \\
B^{21}(u^*_2, u_1) + B^{22}(u^*_2, u_2) = l^2(u^*_2)
\end{aligned} \tag{2.45}$$

where, the bilinear and linear functions can be written by comparison to (2.44). The nodal displacements can be approximated over Ω^e by the interpolation:

$$\begin{aligned}
u_1 = \sum_{j=1}^{n} u_{1j}^{(e)} \phi_j^{(e)} \\
u_2 = \sum_{j=1}^{n} u_{2j}^{(e)} \phi_j^{(e)}
\end{aligned} \tag{2.46}$$

Note that $u_{1j}^{(e)}$ and $u_{2j}^{(e)}$ are the nodal values of the primary variables. Substituting in Equation (2.45) yields:

$$\sum_{j=1}^{n} B^{11}\left(\phi_i^{(e)},\phi_j^{(e)}\right)u_{1j}^{(e)} + \sum_{j=1}^{n} B^{12}\left(\phi_i^{(e)},\phi_j^{(e)}\right)u_{2j}^{(e)} = l^1\left(\phi_i^{(e)}\right)$$
$$\sum_{j=1}^{n} B^{21}\left(\phi_i^{(e)},\phi_j^{(e)}\right)u_{1j}^{(e)} + \sum_{j=1}^{n} B^{22}\left(\phi_i^{(e)},\phi_j^{(e)}\right)u_{2j}^{(e)} = l^2\left(\phi_i^{(e)}\right) \tag{2.47}$$

or

$$\left[K^{11(e)}\right]\left\{u_1^{(e)}\right\} + \left[K^{12(e)}\right]\left\{u_2^{(e)}\right\} = \left\{f_1^{(e)}\right\}$$
$$\left[K^{21(e)}\right]\left\{u_1^{(e)}\right\} + \left[K^{22(e)}\right]\left\{u_2^{(e)}\right\} = \left\{f_2^{(e)}\right\} \tag{2.48}$$

where,

$$K_{ij}^{11(e)} = \int_{\Omega^e} \left(c_{11}\frac{\partial\phi_i^{(e)}}{\partial x_1}\frac{\partial\iota_j^{(e)}}{\partial x_1} + c_{33}\frac{\partial\phi_i^{(e)}}{\partial x_2}\frac{\partial\phi_j^{(e)}}{\partial x_2} \right) dx_1 dx_2$$

$$K_{ij}^{12(e)} = K_{ji}^{21(e)} = \int_{\Omega^e} \left(c_{12}\frac{\partial\phi_i^{(e)}}{\partial x_1}\frac{\partial\iota_j^{(e)}}{\partial x_2} + c_{33}\frac{\partial\phi_i^{(e)}}{\partial x_2}\frac{\partial\phi_j^{(e)}}{\partial x_1} \right) dx_1 dx_2$$

$$K_{ij}^{22(e)} = \int_{\Omega^e} \left(c_{33}\frac{\partial\phi_i^{(e)}}{\partial x_1}\frac{\partial\iota_j^{(e)}}{\partial x_1} + c_{22}\frac{\partial\phi_i^{(e)}}{\partial x_2}\frac{\partial\phi_j^{(e)}}{\partial x_2} \right) dx_1 dx_2$$

$$f_i^{1(e)} = \int_{\Gamma^e} \left(t_1\phi_i^{(e)}\right) d\Gamma + \int_{\Omega^e} \left(b_1\phi_i^{(e)}\right) dx_1 dx_2$$

$$f_i^{2(e)} = \int_{\Gamma^e} \left(t_2\phi_i^{(e)}\right) d\Gamma + \int_{\Omega^e} \left(b_2\phi_i^{(e)}\right) dx_1 dx_2$$

$$c_{11} = c_{22} = \frac{2\mu}{1-\nu'}$$

$$c_{12} = \frac{2\nu'\mu}{1-\nu'}$$

$$c_{33} = \mu$$

$\nu' = \nu$ for plane stress, and $\nu' = \dfrac{\nu}{1-\nu}$ for plane strain.

The global system of equations can be obtained by applying the same procedure for each element and assembling the resultant equations to yield:

$$\boldsymbol{K}\,\boldsymbol{u} = \boldsymbol{f} \tag{2.49}$$

where $\boldsymbol{K}$ is the stiffness matrix for the system, and $\boldsymbol{u}$ and $\boldsymbol{f}$ are the nodal displacements and force vectors, respectively.

Note that if, on the other hand, using the principle of virtual work, the basic expressions required for solution can be obtained as [74]

$$\int_{\Omega} \boldsymbol{B}^{T} \sigma \, d\Omega - \boldsymbol{F} - \int_{\Omega} \boldsymbol{N}^{T} \boldsymbol{b} \, d\Omega = 0 \tag{2.50}$$

where, F donates the external applied forces. $\boldsymbol{N}$ and $\boldsymbol{B}$ are the usual matrix of shape functions and the elastic strain-displacement matrix, respectively. Thus the stiffness matrix $\boldsymbol{K}$ will have the following form:

$$K = \int_{\Omega} B^T D\, B\, d\Omega \tag{2.51}$$

where, D is the stress strain matrix.

For the elasto-plastic analysis [31], Equation (2.50) will not be generally satisfied at any stage of computation, and thus:

$$\psi = \int_{\Omega} B^T \sigma\, d\Omega - F - \int_{\Omega} N^T b\, d\Omega \neq 0 \tag{2.52}$$

where, ψ is the residual force vector. For an elasto-plastic situation the material stiffness is continuously varying, and instantaneously the incremental stress/strain relationship is given by:

$$d\sigma = D_{ep}\, d\varepsilon \tag{2.53}$$

where, D_{ep} is the elasto-plastic stress-strain matrix For the purpose of evaluating the material stiffness matrix at any stage, an incremental form of Equation (2.52) must be employed. Thus within an increment of load we have:

$$\Delta\psi = \int_{\Omega} B^T \Delta\sigma\, d\Omega - \Delta F - \int_{\Omega} N^T \Delta b\, d\Omega \tag{2.54}$$

Substituting for $\Delta\sigma$ using Equation (2.53) results in

$$\Delta\psi = K_T \Delta u - (\Delta F + \int_{\Omega} N^T \Delta b\, d\Omega) \tag{2.55}$$

where, the tangential stiffness matrix $K_T = \int_{\Omega} B^T D_{ep} B \, d\Omega$.

For the solution of Equation (2.55), and for each load increment, the incremental nodal displacements and stresses are calculated. The updated stresses are then brought down to the yield surface and are used to calculate the equivalent nodal forces. These nodal forces can be compared with the externally applied loads to form a system of residual forces, which is brought sufficiently close to zero through an iterative process before moving to the next load increment.

2.7 COMPUTATIONAL STEPS OF THE FEM AND BEM

This section broadly defines the basic computational steps followed in the FEM and BEM. The basic steps of the FEM are as follow [20]:

1. **Discretize the problem domain.** The first step is to divide the problem domain into a number of finite elements each of simple geometry. An element has a number of nodal points the locations in space of which are given by coordinates relative to a set of global axes. The shape of each element is defined in terms of these coordinates by interpolation or shape functions. This is known as solid modeling and is not only a feature of finite element analysis.

2. **Assume a variation of the unknown inside each finite element.** An interpolation function is proposed for the variation of the unknown (e.g.

displacement, temperature) inside each element in terms of values at the nodal points.

3. **Find element response matrices.** For each finite element, coefficient matrices that describe the response characteristics of the element are determined. In solid mechanics for example a matrix of stiffness coefficients is computed.

4. **Assemble the element matrices to obtain the response matrix of the problem domain.** To find the response matrix of the system $[\boldsymbol{K}]$ to be modeled, the response matrices of the individual elements are combined to form a matrix equation expressing the behavior of the entire solution region.

5. **Introduce boundary conditions.** The global material response matrix is a singular one. To remove the singularity problem, certain boundary conditions must be invoked before the assembled system of equations can be solved.

6. **Solve system of equations.** In most problems the number of equations is large, thus special solution techniques have to be employed to solve the system efficiently taking advantage of the properties such as symmetry and sparseness of the matrix of equation coefficients.

7. **Determine additional quantities as required.** Using the nodal values and interpolation functions, additional parameters can be determined such as strain and stress inside each element.

The basic steps of the BEM are as follow [20]:

1. **Discretize the boundary of the given problem.** By contrast with the FEM only the boundary of the problem domain need be discretized.

2. **Assume a variation of the unknown inside each boundary element.** This is the same as in finite element method except that only boundary values are interpolated.

3. **Calculate the coefficient matrices.** Unlike the FEM, the coefficient matrices, $[H]$ and $[G]$, are computed directly by integrating over the boundary elements using the fundamental solution which satisfies the governing differential equations exactly.

4. **Solve system of equations.** As in the FEM the system of equations is now solved. The primary unknown values are obtained directly.

5. **Compute values inside the domain.** By contrast to the FEM the solution of the boundary element equations give only unknowns (e.g. displacements, surface tractions) at the boundary surface of the problem domain. If displacements or stress values are required at specific points inside the domain, they can be calculate from those boundary values. This is one of the distinct features of the BEM in that output may be selectively obtained after the analysis has been completed.

The main programming steps of the BEM and FEM are shown in Figure 2.8.

2.8 COMPARISON OF THE FEM AND BEM

Some of the major differences between the two methods are remarked on here. Depending on the application some of these differences can either be considered as advantageous or disadvantageous to a particular scheme. The major differences can be summarized as [30]:

1. **FEM**: Secondary variables on the boundary are less accurate than the primary variables.

   BEM: Both the primary and secondary variables are of the same accuracy.

2. **FEM**: An entire domain mesh is required.

   BEM: A mesh of the boundary only is required.

   Comment: Because of the reduction of the size of the mesh for the BEM, one can say that the problem size is reduced by one dimension. This is one of the major advantages of the BEM as construction of meshes for complicated objects, particularly in 3-D, is a very time consuming exercise.

3. **FEM**: Entire domain solution is calculated as part of the solution.

   BEM: Solution of the boundary is calculated first. Thereafter, the solution at domain points, if required, is found as a separate step.

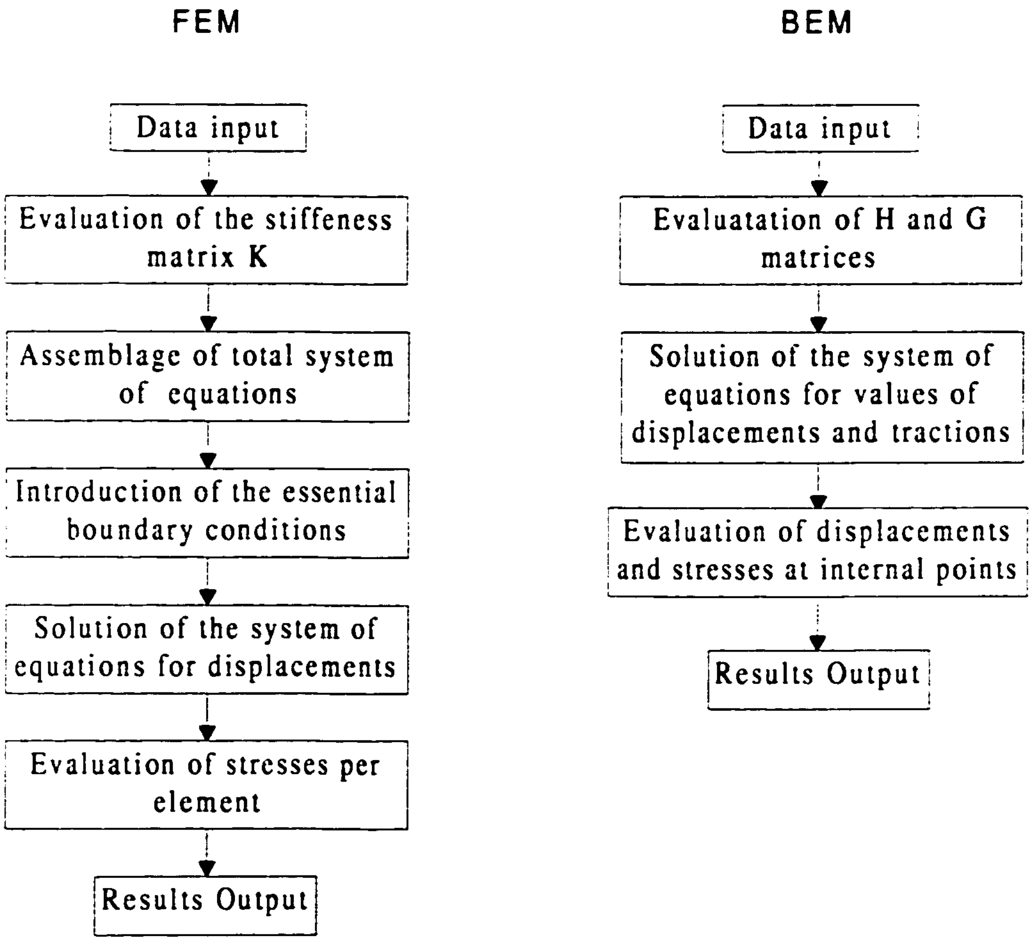

Figure 2.8: FEM versus BEM program

Comment: There are problems where the details of interest occur on the boundary, or localized to a particular part of the domain, and hence an entire domain solution is not required.

4. **FEM**: Differential equations are being approximated.

   BEM: Only boundary conditions are being approximated.

   Comment: The use of the Green-Gauss theorem and a fundamental solution in the formulation means that the BEM involves no approximation of the differential equation in the domain. Approximation is only performed on the boundary conditions.

5. **FEM**: Sparse symmetric matrix generated.

   BEM: Fully populated asymmetric matrix generated.

   Comment: The matrices are generally of different sizes due to the differences in size of the domain mesh compared to the surface mesh. There are problems where either method can give rise to smaller system and quickest solution. This depends partly on the volume to surface ratio. For problems involving infinite or semi-infinite domains, BEM to be favored.

6. **FEM**: Element integrals are easy to evaluate.

BEM: Integrals are more difficult to evaluate, and some contain integrands that become singular.

Comment: BEM integrals are far harder to evaluate. Also the integrals that contain singular integrands have a significant effect on the accuracy of the solution, so these integrals need to be evaluated accurately.

7. **FEM**: Relatively easy to implement.

   BEM: More difficult to implement.

   Comment: The need to evaluate integrals involving singular integrands makes the BEM at least an order of magnitude more difficult to implement than a corresponding finite element procedure.

It is now obvious that both methods have their own range of applications where they are most efficient. To summarize, the FEM is most suitable for problems [20]:

1. with a high ratio of boundary surface to volume;
2. where boundary stresses are not of primary importance;
3. where the material is nonhomogeneous, behaves nonlinearly and/or contain joints and cracks.

The BEM on the other hand, is most suitable for applications involving:

1. a low ratio of boundary surface to volume;

2. a high accuracy of boundary stresses;

3. homogeneous and linear elastic materials.

Typical applications with a high boundary surface to volume ratio are plate and shell structures. Extremely low surface to volume ratios, occur in geomechanics problems where the domain in most cases is assumed to be infinite or semi-infinite. Cases where boundary stresses are of primary importance occur mainly in fracture mechanics and many applications in mechanical engineering.

2.9 COUPLING THE BEM AND FEM METHODS

There are undoubtedly situations, which favor FEM over BEM and vice versa. Often one problem can give rise to a model favoring one method in one region and the other method in another region. In a detailed analysis of stresses around an underground opening, the FEM can be employed to analyze the problem of any shape with complex stress-strain response of the soil media. However, the extent of boundary distance to represent infinite domain and the necessity to discretize large domain introduce some approximation in the results. Furthermore, the preparation and checking of data are tedious and time consuming. The BEM on the other hand requires very small input data, and the elastic infinite domain commonly encountered in the underground openings can be fully represented. An efficient way of solving the problem is to utilize the advantages of both the BEM and FEM by coupling them. For example, in the vicinity of the opening (where the plastic behavior is anticipated), the

FEM can be used, and away from the opening (where the elastic behavior is expected), the BEM can be used.

Both the FEM and BEM are widely employed in fracture mechanics. However neither method is effective for all fracture mechanics problems. Fracture analysis is governed by linear elastic fracture mechanics (LEFM) and elasto-plastic fracture mechanics (EPFM). The former is ideally suited to analysis by the BEM, and there are numerous examples of the application of the BEM for LEFM [32,33]. Although, the BEM is superior to the FEM for LEFM, the BEM is less attractive for EPFM. Coupling of FEM and BEM may be most efficient for certain classes of applications. In EPFM problems, the plastic region around the crack can be modeled by the FEM while the remaining linear elastic region can be modeled by the BEM. In contrast, in the analysis of LEFM problems, it is useful to utilize the BEM at the fracture tip to accurately capture the singular behavior and then to apply the FEM for the rest of the structure where the material properties may be non-homogenous.

For such applications a combination of FEM and BEM seems to be the most efficient way of analysis. In a coupled analysis the user can have the best of both worlds, i.e. utilize the advantages and avoid the limitations of both methods. This may result in an efficient analysis of many engineering problems. Coupling the FEM and BEM is discussed in details in the following chapter.

CHAPTER 3

BACKGROUND ON FEM/BEM COUPLING APPROACHES

3.1 GENERAL

As discussed above, both the FEM and the BEM have their own advantages and disadvantages. It is desirable to develop a combined FEM/BEM technique, which makes use of their advantages and reduces or completely eliminates their disadvantages, and to use the combined technique in situations where it is appropriate. Due to their distinct mathematical formulations, the FEM and the BEM cannot be directly linked. The basic variables in the FEM are nodal displacements and forces, and in the BEM the variables are surface tractions and displacements. Zienkiewicz et al. [34] were the first authors who proposed the coupling of the two methods. Subsequent contribution came from Atluri and Grannell [35] and Brebbia and Georgion [36].

The conventional coupling methods employ an entire unified equation for the whole domain by altering the formulation of one of the methods to make it compatible with the other. The conventional coupling approaches can be classified into FEM hosted and BEM hosted. More recently, coupling the FEM and the BEM has been achieved

using iterative domain decomposition methods. This chapter presents a critical review of the available FEM/BEM coupling approaches.

3.2 FEM HOSTED APPROACH

There are many variations of the FEM hosted approach [34-47]. In general, the FEM hosted approach treats the BEM sub-domain as a large finite element. The displacement-traction equations governing the BEM sub-domain are transformed into FEM-like displacement-force stiffness equations. These stiffness equations are then assembled with those of FEM sub-domain according to the direct stiffness concept.

Considering Figure 3.1, where the domain is decomposed into two sub-domains Ω_B and Ω_F. The decomposed portions are modeled using the BEM and FEM. The corresponding boundary integral equation for the BEM sub-domain is given by:

$$[H]\{u\}=[G]\{t\} \quad \in \Gamma_B \tag{3.1}$$

For the FEM sub-domain, the assembled element equations are:

$$[K]\{u\}=\{f\} \in \Omega_F \tag{3.2}$$

Now, let us define the following vectors:

$\{u_B\}$: displacement in the BEM sub-domain,

$\{u_B^I\}$: displacement on the BEM/FEM interface (but it is approached from the BEM sub-domain),

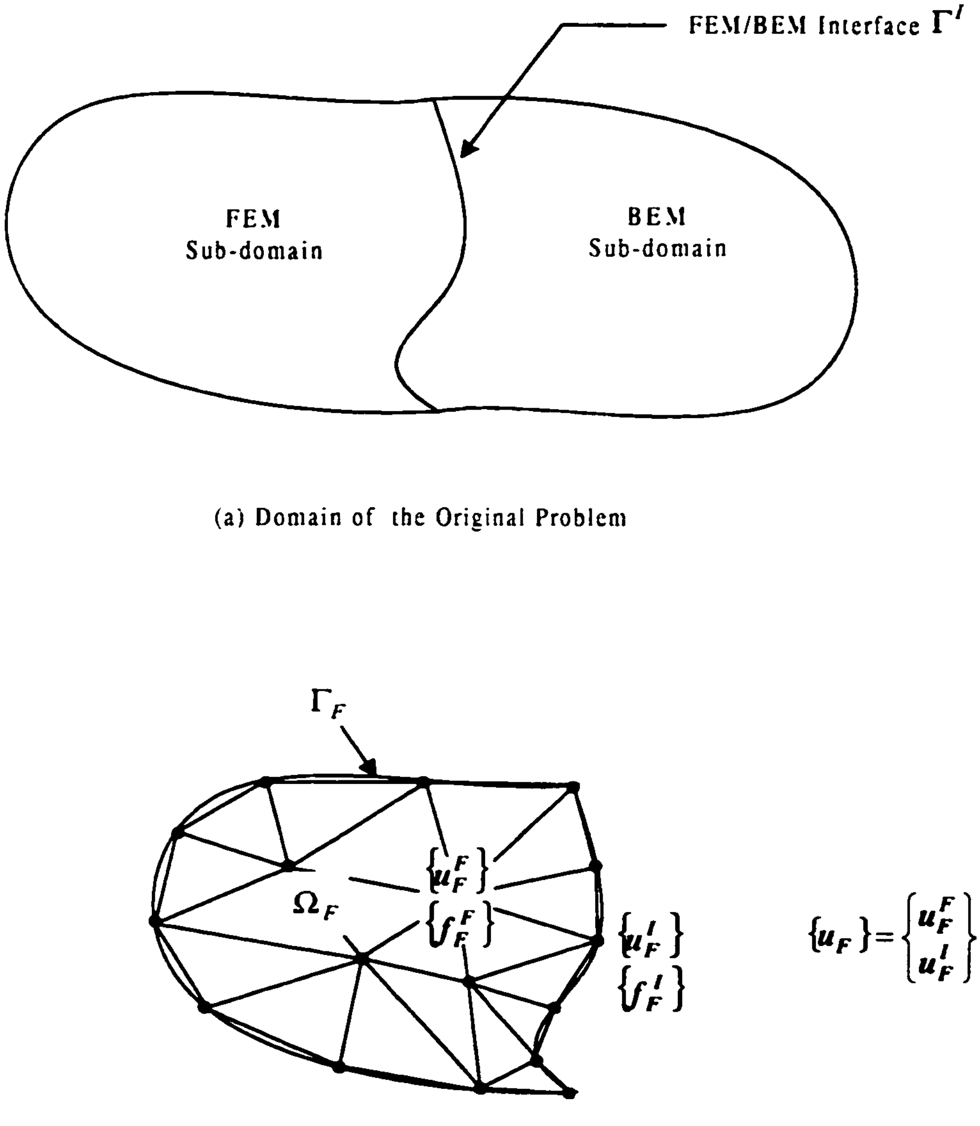

(a) Domain of the Original Problem

(b) FEM Modelling

Figure 3.1: Domain Decomposition

$$\{u_B\} = \begin{Bmatrix} u_B^B \\ u_B^I \end{Bmatrix}$$

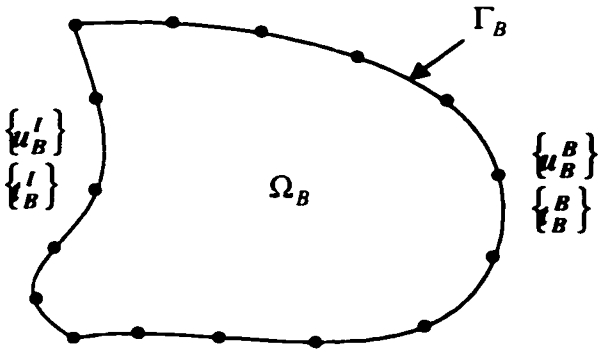

(c) BEM Modelling

Figure 3.1: Continued

$\{u_B^B\}$: displacement in the BEM sub-domain except $\{u_B^I\}$,

$$\{u_B\} = \{u_B^B, u_B^I\}^T$$

$\{u_F\}$: displacement in the FEM sub-domain,

$\{u_F^I\}$: displacement on the BEM/FEM interface (approached from the FEM sub-domain), and

$\{u_F^F\}$: displacement in the FEM sub-domain except $\{u_F^I\}$,

$$\{u_F\} = \{u_F^F, u_F^I\}^T$$

Similarly, one can define the traction and force vectors for the BEM and the FEM sub-domains, respectively.

In order to combine Equations (3.1) and (3.2), the first one can be reduced to a finite element form by inverting G as follows:

$$[G]^{-1}[H]\{u\} = \{t\} \tag{3.3}$$

Next, a relationship between the surface traction and the nodal forces should be established. This relationship can be written as:

$$\{f\} = [M]\{t\} \tag{3.4}$$

where, $[M]$ is the converting matrix due to the weighting of the boundary tractions by the interpolation function on the interface. Equation (3.3) may now be written in the form:

$$[M][G]^{-1}[H]\{u\}=[M]\{t\}=\{\bar{f}\} \tag{3.5}$$

where, the right hand side vector has the same form as that in the FEM. Equation (3.5) may be written as:

$$[\bar{K}]\{u\}=\{\bar{f}\} \tag{3.6}$$

where, $[\bar{K}]=[M][G]^{-1}[H]$ is a stiffness matrix obtained from the boundary element formulation. The equivalent finite element matrices of Equation (3.2) can now be assembled with the matrices corresponding to the sub-domain Ω_B to form a global stiffness matrix.

A major drawback of this approach is that the resulting assembled stiffness matrix is asymmetric and fully populated in contrast to the symmetric sparsely banded stiffness matrix of the FEM.

Zeinckiewicz et al. [34] and Brebbia and Georgion [36] forced a symmetrization on the BEM stiffness matrix on the basis of energy or error minimization considerations, respectively. Although the two symmeterized stiffness matrices are the same, no theoretical justification was made. This forced symmeterization has been followed by many researchers who reported some successful applications, e.g., Beer and Meek [37], Swoboda et al. [38] and Kohno et al. [39]. However, as pointed out by Li et al. [40], Mang et al. [41], and Tullberg and Bolteus [48], that this symmetrization results in a loss of equilibrium in a region near the interface. It was also found in [40,41] that

coupling the asymmetric BEM stiffness with the FEM leads, in general, to more accurate results. Of course, in such a case the resulting total matrix is asymmetric, and hence general matrix equation solvers have to be used which are less efficient than the symmetric equation solvers.

Instead of concentrating on the collocation BEM formulation, many symmetric BEM formulations have been developed that can directly be combined with the FEM. Most of these variational formulations are based on Galerkin or generalized principles of the type proposed by Reissner [49] and Washizu [50], in which the field and boundary variables are taken to be independent of each other, therefore leading to hybrid BEM schemes. One can also mention here the work of Schnack [51], Polizzoto and Zito [52], Sirtori et al. [53], Dummont [54], Felippa [55], Defigueiredo [56], and Brebbia and Defigueiredo [57]. However, attempts for obtaining symmetric BEM were either mechanically inconsistent, due to the inherent nature of the asymmetric BEM matrix, or computationally expensive.

3.3 BEM HOSTED APPROACH

In contrast to the first approach, the BEM hosted approach treats the FEM sub-domain as an equivalent BEM one by converting the stiffness equations of the finite element sub-domain to BEM-like equations. These equations are then coupled with those of the BEM sub-domain while satisfying the continuity and equilibrium along the interface.

Considering Figure 3.1, the governing Equations (3.1) can be decomposed and written in the following form:

$$[H_1 \quad H_2]\begin{Bmatrix} u_B^B \\ u_B^I \end{Bmatrix} = [G_1 \quad G_2]\begin{Bmatrix} t_B^B \\ t_B^I \end{Bmatrix} \tag{3.7}$$

The matrices for the finite element sub-domain can be written in a similar manner using the concept of the converting matrix defined in Equation (3.4),

$$[K_1 \quad K_2]\begin{Bmatrix} u_F^F \\ u_F^I \end{Bmatrix} = [M_1 \quad M_2]\begin{Bmatrix} t_F^F \\ t_F^I \end{Bmatrix} \tag{3.8}$$

At the interface, the compatibility and equilibrium conditions should be satisfied, i.e.,

$$\{u_B^I\} = \{u_F^I\} = \{u^I\} \quad \in \Gamma^I \tag{3.9}$$

$$\{t_B^I\} = -\{t_F^I\} = \{t^I\} \quad \in \Gamma^I \tag{3.10}$$

Using (3.9) and (3.10), Equations (3.7) and (3.8) can be rearranged and written together as:

$$\begin{bmatrix} H_1 & H_2 & -G_2 & 0 \\ 0 & K_2 & M_2 & K_1 \end{bmatrix}\begin{Bmatrix} u_B^B \\ u^I \\ t^I \\ u_F^F \end{Bmatrix} = \begin{bmatrix} G_1 & 0 \\ 0 & M_1 \end{bmatrix}\begin{Bmatrix} t_B^B \\ t_F^F \end{Bmatrix} \tag{3.11}$$

These equations will of course need to be rearranged in accordance with the boundary conditions.

This method of coupling involves no matrix inversion as the FEM hosted procedures. Unlike the first approach, the BEM hosted approach was employed in few investigations [58-60], because in the FEM there is a lot of efficient software available for pre- and post-processing and for solving the final large linear equation system. Furthermore, the BEM hosted approach destroys the positive characteristics of symmetry and bandedness that originally exist in the FEM.

3.4 ITERATIVE DOMAIN DECOMPOSITION METHODS

More recently, the coupling of BEM and FEM has been achieved through the iterative domain decomposition methods. In these coupling methods there is no need to combine the coefficient matrix for the FEM and the BEM sub-domains, as required in most of the conventional coupling methods. A second advantage is that different formulation for the FEM and BEM can be adopted as base programs for coupling the computer codes only. Separate computing for each sub-domain and successive renewal of the variables on the interface of both sub-domains are performed to reach the final convergence.

Gerstle et al. [61] presented a solution method, which was iterative in nature. Their idea was to iteratively apply displacement boundary conditions on the interface of the FEM and BEM sub-domains, calculate the resulting forces on the interface, and then to use the unbalanced force vector on the interface as a predictor for the applied displacements in the next iteration. However, their method was applicable only for symmetric BEM formulation with the disadvantages discussed earlier.

Perera et al. [62] presented a parallel method that was based on the interface equilibrium of Steklov Poincare. Their method may not be suited for certain classes of problems where the natural boundary conditions are specified for the entire external boundary of the FEM or BEM sub-domains. In such case the specification of Neumann boundary conditions over the whole boundary of any sub-domain, will result in non-unique solutions.

Kamiya et al. [63] employed the renewal methods known as Schwarz Neumann-Neumann and Schwarz Dirichlet-Neumann. Both methods, however, are not suited for problems where the natural boundary conditions are specified on the entire external boundary of the FEM sub-domain. Kamiya and Iwase [64] introduced an iterative analysis using conjugate gradient and condensation. However, the conjugate gradient method is only applicable to symmetric BEM formulation.

Lin et al. [65], and Feng and Owen [66] proposed a method which is considered as a sequential form of the Schwarz Dirichlet-Neumann method. The method was based on assigning an arbitrary displacement vector to the interface for the BEM sub-domain. Then, the energy equivalent nodal forces of the solved interface tractions were treated as boundary conditions for the FEM sub-domain to solve for the interfacial displacements. The solution was achieved when these two sets of displacements converge.

In the following sub-sections the formulation of the main iterative domain decomposition methods are critically reviewed.

3.4.1 Parallel Schwarz Neumann-Neumann Method

In Parallel Schwarz Neumann-Neumann method, the traction (Neumann data) is assumed in advance on the FEM/BEM interface [63]. The computations for FEM and BEM are performed in parallel. The iterative method can be described as follows:

1. Set initial values $\{t^I_{B,0}\}=\{\bar{t}\}$
2. Calculate $\{f^I_{F,0}\}=-[M]\{t^I_{B,0}\}$
3. Do for $n=0,1,2,\ldots$

Solve $$[H_1 \quad H_2]\begin{Bmatrix} u^B_B \\ u^I_{B,n} \end{Bmatrix}=[G_1 \quad G_2]\begin{Bmatrix} t^B_B \\ t^I_{B,n} \end{Bmatrix} \text{ for } \{u^I_{B,n}\}$$

$$[K_1 \quad K_2]\begin{Bmatrix} u^F_F \\ u^I_{F,n} \end{Bmatrix}=\begin{Bmatrix} f^F_F \\ f^I_{F,n} \end{Bmatrix} \text{ for } \{u^I_{F,n}\}$$

Apply $$\{t^I_{B,n+1}\}=\{t^I_{B,n}\}+\beta\left(\{u^I_{F,n}\}-\{u^I_{B,n}\}\right)$$

$$\{f^I_{F,n+1}\}=-[M]\{t^I_{B,n}\}$$

where, β is a relaxation parameter to speed up convergence

Until $$\frac{\left\| \{u^I_{B,n+1}\}-\{u^I_{B,n}\} \right\|}{\left\| \{u^I_{B,n+1}\} \right\|}<\varepsilon$$

where, ε is a given tolerance.

A drawback of this method is that it requires a parameter β, which may be empirically selected. Some trial and error and extensive experience are inevitable. Another major drawback is that the method may not be suited for certain classes of

problems where the natural boundary conditions are specified for the entire FEM or BEM sub-domains.

3.4.2 Parallel Schwarz Dirichlet-Neumann Method

In Parallel Schwarz Dirichlet-Neumann method [63], the assumed data on the interface of the BEM sub-domain is the displacement (Dirichlet data), while that of the FEM sub-domain is the traction (Neumann data). The computations for FEM and BEM are performed in parallel. The iterative method is described below:

1. Set the initial guess $\{u^I_{B,0}\} = \{\bar{u}\}$ and $\{f^I_{F,0}\} = \{\bar{f}\}$
2. Do for $n = 0, 1, 2, \ldots$

Solve $$[H_I \quad H_2]\begin{Bmatrix} u^B_B \\ u^I_{B,n} \end{Bmatrix} = [G_I \quad G_2]\begin{Bmatrix} t^B_B \\ t^I_{B,n} \end{Bmatrix} \text{ for } \{t^I_{B,n}\}$$

$$[K_I \quad K_2]\begin{Bmatrix} u^F_F \\ u^I_{F,n} \end{Bmatrix} = \begin{Bmatrix} f^F_F \\ f^I_{F,n} \end{Bmatrix} \text{ for } \{u^I_{F,n}\}$$

Apply $$\{u^I_{B,\,n+I}\} = (1-\gamma)\{u^I_{B,\,n}\} + \gamma\,\{u^I_{F,\,n}\}$$

$$\{f^I_{F,\,n+I}\} = -[M]\{t^I_{B,\,n}\}$$

where, γ is a relaxation parameter to speed up convergence

Until $$\frac{\left\| \{u^I_{B,n+I}\} - \{u^I_{B,n}\} \right\|}{\left\| \{u^I_{B,n+I}\} \right\|} < \varepsilon$$

where, ε is a given tolerance.

The parallel Dirichlet-Neumann method requires the selection of a parameter γ, which demands some trial and error, and extensive experience. Furthermore, the method may not be suited for problems where the natural boundary conditions are specified on the entire external boundary of the FEM sub-domain.

3.4.3 Sequential Schwarz Dirichlet-Neumann Method

The Sequential Schwarz Dirichlet-Neumann iterative method can be described as follows [65,66]:

1. Set the initial guess $\{u^I_{B,0}\} = \{\bar{u}\}$
2. Do for $n = 0, 1, 2, \ldots$

Solve $$[H_I \quad H_2]\begin{Bmatrix} u^B_B \\ u^I_{B,n} \end{Bmatrix} = [G_I \quad G_2]\begin{Bmatrix} t^B_B \\ t^I_{B,n} \end{Bmatrix} \text{ for } \{t^I_{B,n}\}$$

Solve $$[K_I \quad K_2]\begin{Bmatrix} u^F_F \\ u^I_{F,n} \end{Bmatrix} = \begin{Bmatrix} f^F_F \\ -Mt^I_{B,n} \end{Bmatrix} \text{ for } \{u^I_{F,n}\}$$

Apply $$\{u^I_{B,\,n+1}\} = (1-\alpha)\{u^I_{B,\,n}\} + \alpha\,\{u^I_{F,\,n}\}$$

where, α is a relaxation parameter to speed up convergence

Until $$\frac{\left\| \{u^I_{B,n+1}\} - \{u^I_{B,n}\} \right\|}{\left\| \{u^I_{B,n+1}\} \right\|} < \varepsilon$$

where, ε is a given tolerance

The method has the same limitation as that of the parallel Shwarz Dirichlet-Neumann method.

3.5 SUMMARY

This chapter presents a background on the existing FEM/BEM coupling methods. The conventional coupling methods employ an entire unified equation for the whole domain, by combining the discretized equations for the BEM and FEM sub-domains. Although the FEM hosted approach conceived more convenience than the BEM hosted approach, their shortcoming is that the algorithm for constructing the entire equation is highly complicated when compared with that for each single equation. In order to overcome the stated inconvenience, iterative domain decomposition methods were developed. In these methods, separate computing for the BEM and FEM sub-domains and successive renewal of the degrees of freedom on the interface of both sub-domains are performed to reach the final convergence. Different methods were critically reviewed. The iterative FEM/BEM coupling methods presented in Section 3.4 offers many advantages over the conventional coupling methods and appears to be promising. However, the important issue of convergence of the iterative methods is not fully addressed. Also the effect of several parameters such as the initial guess, material and geometrical properties of the sub-domains, and relaxation are not investigated. Moreover, the iterative domain decomposition coupling methods [61-66] are limited only to linear elastic or potential problems, and are not suited for cases where the natural boundary conditions are specified for the entire external boundary of the FEM sub-domain.

CHAPTER 4

CONVERGENCE OF THE SEQUENTIAL DIRICHLET-NEUMANN ITERATIVE COUPLING METHOD

4.1 GENERAL

Several methods for coupling the FEM and BEM were critically reviewed in Chapter 3. Although the iterative FEM/BEM coupling methods offer many advantages over the conventional coupling methods and seem to be promising, the important issue of convergence is still not fully addressed. The objective of this chapter is to establish the convergence conditions for the Sequential Dirichlet-Neumann iterative coupling method presented by Lin et al. [65], and Feng and Owen [66]. Several factors involved in the convergence of the method are discussed. Benchmark examples are presented for validation.

4.2 CONVERGENCE OF THE ITERATIVE METHOD

In this section, the convergence of the Sequential Dirichlet-Neumann iterative coupling method is investigated. The findings will be confirmed by numerical examples in Section 4.3.

For the sake of convergence discussion, the BEM and the FEM equations can be rewritten in more detailed sub-structured forms:

$$\begin{bmatrix} H_{11} & H_{12} \\ H_{21} & H_{22} \end{bmatrix} \begin{Bmatrix} u_B^B \\ u_B^I \end{Bmatrix} = \begin{bmatrix} G_{11} & G_{12} \\ G_{21} & G_{22} \end{bmatrix} \begin{Bmatrix} t_B^B \\ t_B^I \end{Bmatrix} \tag{4.1}$$

and

$$\begin{bmatrix} K_{11} & K_{12} \\ K_{21} & K_{22} \end{bmatrix} \begin{Bmatrix} u_F^F \\ u_F^I \end{Bmatrix} = \begin{Bmatrix} f_F^F \\ f_F^I \end{Bmatrix} \tag{4.2}$$

At the interface, the compatibility and equilibrium conditions are:

$$\{u_B^I\} = \{u_F^I\} \quad \in \Gamma^I \tag{4.3}$$

$$\{f_F^I\} + [M]\{t_B^I\} = 0 \quad \in \Gamma^I \tag{4.4}$$

The FEM/BEM iterations are written as:

$$\{u_{B,\,n+1}^I\} = (1-\alpha)\{u_{B,\,n}^I\} + \alpha\{u_{F,\,n}^I\} \tag{4.5}$$

After applying the boundary conditions and rearranging, Equation (4.1), can be written in the following form:

$$\begin{Bmatrix} X_B^B \\ t_B^I \end{Bmatrix} = \begin{bmatrix} A_{11} & A_{12} \\ A_{21} & A_{22} \end{bmatrix} \begin{Bmatrix} C_B \\ u_B^I \end{Bmatrix} \tag{4.6}$$

where, X_B^B is a vector which contains all unknowns in the BEM sub-domain except the interfacial displacements u_B^I and traction t_B^I. C_B is a vector which contains all BEM known quantities. Similarly, after applying the boundary conditions and rearranging, Equation (4.2) can be written as:

$$\begin{Bmatrix} u_F^F \\ u_F^I \end{Bmatrix} = \begin{bmatrix} F_{11} & F_{12} \\ F_{21} & F_{22} \end{bmatrix} \begin{Bmatrix} C_F \\ f_F^I \end{Bmatrix} \tag{4.7}$$

where, C_F is a vector of known FEM values. Using Equation (4.4) in the second of Equations (4.7) gives:

$$u_F^I = F_{21} C_F - F_{22} M t_B^I \tag{4.8}$$

Using the second of Equations (4.6) in (4.8) gives:

$$u_F^I = C\, u_B^I + E \tag{4.9-a}$$

where

$$C = -F_{22} M A_{22} \tag{4.9-b}$$

and

$$E = F_{21} C_F - F_{22} M A_{21} C_B \tag{4.9-c}$$

Substituting for $u_{F,n}^I$ in Equation (4.5) using Equation (4.9-a) gives:

$$\boldsymbol{u}_{B,n+1}^{I} = \left[(1-\alpha)\boldsymbol{I} + \alpha\,\boldsymbol{C}\right]\boldsymbol{u}_{B,n}^{I} + \alpha\,\boldsymbol{E} \tag{4.10}$$

where, $\boldsymbol{I}$ is the unit matrix. Now, Equation (4.10) is an iterative method of the form:

$$\boldsymbol{X}_{n+1} = \boldsymbol{D}_{\alpha}\boldsymbol{X}_{n} + \boldsymbol{d}_{\alpha} \tag{4.11}$$

which converges if and only if the set of eigenvalues $\sigma(\boldsymbol{D}_{\alpha})$ of the matrix $\boldsymbol{D}_{\alpha}$ is contained in the unit ball $B(0,1)$ in the complex plane [67]. Equation (4.10) converges if and only if:

$$\sigma\left((1-\alpha)\boldsymbol{I} + \alpha\,\boldsymbol{C}\right) \subseteq B(0,1) \tag{4.12}$$

or

$$\sigma\left(\alpha\,\boldsymbol{C}\right) \subseteq B(\alpha-1,1) \tag{4.13}$$

or

$$\sigma\left(\boldsymbol{C}\right) \subseteq B\left(1-\frac{1}{\alpha},\frac{1}{\alpha}\right) \tag{4.14}$$

The ball is centered at $Z = 1-\frac{1}{\alpha}$, with the radius $\frac{1}{\alpha}$. Next, it can be shown that, if $\lambda = x + iy \in \sigma(\boldsymbol{C})$ with $x < 1$, then $\lambda \in B\left(1-\frac{1}{\alpha},\frac{1}{\alpha}\right)$ for some α. For this the following inequality has to be satisfied:

$$\left|\lambda - (1 - \frac{1}{\alpha})\right| < \frac{1}{\alpha} \tag{4.15}$$

or

$$\left[x - (1 - \frac{1}{\alpha})\right]^2 + y^2 < \frac{1}{\alpha^2} \tag{4.16}$$

which, upon simplification, gives:

$$(1 - x)^2 + y^2 < \frac{2(1 - x)}{\alpha} \tag{4.17}$$

Note that inequality (4.17) immediately implies the necessary condition $x < 1$. Inequality (4.17) can be rewritten as:

$$\alpha < \frac{2(1 - x)}{(1 - x)^2 + y^2} \tag{4.18}$$

The foregoing discussion shows that if $\boldsymbol{\lambda}_1 = \boldsymbol{x}_1 + i\boldsymbol{y}_1, \ldots, \boldsymbol{\lambda}_N = \boldsymbol{x}_N + i\boldsymbol{y}_N$ are the eigenvalues of $\boldsymbol{C}$, then,

$$\alpha < \min_{1 \le i \le N} \left\{ \frac{2(1 - \boldsymbol{x}_i)}{(1 - \boldsymbol{x}_i)^2 + \boldsymbol{y}_i^{\,2}} \right\}$$

$$\text{and } \boldsymbol{x}_i < 1, \quad i = 1, 2, \ldots, N \tag{4.19}$$

are the necessary conditions for the convergence of the Sequential Dirichlet-Neumann iterative coupling method.

For a proper choice of α, the specteral radius of the iteration matrix $((1-\alpha)\boldsymbol{I}+\alpha\,\boldsymbol{C})$, which may be denoted by $\rho((1-\alpha)\boldsymbol{I}+\alpha\,\boldsymbol{C})$, may be minimized.

Let

$$\boldsymbol{\lambda}' = (\lambda_1 \quad \lambda_2 \dots \lambda_n) \tag{4.20-a}$$

and

$$\boldsymbol{I}' = (1 \quad 1 \dots 1) \tag{4.20-b}$$

then

$$\rho((1-\alpha)\boldsymbol{I}+\alpha\,\boldsymbol{C}) = \max_{1\le i\le N}\{\,|\,(1-\alpha)+\alpha\,\lambda_i\,|\,\} = \|\,(1-\alpha)\,\boldsymbol{I}+\alpha\,\boldsymbol{\lambda}\,\|_\infty . \tag{4.20-c}$$

where, $\|\,(1-\alpha)\,\boldsymbol{I}+\alpha\,\boldsymbol{\lambda}\,\|_\infty$ is the infinity norm of the iteration matrix. The problem now is to choose α such that $\|\,(1-\alpha)\,\boldsymbol{I}+\alpha\,\boldsymbol{\lambda}\,\|_\infty$ is minimized. Due to the fact that $\|\cdot\|_\infty$ is not differentiable, an explicit value for the optimum α is not readily obtainable.

However, noting that $\frac{1}{\sqrt{N}}\|x\|_2 \le \|x\|_\infty \le \|x\|_2$, one can try to obtain a value of the relaxation parameter ($\bar{\alpha}$) that minimizes the Euclidean norm. If for such $\bar{\alpha}$, it turns out that $\|\,(1-\bar{\alpha})\,\boldsymbol{I}+\bar{\alpha}\;\;\boldsymbol{\lambda}\,\|_2 < 1$, then so will be the infinity norm and consequently the spectral radius of the iteration matrix. Proceeding with this idea let

$$F(\alpha) = \| (1-\alpha)\, \boldsymbol{1} + \alpha\, \boldsymbol{\lambda} \|_2^{\,2} \tag{4.21-a}$$

then

$$F'(\alpha) = 2\,\mathrm{Re}(\boldsymbol{1}^T (\boldsymbol{\lambda} - \boldsymbol{1})) + 2\alpha \| \boldsymbol{\lambda} - \boldsymbol{1} \|^2 \tag{4.21-b}$$

and

$$F''(\alpha) = 2\,\|\boldsymbol{\lambda} - \boldsymbol{1}\|^2 > 0 \tag{4.21-c}$$

The initial values (4.21-a) correspond to the minimum α. Now setting $F'(\alpha) = 0$, the following equations are obtained:

$$\overline{\alpha} = -\frac{\mathrm{Re}(\boldsymbol{1}^t (\boldsymbol{\lambda} - \boldsymbol{1}))}{\|\boldsymbol{\lambda} - \boldsymbol{1}\|^2} \tag{4.22}$$

and

$$F_{\min} = N - \frac{\left|\mathrm{Re}(\boldsymbol{1}^t (\boldsymbol{\lambda} - \boldsymbol{1}))\right|^2}{\|\boldsymbol{\lambda} - \boldsymbol{1}\|^2} \tag{4.23}$$

Then a sufficient condition for convergence in this case is $F_{\min} < 1$. Moreover, this condition implies that $\overline{\alpha}$ necessarily satisfies Equation (4.19).

The two conditions for convergence depicted by Equations (4.19) give rise to a set of factors that control convergence. The most important one is the selection of the

parameter α, which greatly affects the convergence of the Sequential Dirichlet-Neumann iterative coupling method. Beyond the values given by Equation (4.19), the method does not converge. Also from the discussion given in this section, it can be concluded that convergence is dependent on the eigenvalues of the matrix $\boldsymbol{C}$, which in turn are dependent on $\boldsymbol{K}$, $\boldsymbol{H}$, $\boldsymbol{G}$ and $\boldsymbol{M}$ matrices. This indicates that convergence is dependent on the mesh density on the interface, specified type of the boundary conditions for the given sub-domains, and the geometrical and material properties of the sub-domains. It is interesting to note that the initial guess is not involved in the conditions for convergence.

4.3 BENCHMARK EXAMPLES

The conditions for convergence were established theoretically in the previous section. Also, the factors that affect convergence of the method were clarified. Two benchmark examples are given for validation. These examples also serve to clarify some issues related to the convergence of the Sequential Dirichlet-Neumann iterative coupling method.

4.3.1 Potential Flow Problem

The first benchmark example (Figure 4.1) is a potential flow in a rectangular domain governed by Laplace equation, i.e., $k_i \nabla^2 u = 0$ in Ω_i, where k_i is the material property in the sub-domain Ω_i and u is the potential. The decomposed portions are modeled using the BEM and FEM. The domain is decomposed to the FEM and BEM

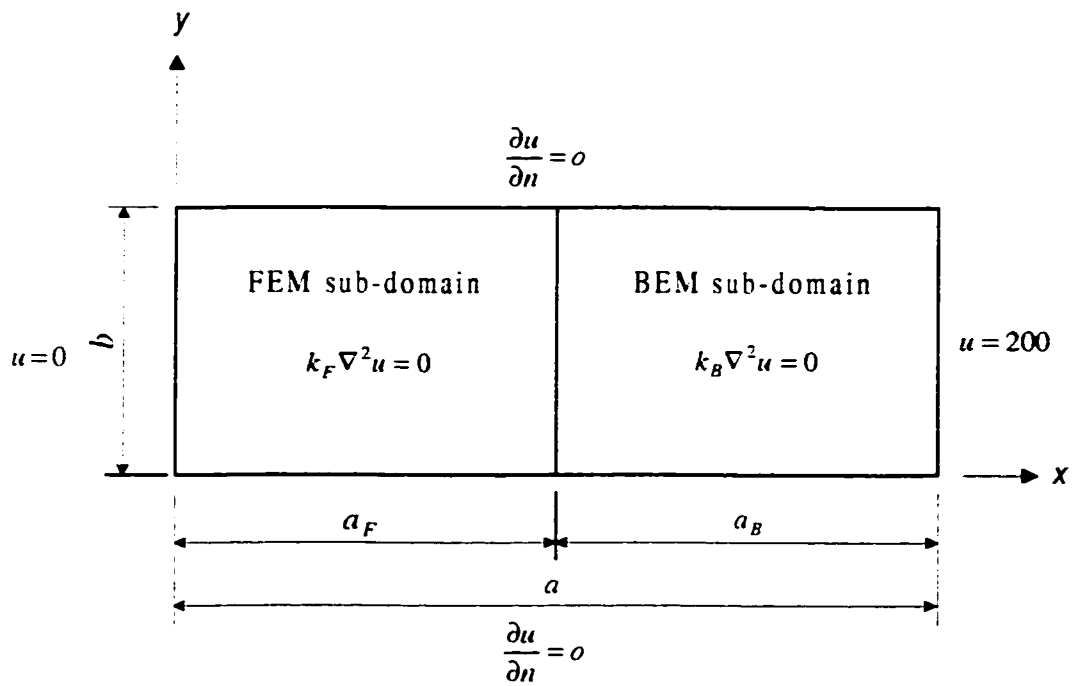

Figure 4.1: Potential Flow Problem

sub-domains with $0 \leq x \leq a$ and $0 \leq y \leq b$. The boundary conditions are selected as $u(0, y) = 0$, $u(a, y) = 200$, and zero flux ($k_i \nabla u$) elsewhere. The effect of the relative material properties (k_B/k_F), relative size of the computational sub-domains (a_B/a_F), and initial guess is investigated. For $a_B/a_F = 1$, the domain is modeled using 18 linear boundary elements and 40 linear triangular elements (Figure 4.2). Due to the simplicity of the problem, the results agree very well with the exact solution and therefore, they are not given here.

The effect of k_B/k_F on the convergence of the solution is shown in Figure 4.3, which clearly indicate that both the optimum value and the applicable range of α vary with k_B/k_F. The Figure also shows the crucial role of α in achieving the convergence. As an example, for $k_B/k_F = 8$, α should be within the range of 0.02 to 0.20, in order to assure convergence. Beyond the value of 0.20, the iterative method does not converge.

Similarly, Figure 4.4 gives the applicable range of α for different relative sizes of the computational sub-domains (a_B/a_F) with $k_B/k_F = 1$. For example, Figure 4.4 indicates that for $a_B/a_F = 0.2$, the convergence can not be achieved when $\alpha > 0.32$.

The optimum value and applicable range of α for different combinations of a_B/a_F and k_B/k_F are given in Table 4.1. It is interesting to observe that for combinations of very high values of k_B/k_F and low values of a_B/a_F, applicable range of α

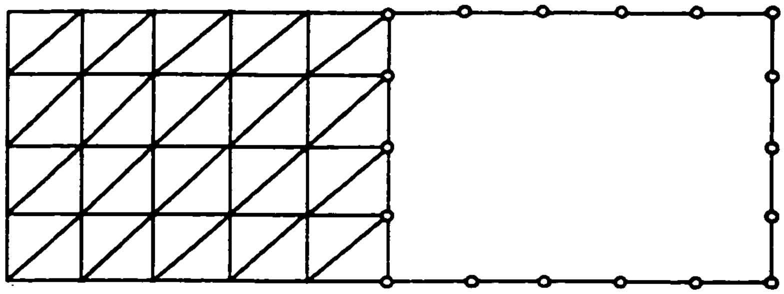

Figure 4.2: Discretization for the Potential Flow Problem

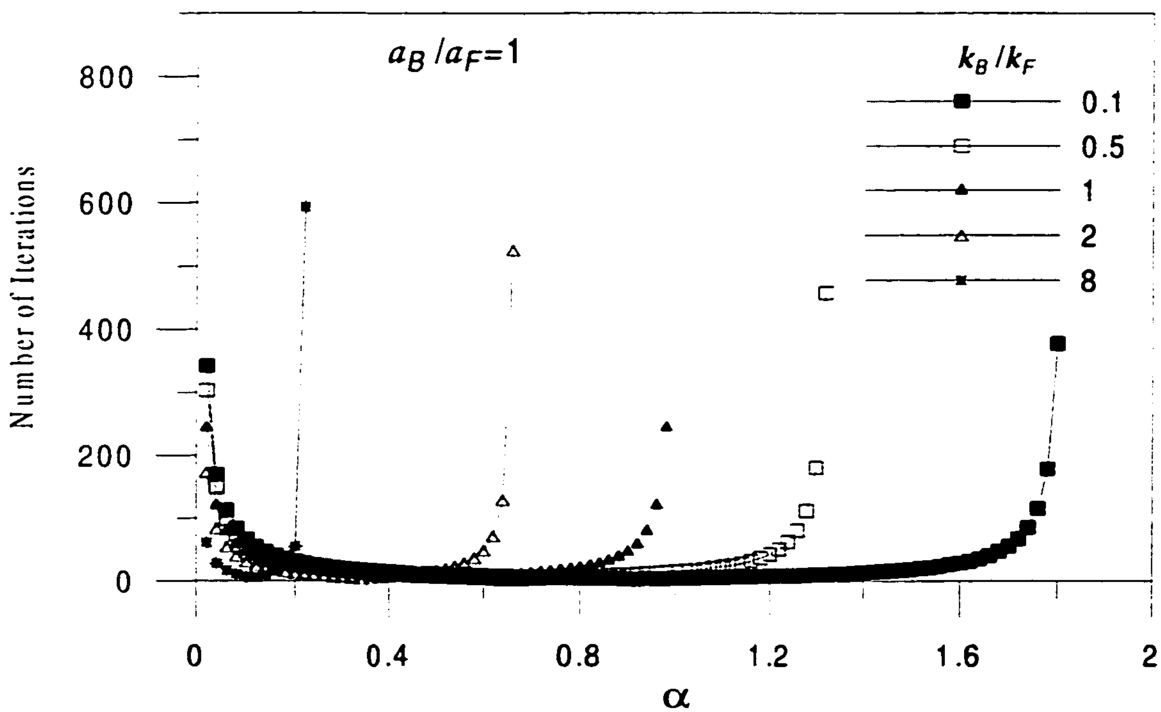

Figure 4.3: Required Iterations vs. α for Different Values of k_B/k_F

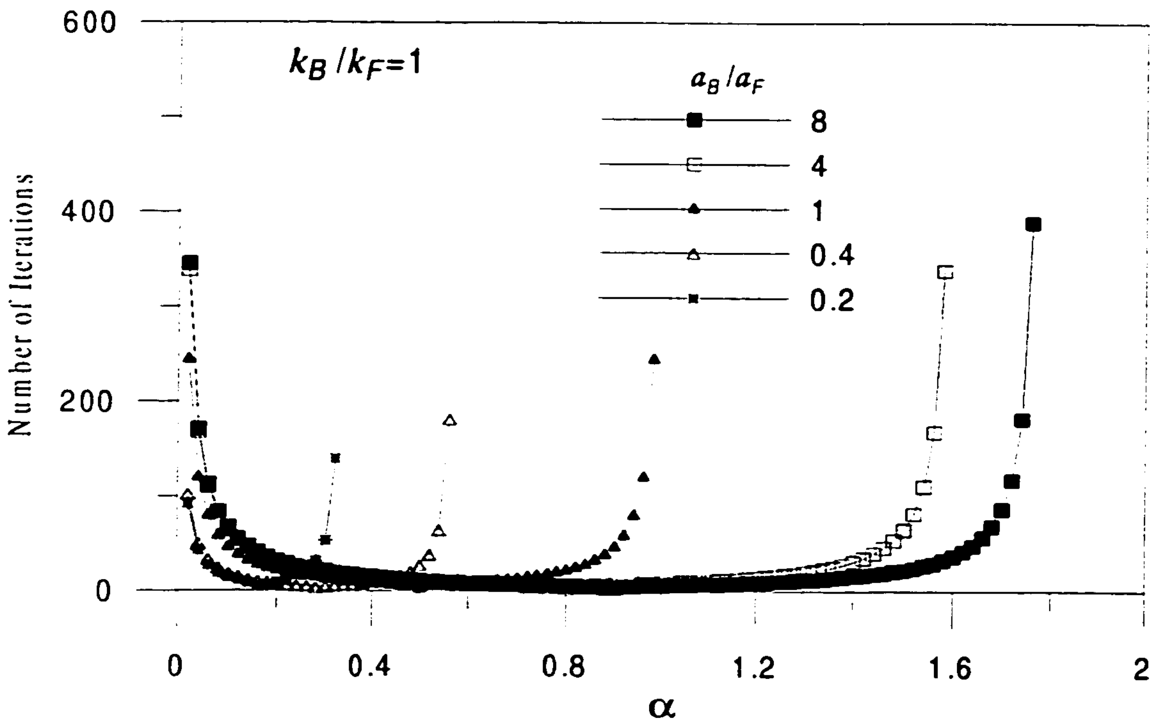

Figure 4.4: Required Iterations vs. α for Different Values of a_B/a_F

Table 4.1: Applicable Range and optimum values of α for Different Values of a_B/a_F and k_B/k_F

a_B/a_F		k_B/k_F 0.1	0.50	1.0	2.0	8.0
0.2	Range	0.02-1.32	0.02-0.56	0.02-0.32	0.02-0.18	0.02-0.04
	Optimum	0.68	0.28	0.16	0.1	0.02
0.4	range	0.02-1.58	0.02-0.88	0.02-0.56	0.02-0.32	0.02-0.08
	Optimum	0.8	0.44	0.28	0.16	0.04
1.0	range	0.02-1.8	0.02-1.32	0.02-0.98	0.02-0.64	0.02-0.20
	Optimum	0.9	0.66	0.5	0.34	0.12
4.0	range	0.02-1.94	0.02-1.76	0.02-1.58	0.02-1.32	0.02-0.66
	Optimum	0.96	0.88	0.8	0.66	0.34
8.0	range	0.02-1.96	0.02-1.88	0.02-1.76	0.02-1.58	0.02-0.98
	Optimum	0.98	0.94	0.9	0.8	0.50

reduces to a very narrow range. The limit and optimum values given by Table 4.1 are found to be in good agreement with those determined using Equations (4.19) and (4.22).

In order to investigate the effect of the initial guess of the potential u^I on the interface, the same problem is reinvestigated with $a_B/a_F = 0.4$ and $k_B/k_F = 1$, and different values of u^I. The results (Figure 4.5) show that, the arbitrary assigned u^I values have an insignificant effect on the speed of convergence. The applicable range of α, remains between 0.02 to 0.56 for this problem. It is reasonable to start with values of zeros on the interface for the initial potentials, which seems convenient as well as, appropriate from the physical realization.

4.3.2 Steel Cantilever Beam Subjected to Uniform Tension

The steel cantilever beam shown in Figure 4.6 is analyzed, and the results are compared with those from elasticity theory. The cantilever beam is subjected to a uniform tensile loading of $20\text{x}10^3$ units at its free end, and is considered to be in a state of plane stress with an elastic modulus, $E = 29\text{x}10^6$ units, and a Poison's ratio $\nu = 0.3$. The beam is 20 units long and 10 units high, and is assumed to be weightless. The results obtained from the coupled BEM/FEM approach, using different meshes as shown in Figure 4.7, match very well with the analytical solutions.

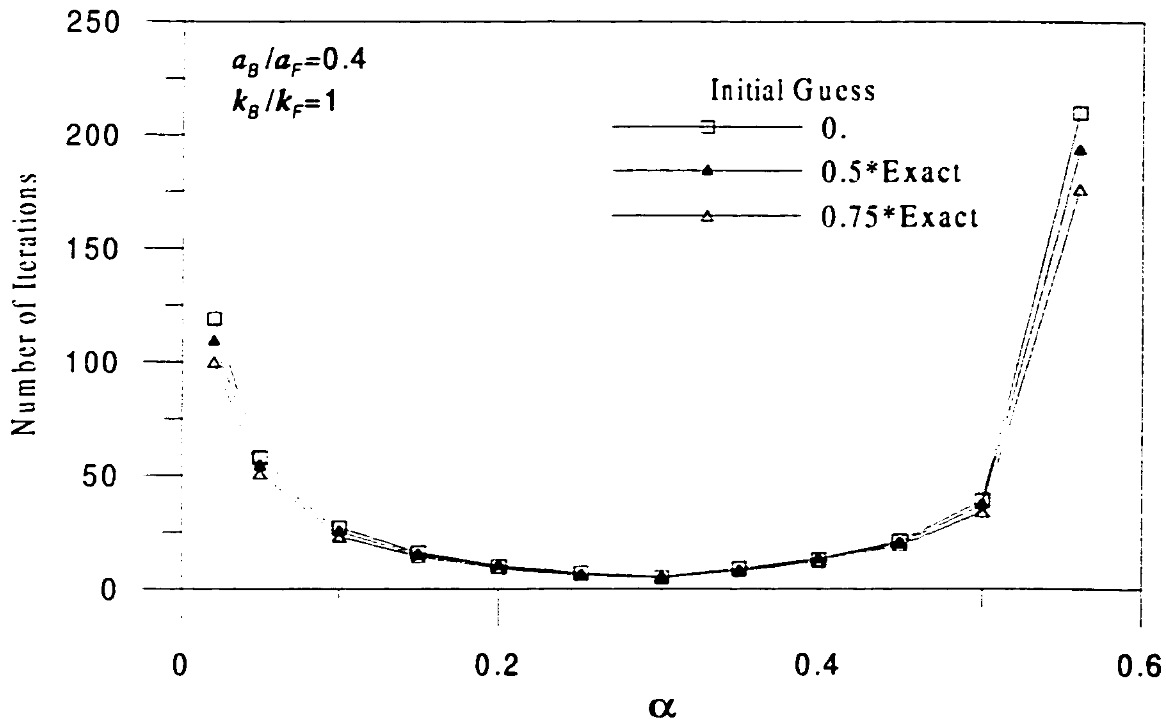

Figure 4.5: Effect of Initial Guess on the Convergence of the Solution

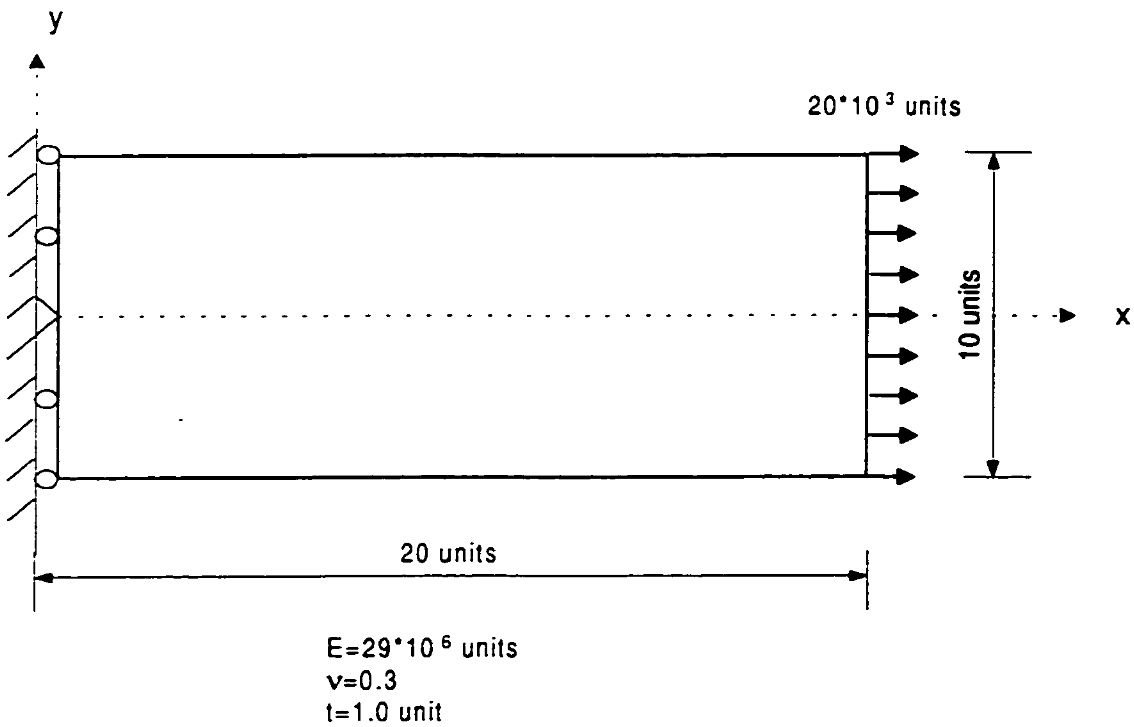

Figure 4.6: Cantilever Beam Subjected to Uniform Loading

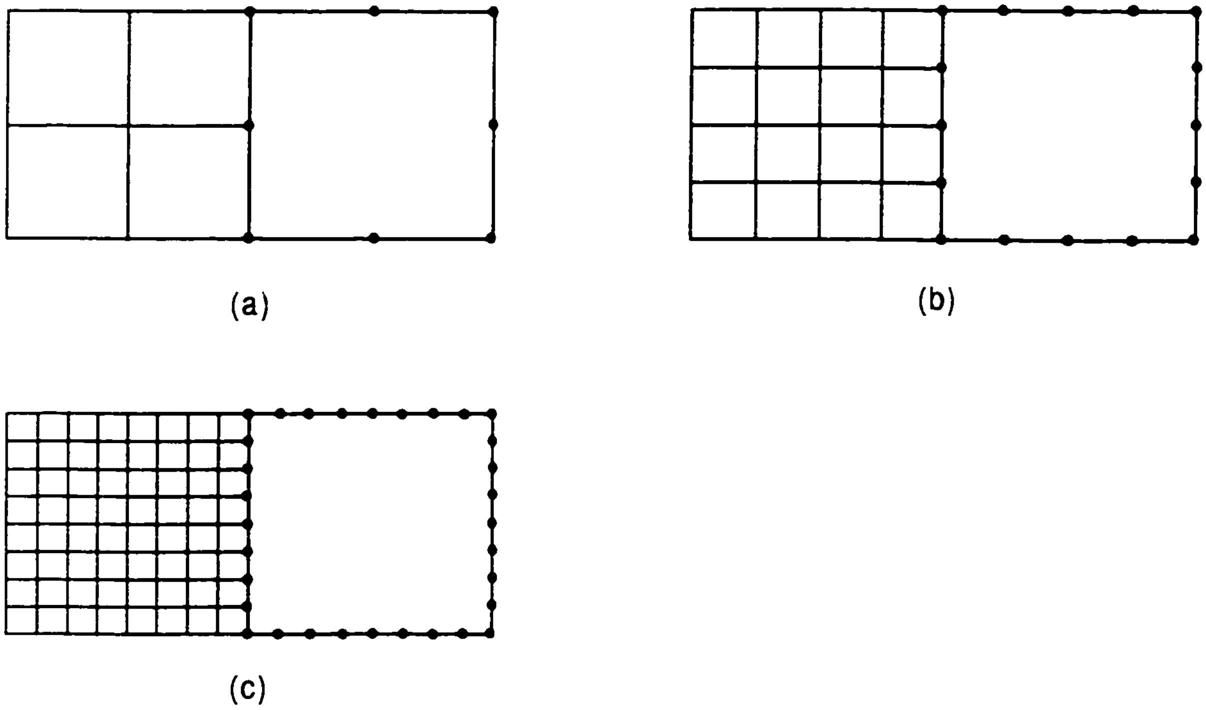

Figure 4.7: BEM/FEM Discretization (a) 3 Nodes at Interface (b) 5 Nodes at Interface (c) 9 Nodes at Interface

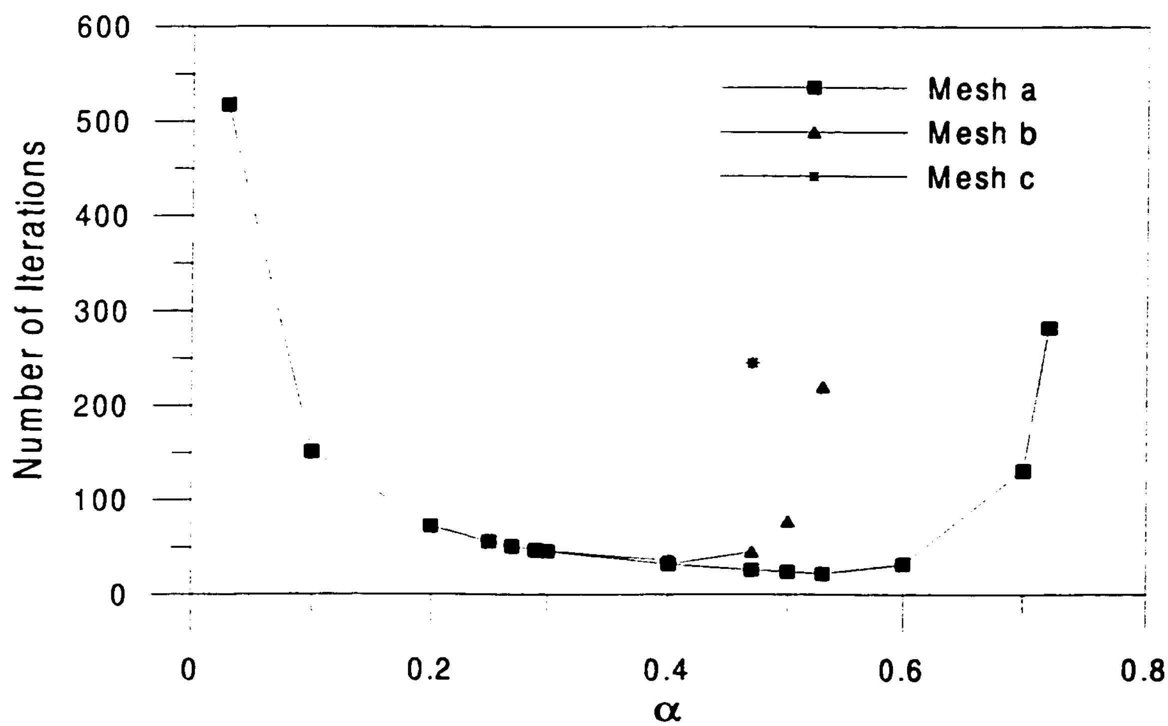

Figure 4.8: Effect of the Number of Nodes on the BEM/FEM Interface on α

Figure 4.8 illustrates the effect of the mesh size on the convergence of solution. It is observed that the applicable range of α to assure solution convergence, varies with the number of the interfacial nodes. For mesh (a), α should be within the range of 0.03 to 0.72, whilst the range for mesh (c) is 0.03 to 0.47. Beyond these values the method does not converge. The range from which the relaxation parameter to be chosen becomes narrower with the increase in the number of nodes on the interface. Moreover, it is observed that different optimal values of α exist for different FEM and BEM meshes.

In order to address the effect of the geometry of the computational sub-domains on solution convergence, the problem is investigated for different relative areas of the finite and boundary element sub-domains, as shown in Figure 4.9. From Figure 4.10, it is observed that the minimum applicable range of α is for problems having equal finite and boundary element areas ($a_B/a_F = 1$). As a_B/a_F increases or decreases, the applicable range of α increases.

Using mesh (b) of Figure 4.7, the problem is investigated for different relative values of modulus of elasticity for the BEM and FEM sub-domains (E_B / E_F). Figure 4.11 indicates that as E_B / E_F decreases the applicable range of α increases. This range reduces to a very narrow one for higher values of E_B / E_F.

Using the equivalent two different types of boundary conditions as shown in Figure 4.12, mesh (b) of Figure 4.7 is also analyzed. As can be seen from Figure 4.13,

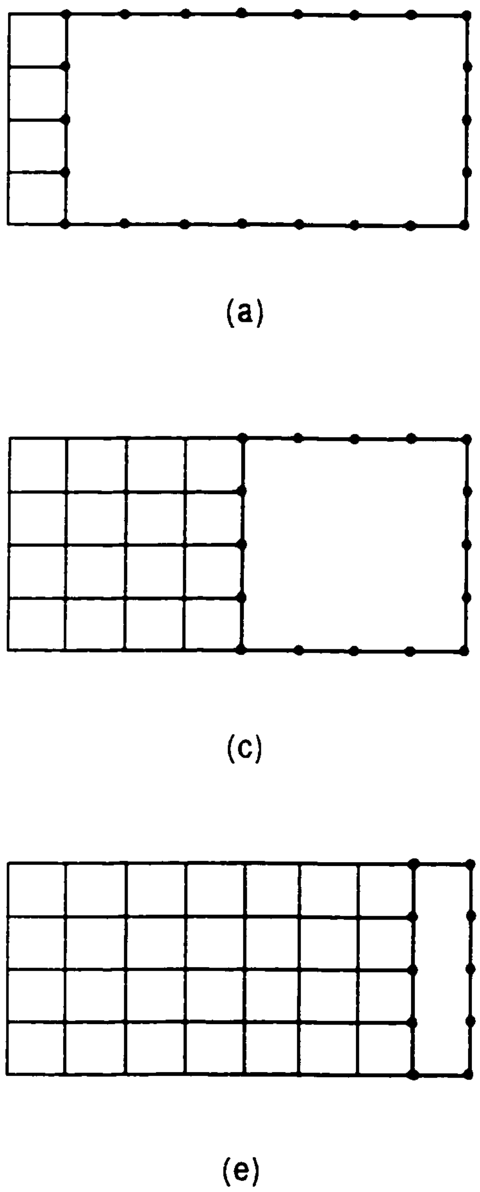

Figure 4.9: Relative BEM to FEM Computational Sub-Domains

(a) $\frac{a_B}{a_F} = 7$ (b) $\frac{a_B}{a_F} = 3$ (c) $\frac{a_B}{a_F} = 1$ (d) $\frac{a_B}{a_F} = \frac{1}{3}$ (e) $\frac{a_B}{a_F} = \frac{1}{7}$

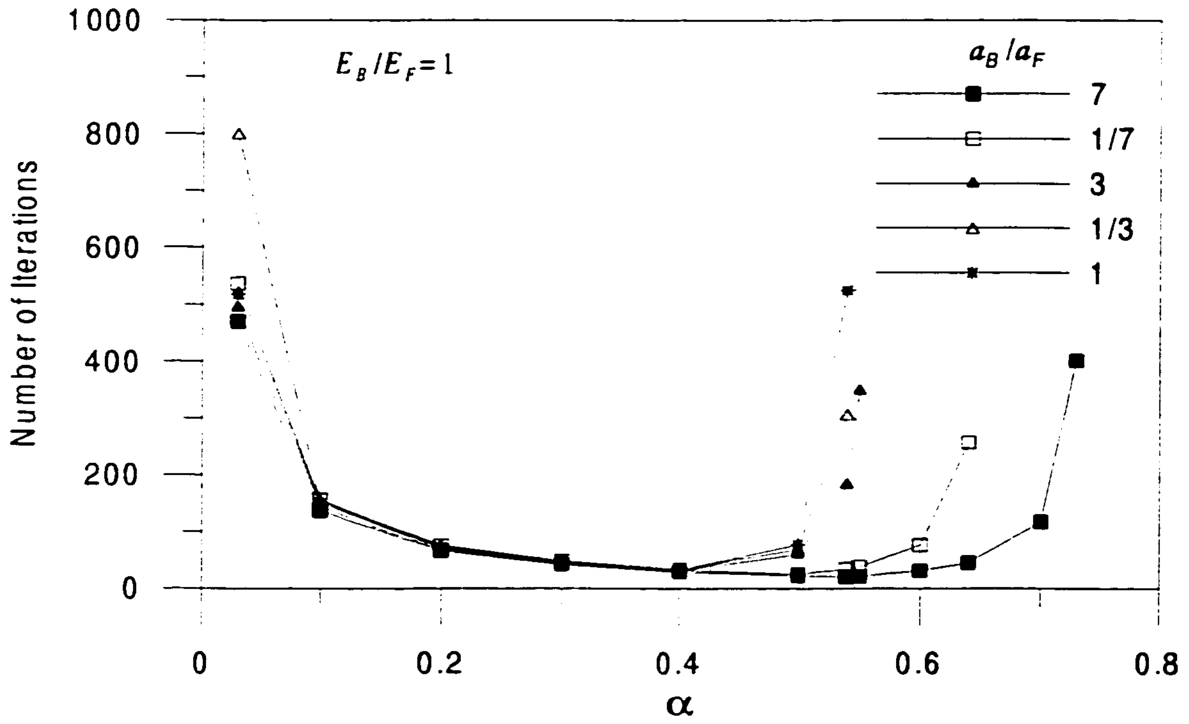

Figure 4.10: Effect of the Geometry of the Computational Sub-Domains on α

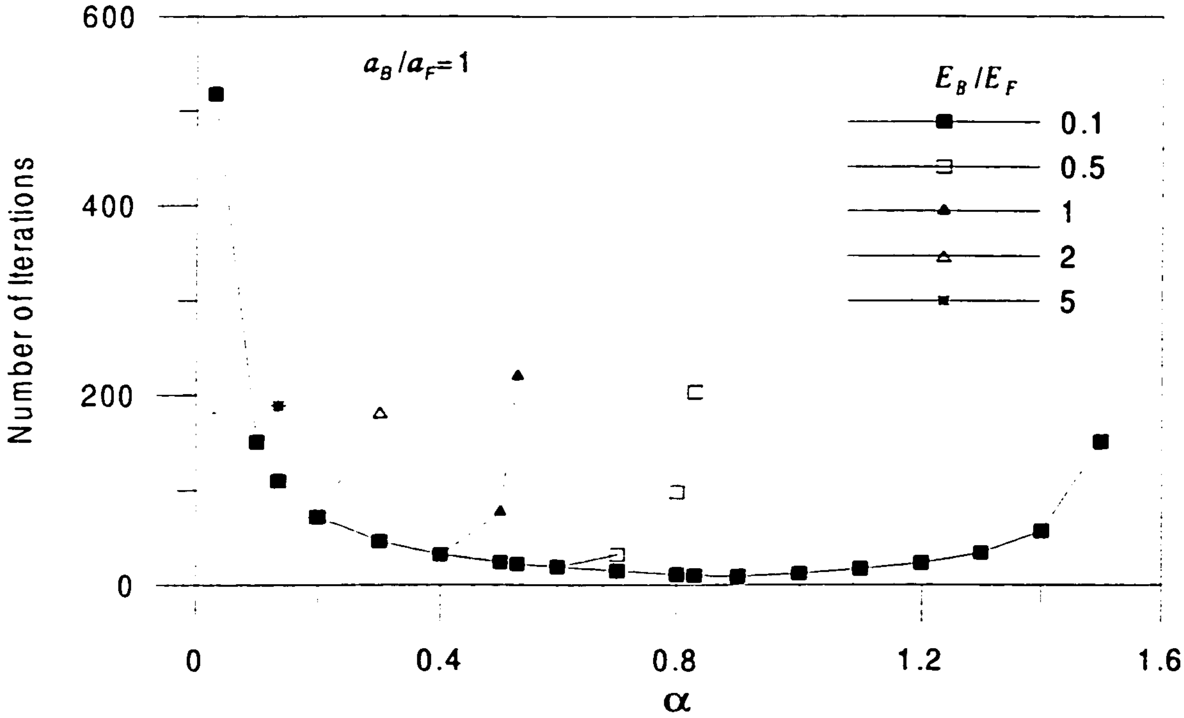

Figure 4.11: Effect of Material Properties of the Sub-Domains on α

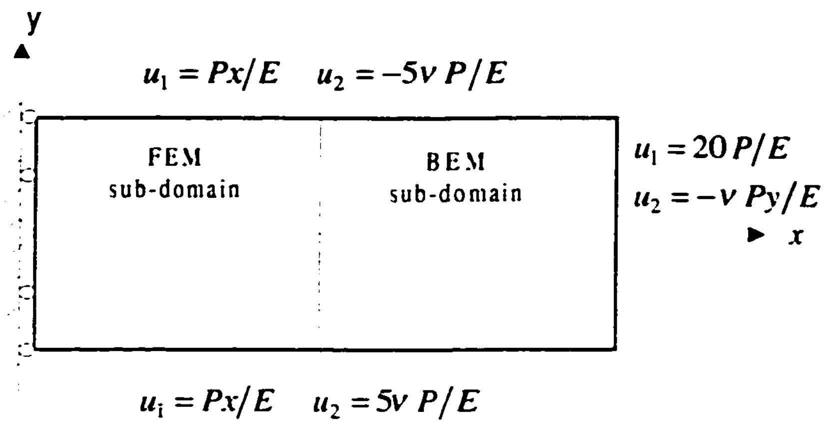

Dirichlet BC

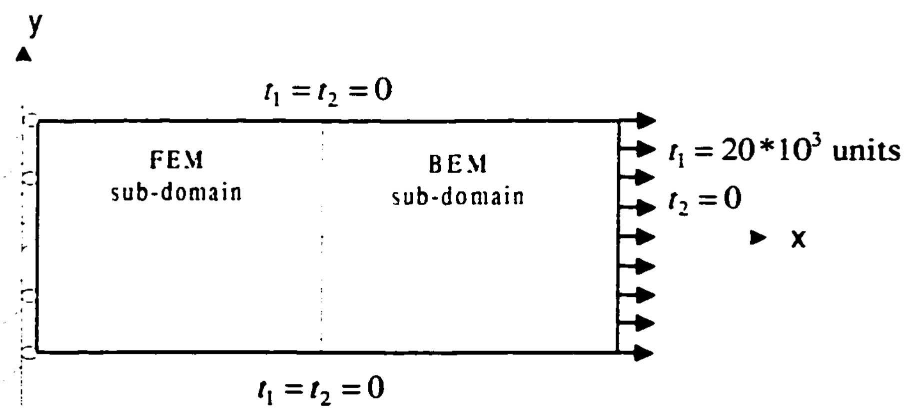

Neumann BC

Figure 4.12: Boundary Conditions

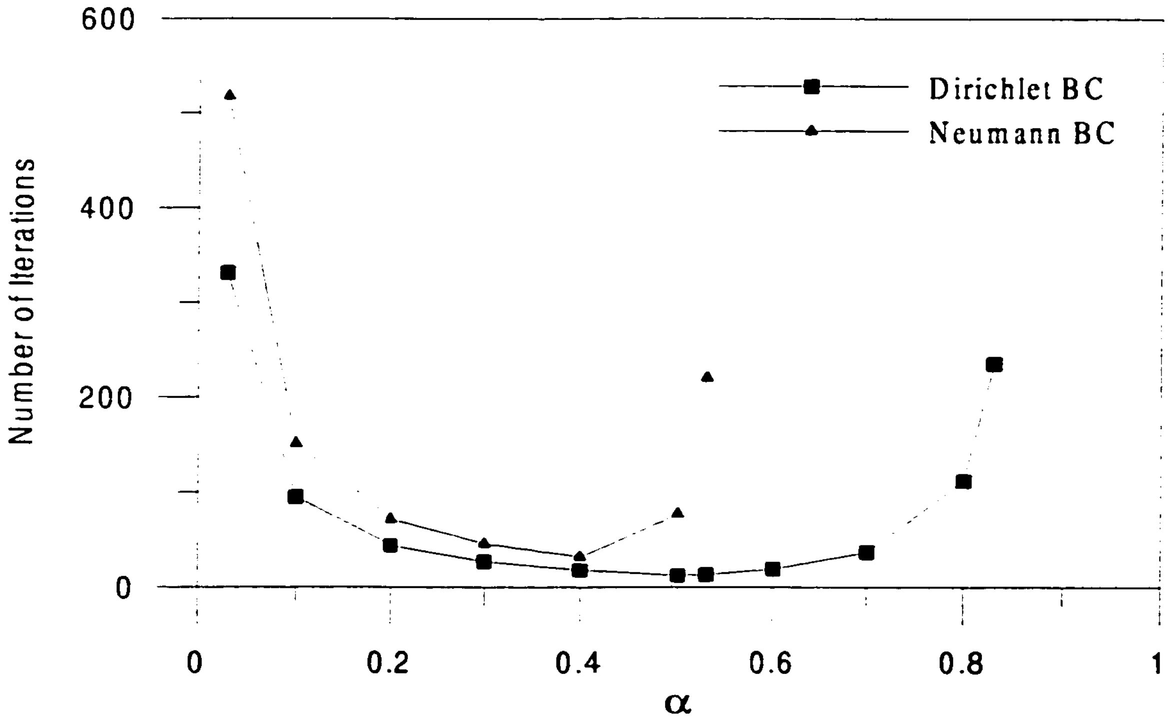

Figure 4.13: Effect of Boundary Conditions on α

different types of boundary conditions results in different optimum values and applicable ranges of the parameter α.

In order to investigate the effect of the initial guess of the degrees of freedom on the interface, the same problem is reinvestigated using mesh (b) in Figure 4.7, and different values of u^I. Again, the results in Figure 4.14 show that, the arbitrary assigned initial values of u^I have an insignificant effect on the speed of convergence. The allowable range remains between 0.03 to 0.53 for this problem. It is reasonable to start with values of zeros on the interface for the initial displacements, which seems convenient as well as appropriate from the physical realization.

Again, the numerical results obtained for this problem match with those of Equations (4.19) and (4.22).

4.4 SELECTION OF THE RELAXATION PARAMETER

The theoretical analysis and benchmark examples presented in Sections 4.2 and 4.3, respectively, clearly identify the factors that control the convergence of the Sequential Dirichlet-Neumann iterative coupling method. These factors include the geometrical and material properties of the FEM and BEM sub-domains, specified type of boundary conditions of the sub-domains, and the number of nodes on the FEM/BEM interface. The most important issue regarding convergence, is the selection of the parameter α. Beyond the values given by Equation (4.19) the iterative method does not converge.

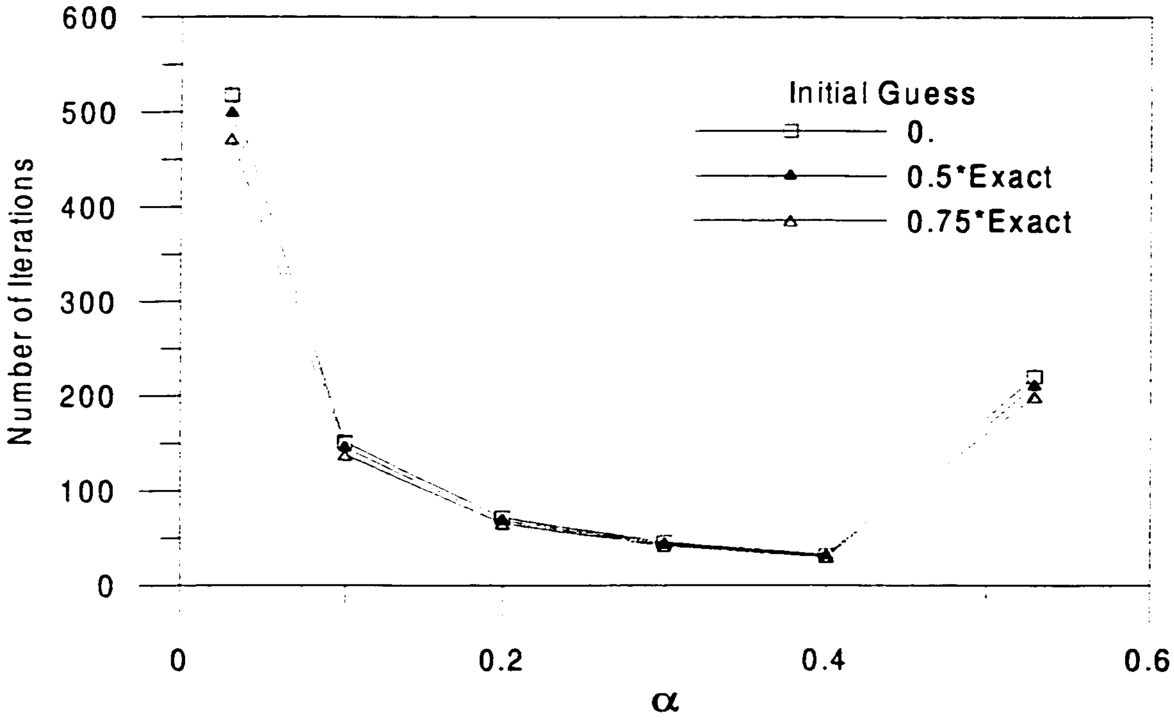

Figure 4.14: Effect of the Initial Guess on α

It is also concluded that the initial guess is not involved in the conditions for convergence and it has an insignificant effect on the speed of convergence. A further examination of Equation (4.22) indicates that the optimum value of α is independent on the initial guess of the potentials or displacements on the FEM/BEM interface. This is also confirmed by the benchmark examples. It is reasonable to start with values of zeros for the initial potentials or displacements on the interface.

For the selection of the parameter α, Equations (4.19) and (4.22) should be utilized. Alternatively, and to avoid the calculations required by Equations (4.19) and (4.22), some trial and error and deep experience are required. However, the following guidelines may be helpful in selecting the parameter α:

1. For combinations of low values of the relative sizes of the BEM to FEM sub-domains, and high values of the relative stiffness of the BEM to FEM sub-domains, the parameter α is assigned a relatively low value.

2. For combinations of high values of the relative sizes of the BEM to FEM sub-domains, and low values of the relative stiffness of the BEM to FEM sub-domains, the applicable range of α becomes wider. Fortunately, most of the FEM/BEM coupling applications satisfy these two criteria. In such case α may be assigned a relatively higher value.

CHAPTER 5

OVERLAPPING ITERATIVE DOMAIN DECOMPOSITION METHOD FOR COUPLING THE FEM AND BEM

5.1 GENERAL

A new iterative domain decomposition method for Coupling the BEM and FEM is presented in this chapter. The method has the advantage of allowing different formulation for the FEM and BEM, while preserving the identity of each method. It utilizes a common region that is modeled by both methods. The method avoids the limitations of the existing iterative coupling methods. It allows for the asymmetric formulation of the BEM avoiding the limitation of the conjugate gradient method presented by Gerstle et al. [61], and Kamiya and Iwase [64]. Furthermore, the method is capable of handling situations where the natural boundary conditions are prescribed on the entire external boundary of the FEM or BEM sub-domains. Such situations cannot be modeled using the iterative methods presented by Perera et al. [62], Kamiya et al. [63], Lin et al. [65], and Feng and Owen [66] as discussed earlier in Chapter 3.

The convergence of the method is investigated. Benchmark examples are given. The method is also presented to solve problems involving infinite and semi-infinite regions.

5.2 OVERLAPPING ITERATIVE COUPLING METHOD

In this section an iterative overlapping domain decomposition method is presented. The domain of the original problem is subdivided into FEM and BEM sub-domains, such that the two sub-domains partially overlap each other. The common region is modeled by both methods (Figure 5.1). The FEM/BEM interfaces (Γ^{I1} and Γ^{I2}) are also shown in the figure. Now, let us define the following vectors:

$\boldsymbol{u}_B$: displacement in the BEM sub-domain,

$\boldsymbol{u}_B^{I1}$: displacement on Γ^{I1} approached from the BEM sub-domain,

$\boldsymbol{u}_B^{B}$: displacement in the BEM sub-domain except $\boldsymbol{u}_B^{I1}$

$$\boldsymbol{u}_B = [\boldsymbol{u}_B^B, \boldsymbol{u}_B^{I1}]^T .$$

$\boldsymbol{u}_B^{I2}$: displacement on Γ^{I2} calculated as internal points for the BEM sub-domain,

$\boldsymbol{u}_F$: displacement in the FEM sub-domain,

$\boldsymbol{u}_F^{I1}$: displacement on Γ^{I1} approached from the FEM sub-domain

$\boldsymbol{u}_F^{I2}$: displacement on Γ^{I2} approached from the FEM sub-domain, and

$\boldsymbol{u}_F^{F}$: displacement in the FEM sub-domain except $\boldsymbol{u}_F^{I1}$ and $\boldsymbol{u}_F^{I2}$

$$\boldsymbol{u}_F = [\boldsymbol{u}_F^F, \boldsymbol{u}_F^{I1}, \boldsymbol{u}_F^{I2}]^T$$

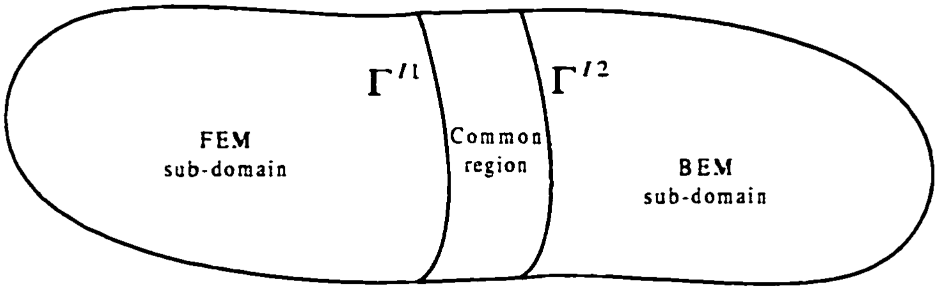

(a) Domain of the Original Problem

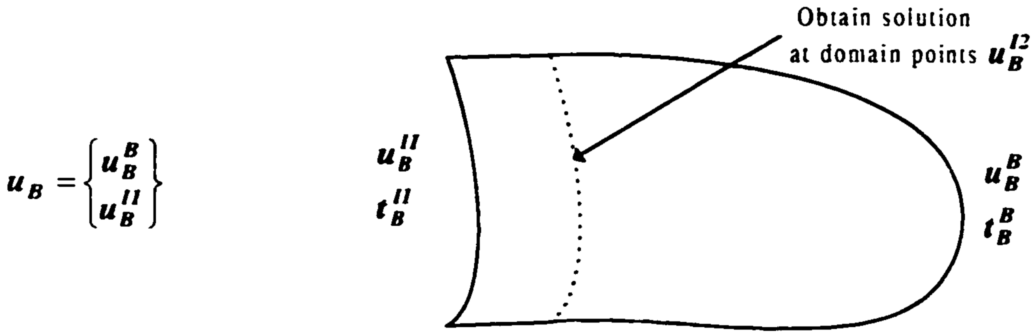

(b) BEM Modelling

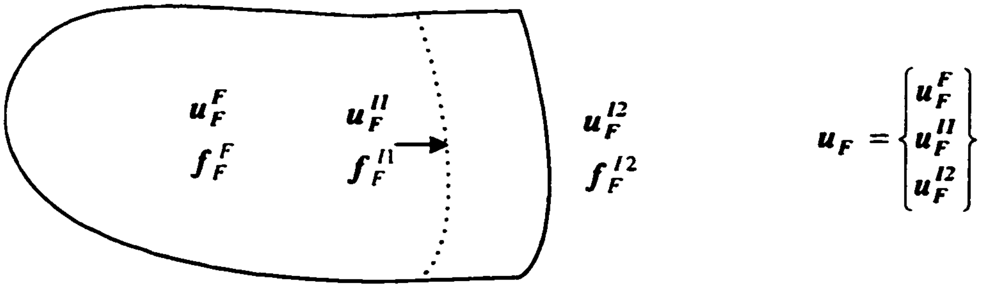

(c) FEM Modelling

Figure 5.1: Overlapping Domain Decomposition

Similarly, the BEM traction are denoted by t_B^B and t_B^{I1}, and the FEM force vectors by f_F^F, f_F^{I1} and f_F^{I2}.

The corresponding boundary integral equation for the BEM sub-domain can be written in sub-structured form as:

$$\begin{bmatrix} H_{11} & H_{12} \\ H_{21} & H_{22} \end{bmatrix} \begin{Bmatrix} u_B^B \\ u_{B,n}^{I1} \end{Bmatrix} = \begin{bmatrix} G_{11} & G_{12} \\ G_{21} & G_{22} \end{bmatrix} \begin{Bmatrix} t_B^B \\ t_{B,n}^{I1} \end{Bmatrix} \tag{5.1}$$

After solving for the unknowns in Equation (5.1), the displacement vector inside the domain $\{u_{B,n}^{I2}\}$ can be obtained as:

$$\{u_{B,n}^{I2}\} = \begin{bmatrix} H_{11}^* & H_{12}^* \\ H_{12}^* & H_{22}^* \end{bmatrix} \begin{Bmatrix} u_B^B \\ u_{B,n}^{I1} \end{Bmatrix} + \begin{bmatrix} G_{11}^* & G_{12}^* \\ G_{21}^* & G_{22}^* \end{bmatrix} \begin{Bmatrix} t_B^B \\ t_{B,n}^{I1} \end{Bmatrix} \tag{5.2}$$

For the FEM sub-domain, the assembled element equations are given by:

$$\begin{bmatrix} K_{11} & K_{12} & K_{13} \\ K_{21} & K_{22} & K_{23} \\ K_{31} & K_{32} & K_{33} \end{bmatrix} \begin{Bmatrix} u_F^F \\ u_{F,n}^{I1} \\ u_{F,n}^{I2} \end{Bmatrix} = \begin{Bmatrix} f_F^F \\ f_F^{I1} \\ f_F^{I2} \end{Bmatrix} \tag{5.3}$$

The proposed method can be described as follows:

1. Set an initial guess $\{u_{B,0}^{I1}\} = \{\overline{u}\}$.

2. Do for $n = 0, 1, 2, \ldots$

Solve $\begin{bmatrix} H_{11} & H_{12} \\ H_{21} & H_{22} \end{bmatrix} \begin{Bmatrix} u_B^B \\ u_{B,n}^{I1} \end{Bmatrix} = \begin{bmatrix} G_{11} & G_{12} \\ G_{21} & G_{22} \end{bmatrix} \begin{Bmatrix} t_B^B \\ t_{B,n}^{I1} \end{Bmatrix}$ for $\{t_{B,n}^{I1}\}$ and the boundary unknowns

Solve $\{u_{B,n}^{I2}\} = \begin{bmatrix} H_{11}^* & H_{12}^* \\ H_{12}^* & H_{22}^* \end{bmatrix} \begin{Bmatrix} u_B^B \\ u_{B,n}^{I1} \end{Bmatrix} + \begin{bmatrix} G_{11}^* & G_{12}^* \\ G_{21}^* & G_{22}^* \end{bmatrix} \begin{Bmatrix} t_B^B \\ t_{B,n}^{I1} \end{Bmatrix}$

Solve $\begin{bmatrix} K_{11} & K_{12} & K_{13} \\ K_{21} & K_{22} & K_{23} \\ K_{31} & K_{32} & K_{33} \end{bmatrix} \begin{Bmatrix} u_F^F \\ u_{F,n}^{I1} \\ u_{B,n}^{I2} \end{Bmatrix} = \begin{Bmatrix} f_F^F \\ f_F^{I1} \\ f_F^{I2} \end{Bmatrix}$ for $\{u_{F,n}^{I1}\}$

Apply $\{u_{B,\,n+1}^{I1}\} = (1-\alpha)\{u_{B,\,n}^{I1}\} + \alpha\ \{u_{F,\,n}^{I1}\}$

where, α is a relaxation parameter

Until $\dfrac{\left\| \{u_{B,n+1}^{I1}\} - \{u_{B,n}^{I1}\} \right\|}{\left\| \{u_{B,n+1}^{I1}\} \right\|} < \varepsilon$

where, ε is a given tolerance.

The current method avoids the prescription of natural boundary conditions on the interface Γ^{I1} or Γ^{I2}, and therefore it overcomes the problem encountered in the iterative methods presented in [62, 63, 65, and 66]. Another advantage is that the method does not require the transformation of the BEM tractions on the interface to the corresponding FEM forces.

5.3 CONVERGENCE CONDITIONS

A convergence analysis of the new overlapping method is presented in this section. After applying the boundary conditions, rearranging and conducting a series of matrix operations on Equation (5.1) and (5.2), the vector of unknowns $\{u_{B,n}^{I2}\}$ can be written as:

$$\{u_{B,n}^{I2}\} = [A_{11} \quad A_{12}]\begin{Bmatrix} C_B \\ u_{B,n}^{I1} \end{Bmatrix} \tag{5.4}$$

where, C_B is a vector of known BEM values and they are obtained from the initial boundary conditions for the BEM sub-domain. Similarly for the FEM after applying the boundary conditions, rearranging and performing a series of matrix operations on Equation (5.3) the following equation is obtained:

$$\begin{Bmatrix} u_F^F \\ u_{F,n}^{I1} \\ u_{F,n}^{I2} \end{Bmatrix} = \begin{bmatrix} F_{11} & F_{12} & F_{13} \\ F_{21} & F_{22} & F_{23} \\ 0 & 0 & 1 \end{bmatrix} \begin{Bmatrix} C_F^F \\ C_F^{I1} \\ u_{F,n}^{I2} \end{Bmatrix} \tag{5.5}$$

Note that C_F^F and C_F^{I1} are vectors of known FEM values and they are obtained from the initial boundary conditions for the FEM sub-domain. Substituting Equation (5.4) in the second of Equations (5.5) gives:

$$u_{F,n}^{I1} = C\, u_{B,n}^{I1} + E \tag{5.6}$$

where,

$$\boldsymbol{C} = \boldsymbol{F}_{23}\boldsymbol{A}_{12}$$

and

$$\boldsymbol{E} = \boldsymbol{F}_{21}\boldsymbol{C}_F^F + \boldsymbol{F}_{22}\boldsymbol{C}_F^{II} + \boldsymbol{F}_{23}\boldsymbol{A}_{11}\boldsymbol{C}_B$$

Substituting for $\boldsymbol{u}_{F,n}^{II}$ in the iterations $\boldsymbol{u}_{B,n+1}^{II} = (1-\alpha)\boldsymbol{u}_{B,n}^{II} + \alpha\,\boldsymbol{u}_{F,n}^{II}$ gives:

$$\boldsymbol{u}_{B,n+1}^{II} = [(1-\alpha)\boldsymbol{I} + \alpha\,\boldsymbol{C}]\,\boldsymbol{u}_{B,n}^{II} + \alpha\,\boldsymbol{E} \tag{5.7}$$

which has the same form as obtained for the Sequential Dirichlet-Neumann method. It can be concluded that if $\lambda_1 = \boldsymbol{x}_1 + i\boldsymbol{y}_1, \ldots, \lambda_N = \boldsymbol{x}_N + i\boldsymbol{y}_N$ are the eigenvalues of $\boldsymbol{C}$, then,

$$\alpha < \min_{1\le i\le N}\left\{\frac{2(1-\boldsymbol{x}_i)}{(1-\boldsymbol{x}_i)^2 + \boldsymbol{y}_i^{\,2}}\right\}$$

$$\text{and } \boldsymbol{x}_i < 1, \quad i = 1,2,\ldots,N \tag{5.8}$$

are the necessary conditions for the convergence of the new iterative method. The optimum α is obtained as:

$$\overline{\alpha} = -\frac{\mathrm{Re}(\boldsymbol{I}'(\lambda - \boldsymbol{I}))}{\|\lambda - \boldsymbol{I}\|^2} \tag{5.9}$$

5.4 INFINITE AND SEMI-INFINITE PROBLEMS

The new overlapping iterative method can be effectively used to solve problems with infinite and semi-infinite domains. Consider the case of a shallow tunnel as shown in Figure 5.2. This problem cannot be solved using the iterative methods presented in [62, 63, 65, and 66], as these methods require the specification of the natural boundary conditions on the FEM/BEM interface. According to the nature of the problem this will result in non-unique solutions for the FEM sub-domain. Thus, the iterative methods presented in [62, 63, 65, and 66] are not applicable for such cases. The procedure for applying the overlapping method to the semi-infinite and infinite problems is given below.

Consider Figure 5.3; where a finite region close to the opening is modeled by the FEM while the remaining infinite or semi-infinite region is modeled by the BEM. The two sub-domains overlap over a finite common region. The proposed method can be described as follows:

1. Set initial guess $\{u^{I1}_{B,0}\} = \{\bar{u}\}$.

2. Do for $n = 0, 1, 2, \ldots$

   Solve $[H]\{u^{I1}_{B,n}\} = [G]\{t^{I1}_{B,n}\}$ for $\{t^{I1}_{B,n}\}$

   Solve $\{u^{I2}_{B,n}\} = [H^{*}]\{u^{I1}_{B,n}\} + [G^{*}]\{t^{I1}_{B,n}\}$

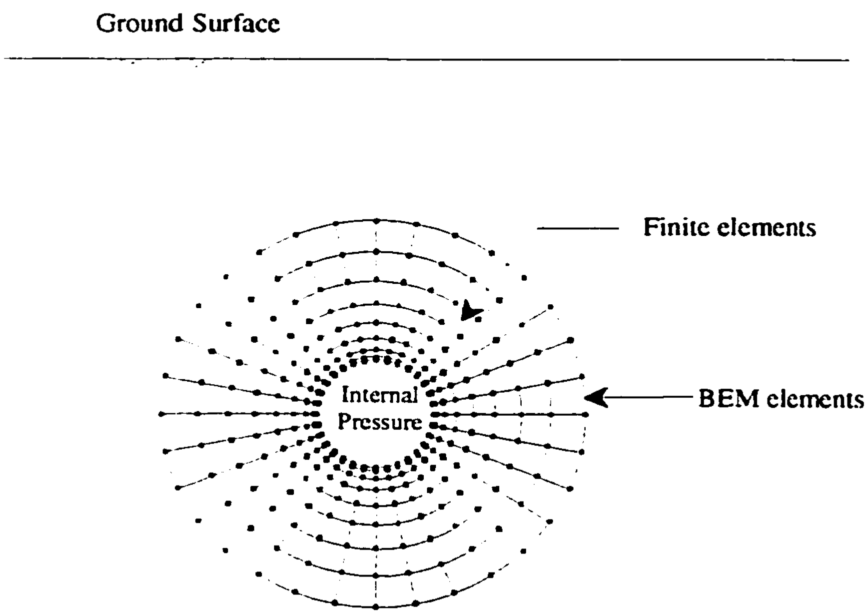

Figure 5.2: Shallow Tunnel Modeled by the Coupled FEM/BEM

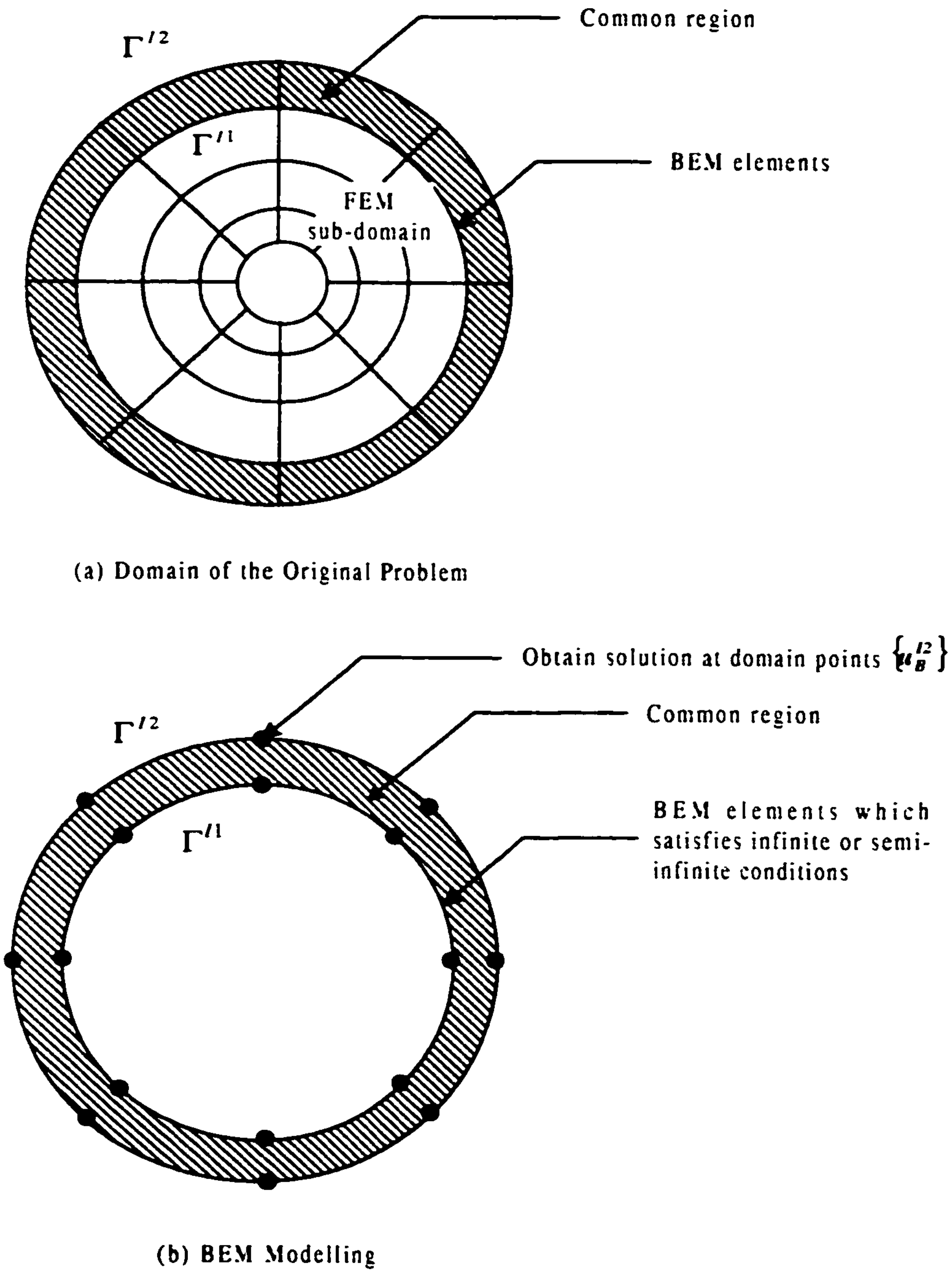

Figure 5.3: Domain Decomposition for Infinite and Semi-Infinite Problems

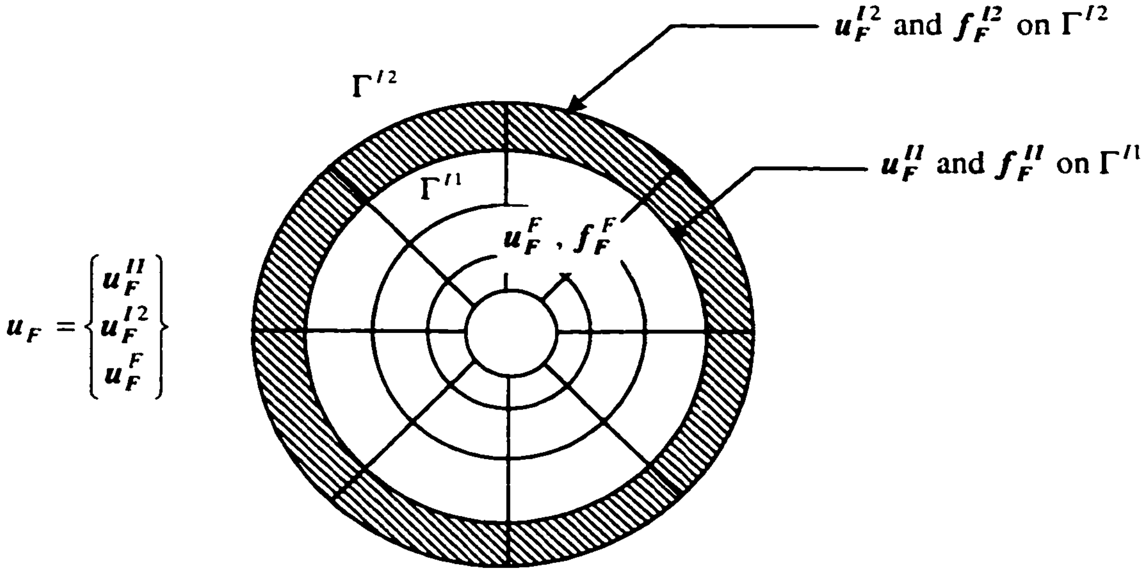

(b) FEM Modelling

Figure 5.3: Continued

$$\text{Solve} \quad \begin{bmatrix} K_{11} & K_{12} & K_{13} \\ K_{21} & K_{22} & K_{23} \\ K_{31} & K_{32} & K_{33} \end{bmatrix} \begin{Bmatrix} u_F^F \\ u_{F,n}^{I1} \\ u_{B,n}^{I2} \end{Bmatrix} = \begin{Bmatrix} f_F^F \\ f_F^{I1} \\ f_F^{I2} \end{Bmatrix} \quad \text{for } \{u_{F,n}^{I1}\}$$

$$\text{Apply} \quad \{u_{B,n+1}^{I1}\} = (1-\alpha)\{u_{B,n}^{I1}\} + \alpha\{u_{F,n}^{I1}\}$$

$$\text{Until} \quad \frac{\left\| \{u_{B,n+1}^{I1}\} - \{u_{B,n}^{I1}\} \right\|}{\left\| \{u_{B,n+1}^{I1}\} \right\|} < \varepsilon$$

5.5 BENCHMARK EXAMPLES

In this section two benchmark examples that show the efficiency of the new overlapping iterative coupling method are given. The two examples show the applicability of the new method to problems involving natural boundary conditions on the entire FEM sub-domain. The two examples considered here can not be solved using the iterative methods presented in [62, 63, 65, and 66]. Practical applications are given in Chapter 7.

5.5.1 Potential Flow Example

Consider the potential flow example given in Chapter 4 with the following boundary conditions: $t(0,y) = -100$, $u(a,y) = 200$, and zero flux elsewhere as shown in Figure 5.4. The geometrical and material properties are such that a_B, a_F, k_B and k_F are fixed to unity. The problem is modeled using 30 linear boundary elements and 55 linear quadrilateral finite elements with an overlapping distance $a_c = 0.1$. The

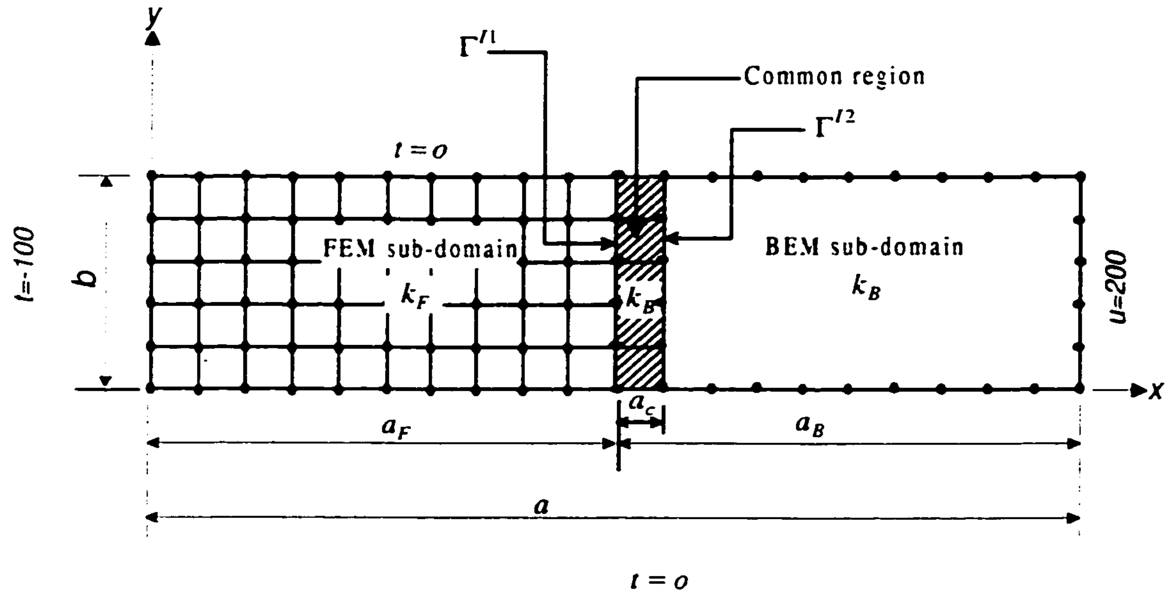

Figure 5.4: Potential Flow Example Using the New Overlapping Iterative Method. (Neumann Boundary Conditions are specified for the entire FEM sub-domain)

overlapping iterative method gives a solution that is in good agreement with the exact solution. The range for the parameter α is obtained as 0.02-20, with an optimum value of 10.

5.5.2 Elasticity Example

Consider a circular hole in an infinite plane subjected to uniform pressure. The example is indicated in Figure 5.5 while the FEM/BEM discretization is shown in Figure 5.6.

Figure 5.7 shows the radial displacements with the overlapping iterative method compared with the exact solution [72]. The results clearly show the excellent agreement between the coupled FEM/BEM and the exact solutions. The applicable range of the parameter α is obtained as 0.02-6.6, with an optimum value of 4.

5.6 SELECTION OF THE COMMON REGION

In order to examine the selection of the common region, the potential flow example given in Chapter 4 is reinvestigated using the new overlapping iterative coupling method (Figure 5.8). The problem is investigated for different values of a_B/a_F and k_B/k_F. For $a_B/a_F = 1$, the problem is modeled using 30 linear boundary elements and 55 linear quadrilateral finite elements (Figure 5.8).

The combined effect of the size of the common region (a_c), and the relative material properties (k_B/k_F), on the convergence of the solution is shown in Figure 5.9. The

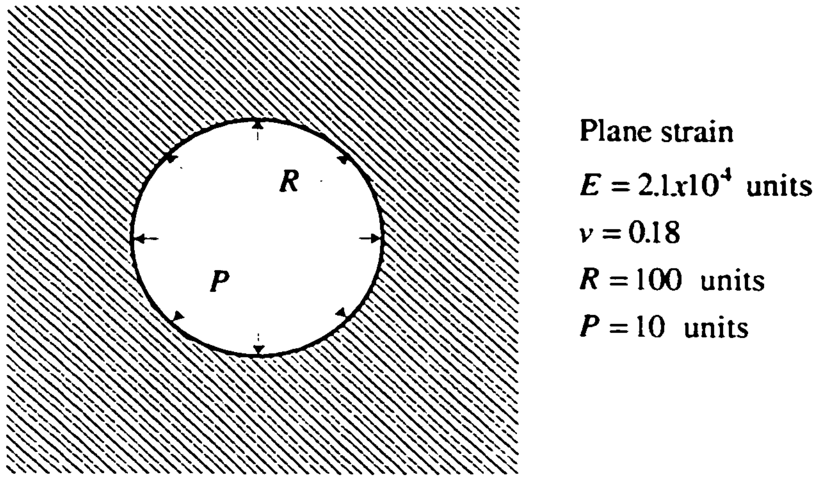

Figure 5.5: Circular Hole in an Infinite Elastic Domain Subjected to Uniform Pressure

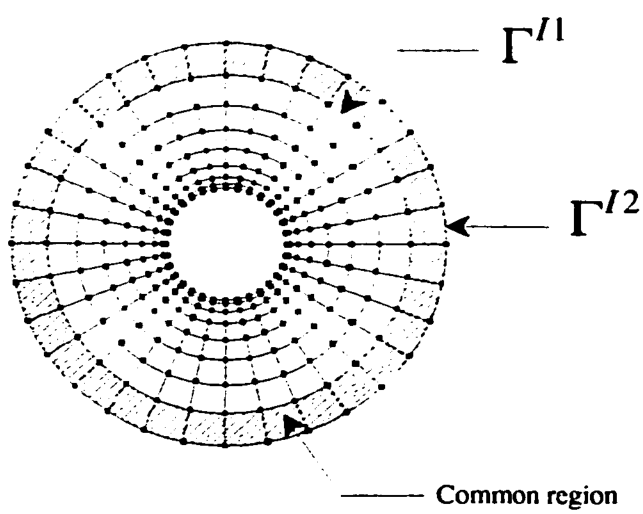

Figure 5.6: Discretization of the Circular Hole Example

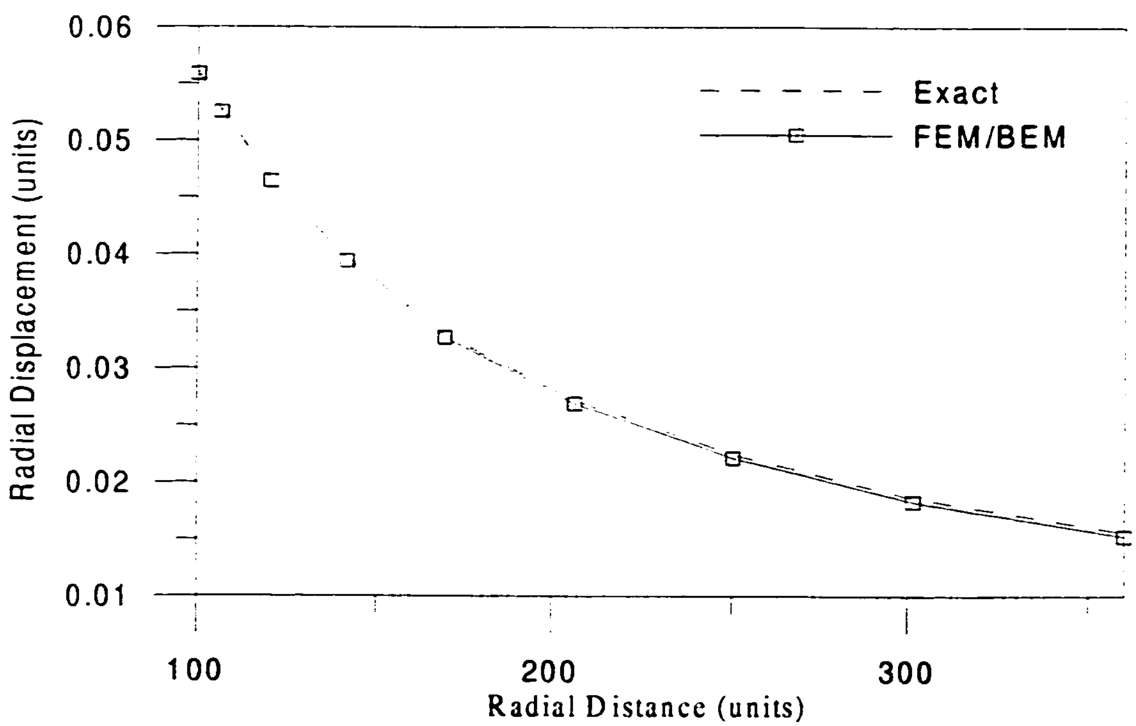

Figure 5.7: Radial Displacements for the Circular Hole Example

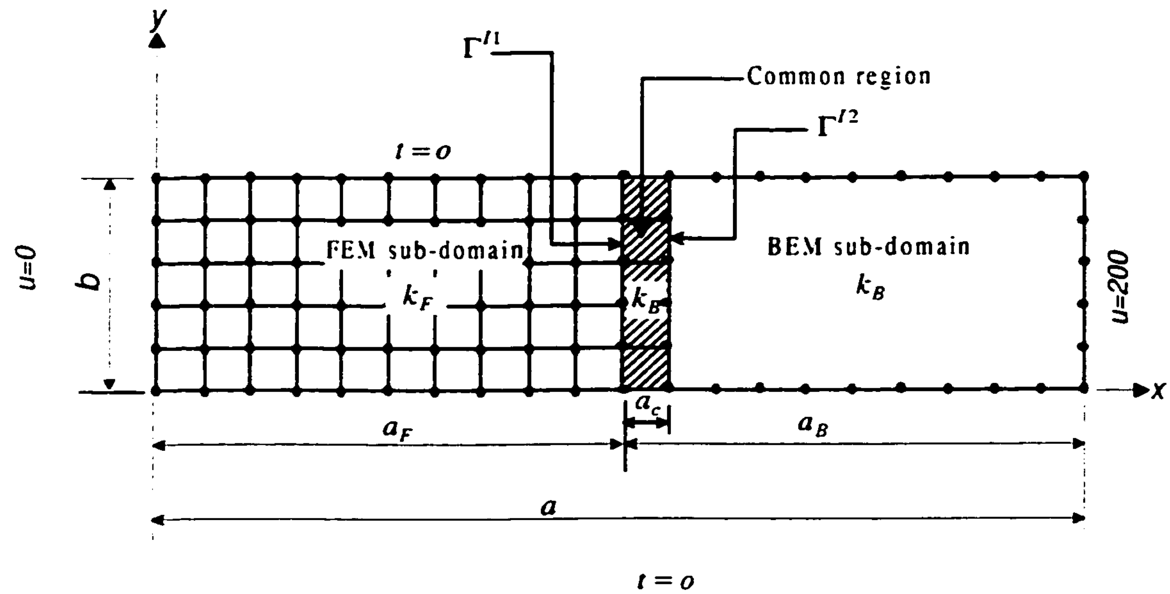

Figure 5.8: Potential Flow Example Using the New Overlapping Iterative Coupling Method

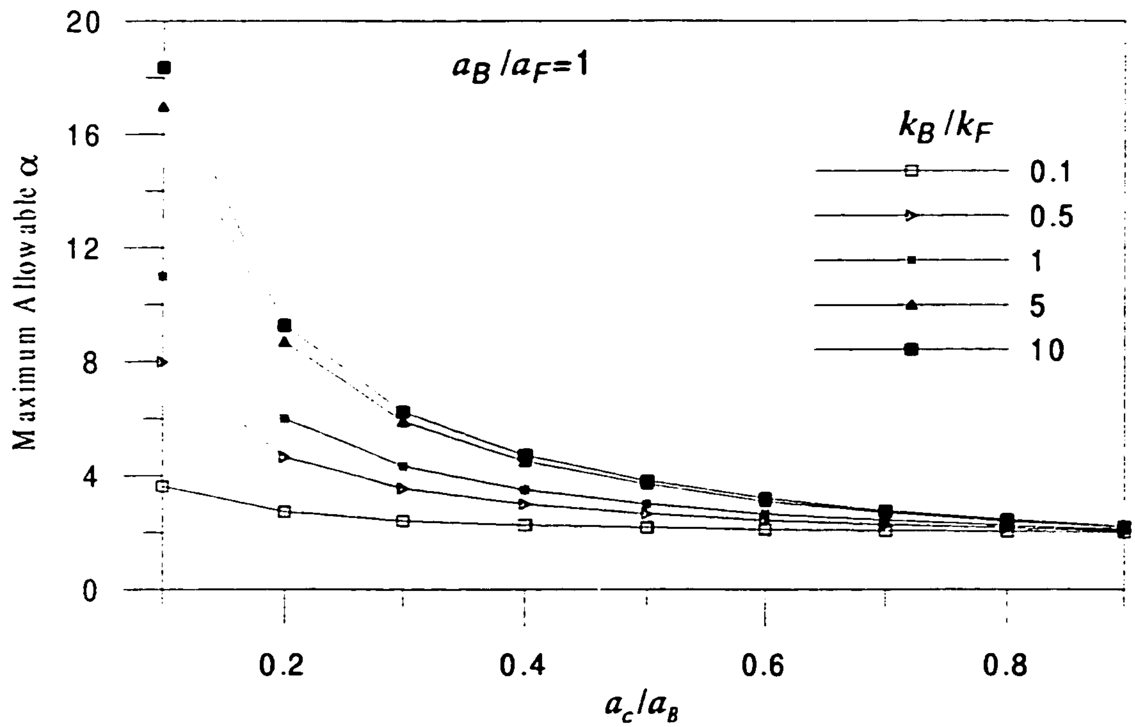

Figure 5.9: Maximum Allowable α vs. a_c/a_B for Different Values of k_B/k_F ($a_B/a_F = 1$)

figure gives the maximum allowable α for different combinations of k_B/k_F using different values of a_c/a_B. Figure 5.9 is self-explanatory, and it clearly indicates that the applicable range of α vary with k_B/k_F. As a_c/a_B decreases the applicable range of α increases. Also it is observed from the figure that the new overlapping method provides a wider applicable range of α compared to the Sequential Dirichlet-Neumann iterative method, which is more advantageous. As an example the applicable range is 0.02-0.18 for $k_B/k_F = 10$ using the Sequential Dirichlet-Neumann iterative coupling method as compared to 0.02-18.36 using the new overlapping iterative method with $a_c/a_B = 0.1$. It is also concluded from Figure 5.9 that it is more advantageous to choose a common region, which is relatively small.

Similarly, Figures 5.10 through 5.12 give the maximum allowable α for different relative sizes of the computational sub-domains $a_B/a_F = 3$, 10, and 1/3, respectively. Similar observations can be made as for $a_B/a_F = 1$.

It is interesting to observe that for all cases studied, and for different combinations of k_B/k_F, a_B/a_F, and a_c/a_B, the applicable range of the parameter α is very wide compared to the Sequential Dirichlet-Neumann iterative coupling method. The maximum allowable α has a minimum value of 2, and only for combinations with high a_c/a_B values. As the size of the common region decreases, the applicable range of α increases. The limit values given by Figures 5.9 through 5.12 are found to be in good agreement with those determined using Equation (5.8).

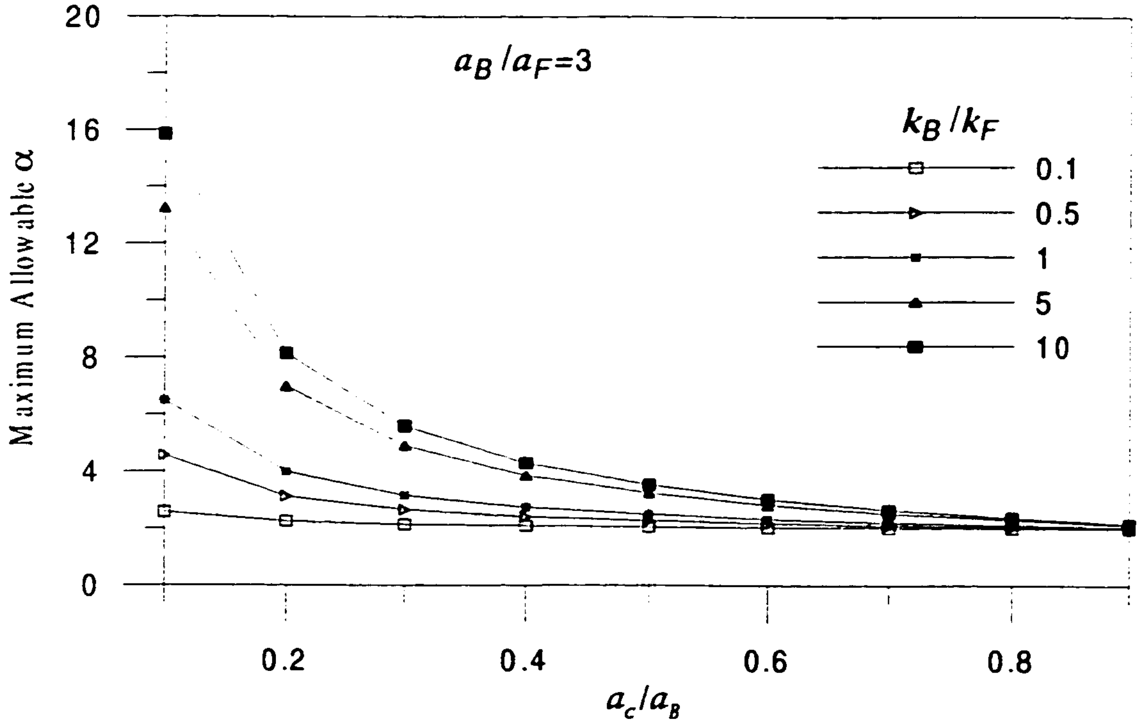

Figure 5.10: Maximum Allowable α vs. a_c/a_B for Different Values of k_B/k_F ($a_B/a_F = 3$)

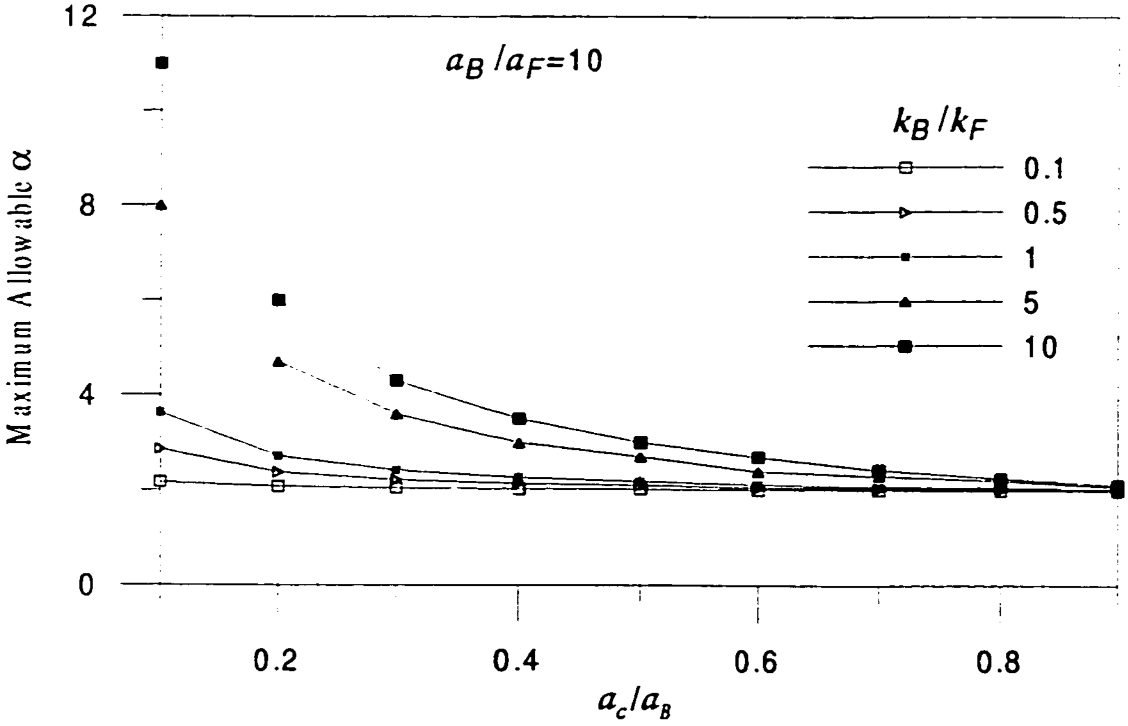

Figure 5.11: Maximum Allowable α vs. a_c/a_B for Different Values of k_B/k_F ($a_B/a_F = 10$)

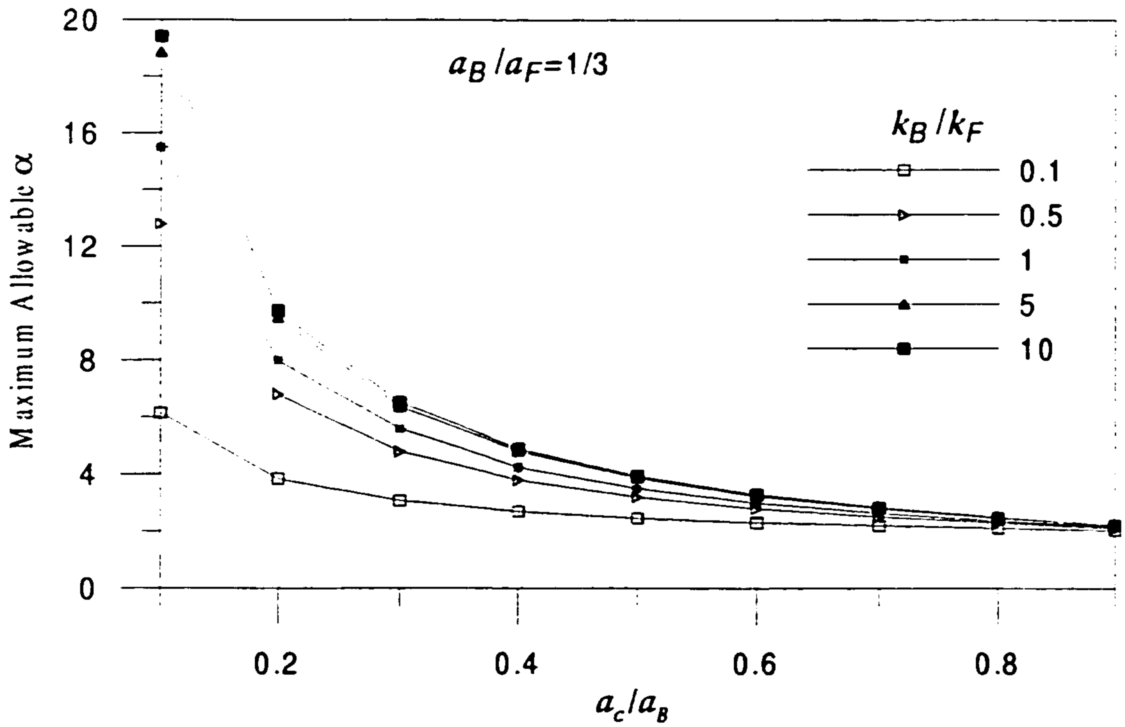

Figure 5.12: Maximum Allowable α vs. a_c/a_B for Different Values of k_B/k_F ($a_B/a_F = 1/3$)

It is clear from the analysis conducted that the size of the common region can be arbitrary chosen. However, the following guidelines may be helpful regarding the selection of the common region (a_c):

1. The width of the common region a_c should not be too small in order to avoid the computation of singular boundary integrals.

2. The choice of a_c should be small enough to have a wider range of α and to avoid the reduction in the efficiency of the method, due to the increase in the number of the coupling equations.

3. A reasonable decision is to choose a common region with a_c being equal to the length of the boundary element on the BEM interface.

CHAPTER 6

EXTENSION OF THE ITERATIVE COUPLED FEM/BEM METHODS TO ELASTO-PLASTICITY

6.1 GENERAL

As mentioned earlier, the conventional methods of coupling the finite element and boundary element methods employ an entire unified equation for the whole domain by combining the discretized equations for the BEM and FEM sub-domains. Applications of the conventional coupling methods in elasto-plasticity can be found in [69-71]. The iterative domain decomposition methods [61-66] were developed to overcome some limitations of the conventional coupling methods. Unfortunately, these investigations [61-66] are limited to linear potential or elasticity problems. In this chapter, the extension of the Sequential Dirichlet-Neumann iterative coupling method and the new iterative overlapping coupling method to elasto-plasticity is presented. Practical applications are given in Chapter 7.

6.2 THE DIRICHLET-NEUMANN METHOD IN ELASTO-PLASTICITY

In this section, the extension of the Sequential Dirichlet-Neumann iterative coupling method to elasto-plasticity problems is presented. Considering Figure 3.1 where the

domain of the original problem is decomposed to FEM and BEM sub-domains. The FEM only needs to be applied to the plastic region and the BEM to the remaining elastic region. The FEM equations in elasto-plasticity are given in Section 2.6. An incremental form of the FEM equations can be written as:

$$\{\Delta\psi\}=[K_T]\{\Delta u\}-\{\Delta f\} \tag{6.1}$$

It should be noted that for each load increment, Equations (6.1) are nonlinear and therefore are solved iteratively. The iterative coupling method can be described as follows:

1. Set an initial guess $\{u^I_{B,0}\}=\{\bar{u}\}$
2. Do for $n=0, 1, 2, \ldots$

   Solve $\begin{bmatrix} H_{11} & H_{12} \\ H_{21} & H_{22} \end{bmatrix}\begin{Bmatrix} u^B_B \\ u^I_{B,n} \end{Bmatrix}=\begin{bmatrix} G_{11} & G_{12} \\ G_{21} & G_{22} \end{bmatrix}\begin{Bmatrix} t^B_B \\ t^I_{B,n} \end{Bmatrix}$ for $\{t^I_{B,n}\}$

   Solve $\{f^I_{F,n}\}=-[M]\{t^I_{B,n}\}$

   For the FEM region

   For $i=1, 2, \ldots, m$

   where, m is a specified number of increments such that:

   $\{f_{F,n}\}=\{\Delta f_{F,n}\}_1+\{\Delta f_{F,n}\}_2+\cdots+\{\Delta f_{F,n}\}_i+\cdots+\{\Delta f_{F,n}\}_m$

   Solve $\begin{Bmatrix} \Delta\psi^F_{F,n} \\ \Delta\psi^I_{F,n} \end{Bmatrix}_i=\begin{bmatrix} K_{T11} & K_{T12} \\ K_{T21} & K_{T22} \end{bmatrix}_i\begin{Bmatrix} \Delta u^F_{F,n} \\ \Delta u^I_{F,n} \end{Bmatrix}_i-\begin{Bmatrix} \Delta f^F_{F,n} \\ \Delta f^I_{F,n} \end{Bmatrix}_i$

$$\text{Until} \quad \frac{\left\| \begin{Bmatrix} \Delta u^F_{F,n} \\ \Delta u^I_{F,n} \end{Bmatrix}^r_i - \begin{Bmatrix} \Delta u^F_{F,n} \\ \Delta u^I_{F,n} \end{Bmatrix}^{r-1}_i \right\|}{\left\| \begin{Bmatrix} \Delta u^F_{F,n} \\ \Delta u^I_{F,n} \end{Bmatrix}^r_i \right\|} \le \delta$$

where, δ is a specified tolerance, and $r-1$ and r denote successive iterations

$$\text{Apply} \quad \begin{Bmatrix} u^F_{F,n} \\ u^I_{F,n} \end{Bmatrix}_i = \begin{Bmatrix} u^F_{F,n} \\ u^I_{F,n} \end{Bmatrix}_{i-1} + \begin{Bmatrix} \Delta u^F_{F,n} \\ \Delta u^I_{F,n} \end{Bmatrix}_i$$

$$\begin{Bmatrix} u^F_{F,n} \\ u^I_{F,n} \end{Bmatrix} = \begin{Bmatrix} u^F_{F,n} \\ u^I_{F,n} \end{Bmatrix}_m$$

$$\text{Apply} \quad \left\{u^I_{B,n+1}\right\} = (1-\alpha)\left\{u^I_{B,n}\right\} + \alpha \left\{u^I_{F,n}\right\}$$

$$\text{Until} \quad \frac{\left\| \left\{u^I_{B,n+1}\right\} - \left\{u^I_{B,n}\right\} \right\|}{\left\| \left\{u^I_{B,n+1}\right\} \right\|} < \varepsilon .$$

An elasto-plastic coupled FEM/BEM Fortran computer program **EPFBE** (**E**lasto-**P**lastic **F**inite **B**oundary **E**lement) is developed using the algorithm presented above. The program permits the solution of the elasto-plastic problems by the tangential stiffness, the initial stiffness, or a combination of both. It has options for Tresca, Von Mises, Mohr-Coulomb and Drucker-Prager yield criteria. Figure 6.1 shows the primary subroutines called from **EPFBE**. The FEM subroutines such as **INPUT, DIMEN, LOADPS, ZERO, INCREM, ALGOR, STIFP, FRONT, RESIDU,**

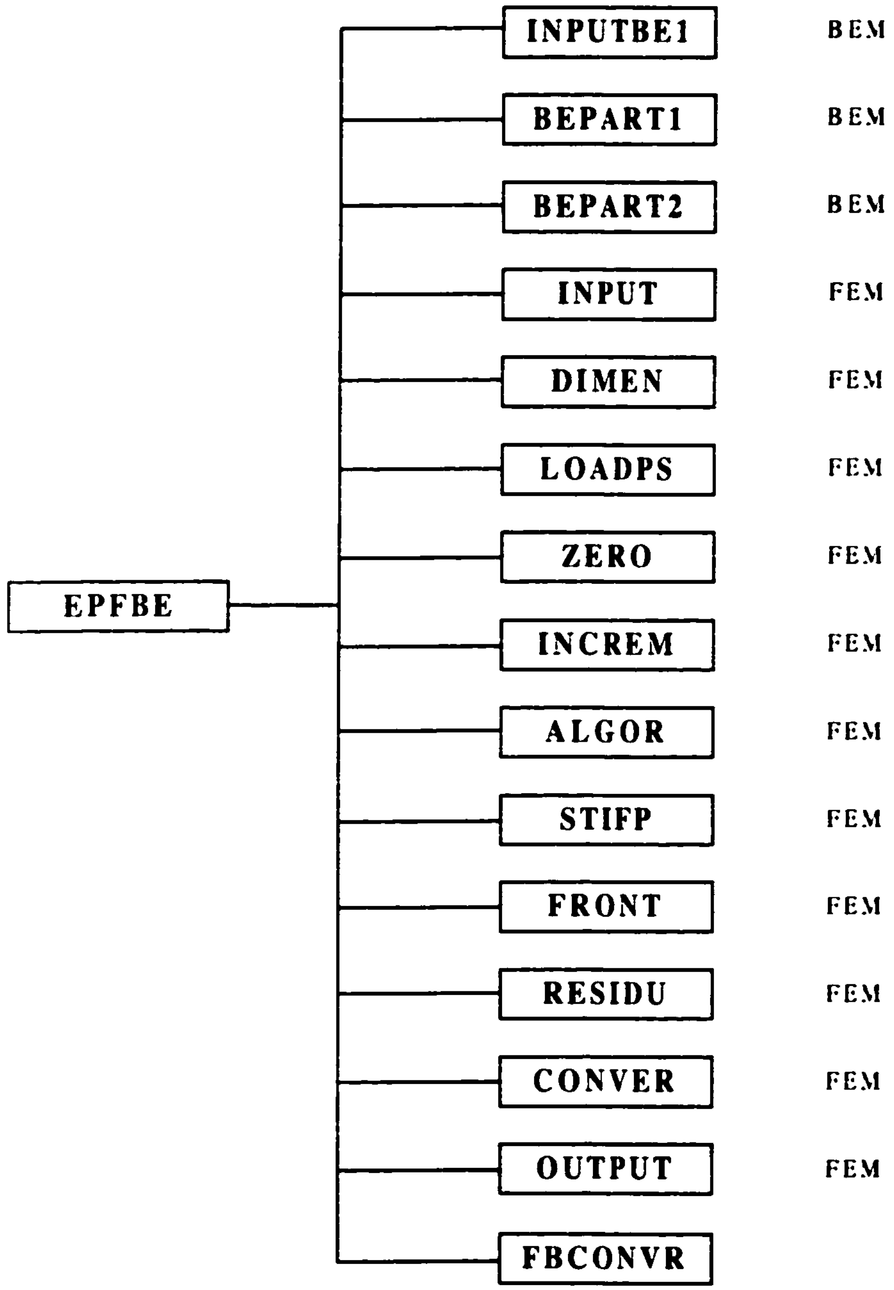

Figure 6.1: Structure of **EPFBE** Program

CONVER, and **OUTPUT** have been adopted from reference [31]. The BEM subroutines such as **INPUTBE, BEPART1,** and **BEPART2**, are developed for the solution of two-dimensional elastostatic problems using linear boundary elements.

The FEM subroutines are briefly described below [31]:

INPUT: It accepts most of the input data required for the FEM sub-domain.

DIMEN: The function of this subroutine is to preset the values of FEM variables employed in the program.

LOADPS: The purpose of this subroutine is to evaluate the consistent nodal forces for each element due to discrete point loads, gravity loading and distributed edge loading.

ZERO: This subroutine merely sets to zero the contents of several arrays employed for the FEM sub-domain.

INCREM: The role of this subroutine is to increment the applied loading or any prescribed displacements for the FEM sub-domain, according to the load factors specified as input.

ALGOR: The function of this subroutine is to set an indicator to identify the solution algorithm, e.g., initial stiffness, tangential stiffness, etc.

STIFP: This subroutine evaluates the stiffness matrix for each element.

FRONT: The function of this subroutine is to assemble the contribution from each element to form the global stiffness matrix and global load vector, and to solve the resulting set of simultaneous equations by gausssian direct elimination. The main feature of the frontal solution technique is that it assembles the equations and eliminates the variables at the same time.

RESIDU: The function of this subroutine is to evaluate the nodal forces, which are statically equivalent to the stress field satisfying elasto-plastic conditions. Comparison of these equivalent nodal forces with the applied loads gives the residual force.

CONVER: This subroutine monitors the convergence of the nonlinear solution iteration process.

OUTPUT: This subroutine outputs FEM sub-domain results at a frequency determined by the output parameters.

The BEM subroutines along with **FBCONVR** are briefly described below:

INPUTBE: This subroutine reads the input data required for the BEM sub-domain.

BEPART1: This subroutine employs the BEM using straight elements characterized by linear displacements and linear tractions to evaluate $[H]$ and $[G]$ matrices. The leading diagonal sub-matrices

corresponding to $[H]$ are calculated using rigid body translations. It also reorders the system of equations based on known boundary conditions.

BEPART2: The function of this subroutine is to solve the linear system of equations. It prints the results for the boundary displacements and tractions. It also employs the BEM to calculate the displacements and stresses at selected domain points. The subroutine evaluates matrix $[M]$ and it transfers the BEM interfacial tractions into FEM interfacial forces according to Equation (4.4).

FBCONVR: The function of this subroutine is to check the convergence of the iterative FEM/BEM solution process according to a predefined tolerance ε. It also assigns new values for the BEM interfacial displacements $\{u^{I}_{B,n+1}\}$ for the new iteration.

An outline of **EPFBE** is given in Figure 6.2.

6.3 OVERLAPPING COUPLING METHOD IN ELASTO-PLASTICITY

Considering Figure 5.1, the overlapping method presented in Chapter 5 can be modified to solve elasto-plasticity problems and is described below:

1. Set an initial guess $\{u^{II}_{B,0}\}=\{\overline{u}\}$

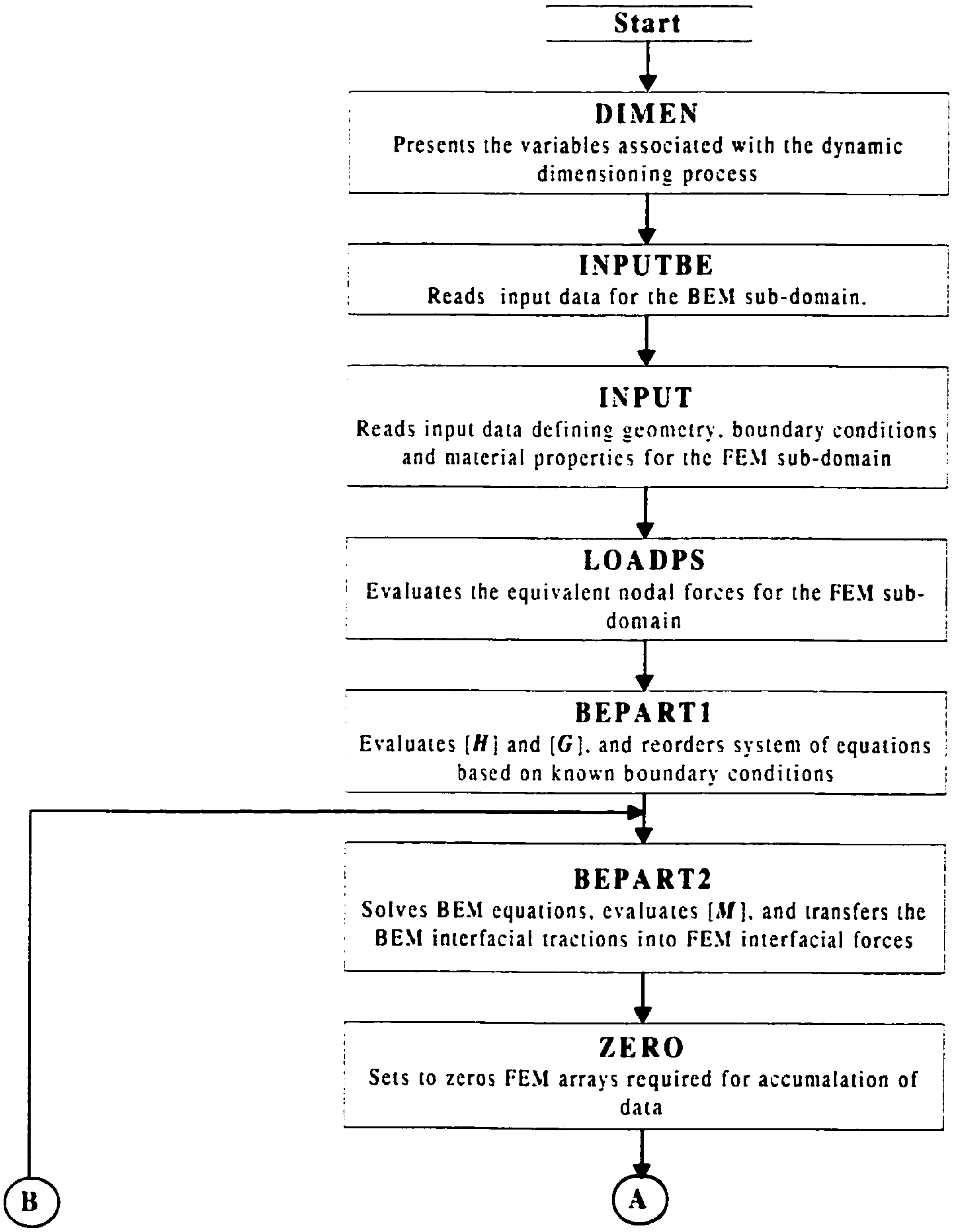

Figure 6.2: **EPFBE** Program Organization

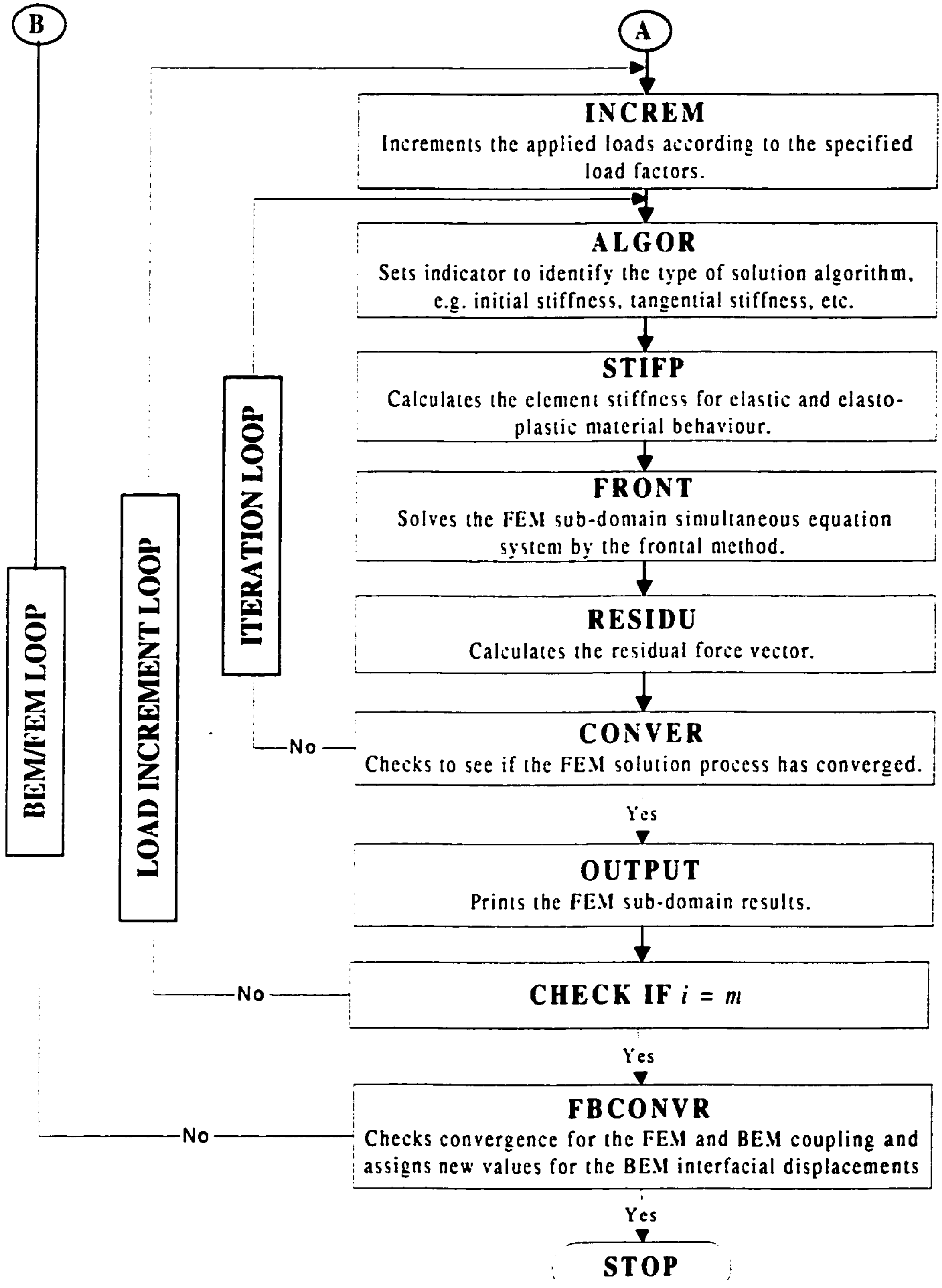

Figure 6.2: Continued

2. Do for $n = 0, 1, 2, \ldots$

Solve $\begin{bmatrix} H_{11} & H_{12} \\ H_{21} & H_{22} \end{bmatrix} \begin{Bmatrix} u_B^B \\ u_{B,n}^I \end{Bmatrix} = \begin{bmatrix} G_{11} & G_{12} \\ G_{21} & G_{22} \end{bmatrix} \begin{Bmatrix} t_B^B \\ t_{B,n}^I \end{Bmatrix}$ for $\{t_{B,n}^I\}$ and boundary unknowns

Solve $\{u_{B,n}^{I2}\} = \begin{bmatrix} H_{11}^* & H_{12}^* \\ H_{12}^* & H_{22}^* \end{bmatrix} \begin{Bmatrix} u_B^B \\ u_{B,n}^{I1} \end{Bmatrix} + \begin{bmatrix} G_{11}^* & G_{12}^* \\ G_{21}^* & G_{22}^* \end{bmatrix} \begin{Bmatrix} t_B^B \\ t_{B,n}^{I1} \end{Bmatrix}$

For the FEM region

Set $\{u_F^{I2}\} = \{u_B^{I2}\}$

For $i = 1, 2, \ldots, m$

where, m is a specified number of increments such that:

$$\{f_{F,n}\} = \{\Delta f_{F,n}\}_1 + \{\Delta f_{F,n}\}_2 + \cdots + \{\Delta f_{F,n}\}_i + \cdots + \{\Delta f_{F,n}\}_m$$

Solve

$$\begin{Bmatrix} \Delta\psi_F^F \\ \Delta\psi_{F,n}^{I1} \\ \Delta\psi_{B,n}^{I2} \end{Bmatrix}_i = \begin{bmatrix} K_{T11} & K_{T12} & K_{T13} \\ K_{T21} & K_{T22} & K_{T23} \\ K_{T31} & K_{T32} & K_{T33} \end{bmatrix}_i \begin{Bmatrix} \Delta u_F^F \\ \Delta u_{F,n}^{I1} \\ \Delta u_{F,n}^{I2} \end{Bmatrix}_i - \begin{Bmatrix} \Delta f_F^F \\ \Delta f_F^{I1} \\ \Delta f_F^{I2} \end{Bmatrix}_i$$

Until $$\frac{\left\| \begin{Bmatrix} \Delta u_F^F \\ \Delta u_{F,n}^{I1} \\ \Delta u_{F,n}^{I2} \end{Bmatrix}_i^r - \begin{Bmatrix} \Delta u_F^F \\ \Delta u_{F,n}^{I1} \\ \Delta u_{F,n}^{I2} \end{Bmatrix}_i^{r-1} \right\|}{\left\| \begin{Bmatrix} \Delta u_F^F \\ \Delta u_{F,n}^{I1} \\ \Delta u_{F,n}^{I2} \end{Bmatrix}_i^r \right\|} \le \delta$$

where, δ is a specified tolerance, and $r-1$ and r denote successive iterations

$$\text{Apply} \quad \begin{Bmatrix} u_F^F \\ u_{F,n}^{I1} \\ u_{F,n}^{I2} \end{Bmatrix}_i = \begin{Bmatrix} u_F^F \\ u_{F,n}^{I1} \\ u_{F,n}^{I2} \end{Bmatrix}_{i-1} + \begin{Bmatrix} \Delta u_F^F \\ \Delta u_{F,n}^{I1} \\ \Delta u_{F,n}^{I2} \end{Bmatrix}_i$$

$$\begin{Bmatrix} u_F^F \\ u_{F,n}^{I1} \\ u_{F,n}^{I2} \end{Bmatrix} = \begin{Bmatrix} u_F^F \\ u_{F,n}^{I1} \\ u_{F,n}^{I2} \end{Bmatrix}_m$$

$$\text{Apply} \quad \left\{u_{B,n+1}^{I1}\right\} = (1-\alpha)\left\{u_{B,n}^{I1}\right\} + \alpha\left\{u_{F,n}^{I1}\right\}$$

$$\text{Until} \quad \frac{\left\|\left\{u_{B,n+1}^{I1}\right\} - \left\{u_{B,n}^{I1}\right\}\right\|}{\left\|\left\{u_{B,n+1}^{I1}\right\}\right\|} < \varepsilon .$$

A Fortran computer program **OVEPFBE** (**OV**erlapping **E**lasto-**P**lastic **F**inite **B**oundary **E**lement) is developed using the new overlapping algorithm. The program permits the solution of the elasto-plastic problems by the tangential stiffness, the initial stiffness, or a combination of both. It has options for Tresca, Von Mises, Mohr-Coulomb and Drucker-Prager yield criteria. The FEM subroutines such as **INPUT, DIMEN, LOADPS, ZERO, INCREM, ALGOR, STIFP, FRONT, RESIDU, CONVER,** and **OUTPUT** have been adopted from reference [31]. The BEM subroutines such as **OINPUTBE, OBEPART1,** and **OBEPART2**, are developed for the solution of two-dimensional elastostatic problems using linear boundary elements for infinite and semi-infinite domains.

The FEM subroutines have been mentioned while describing **EPFBE**. The BEM subroutines and **FBCONVR** are described below:

OINPUTBE: This subroutine reads the input data required for the BEM sub-domain.

OBEPART1: This subroutine employs the BEM using straight elements characterized by linear displacements and linear tractions to evaluate $[H]$ and $[G]$ matrices for infinite or semi-infinite domains. The program utilizes the Kelvin fundamental solution for infinite domains. For the semi-infinite case, the program utilizes Melan fundamental solution for the evaluation of $[H]$ and $[G]$ matrices. The subroutine also reorders the system of equations based on known boundary conditions.

OBEPART2: The function of this subroutine is to solve the linear system of equations. It prints the results for the boundary displacements and tractions. It also employs the BEM to calculate the displacements and stresses at selected domain points. The subroutine also evaluates displacements on Γ^{I2} and sets $\{u_{F,n}^{I2}\} = \{u_{B,n}^{I2}\}$.

OFBCONVR:

The function of this subroutine is to check the convergence of the iterative FEM/BEM solution process according to a predefined

tolerance ε. It also assigns new values for the BEM interfacial displacements $\left\{ \boldsymbol{u}_{B,n+1}^{I1} \right\}$ for the new iteration.

An outline of **OVEPFBE** is given in Figure 6.3.

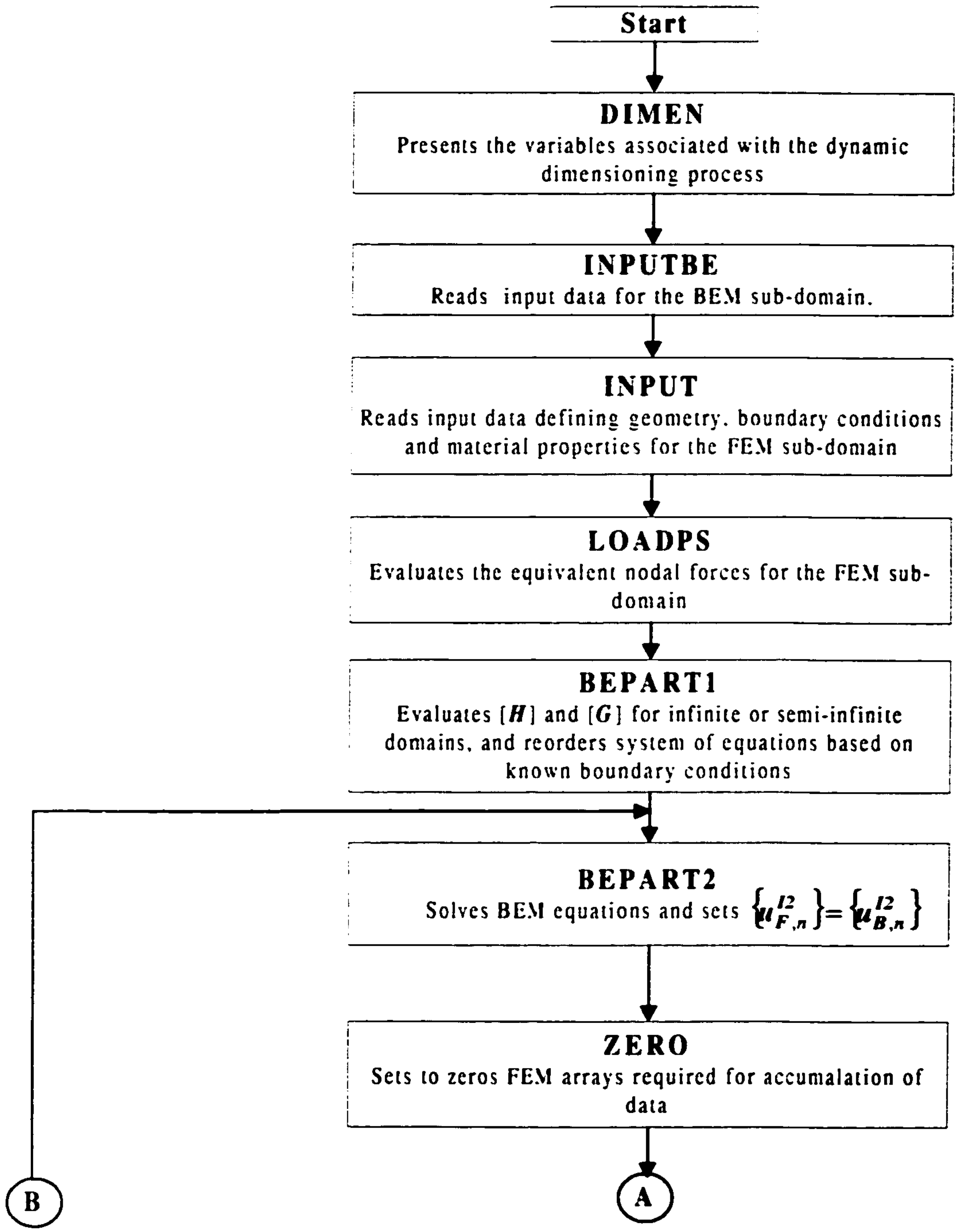

Figure 6.3: **OVEPFBE** Program Organization

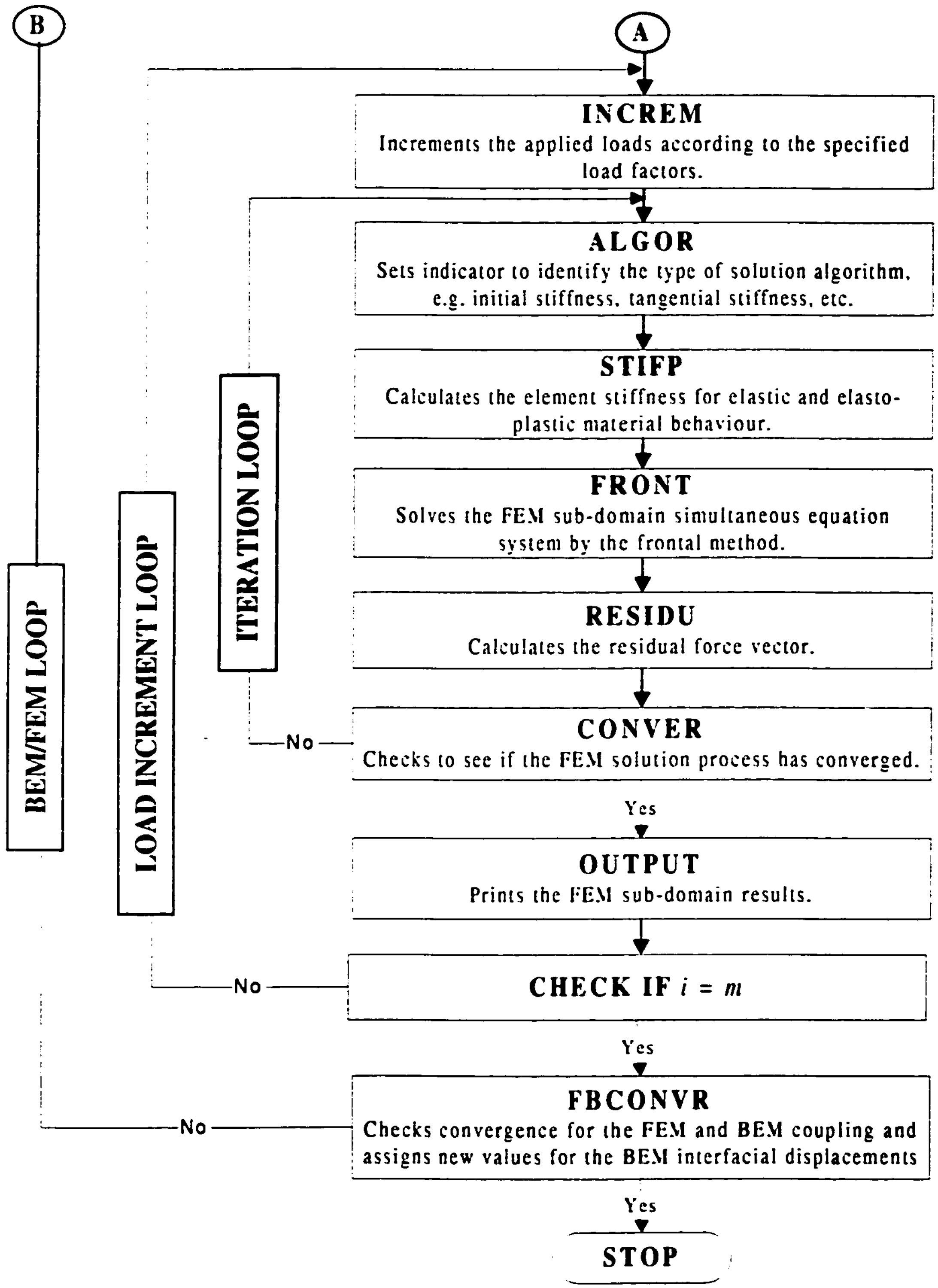

Figure 6.3: Continued

CHAPTER 7

APLLICATIONS

7.1 GENERAL

In this chapter, practical applications, which include two fracture mechanics and deep and shallow tunnels problems are considered. The coupled FEM/BEM solution using **EPFBE** or **OVEPFBE** programs is compared to the theoretical solution, where available, and to the conventional FEM using **PLAST** [31].

7.2 FRACTURE MECHANICS

As mentioned earlier, the coupling of the FEM and BEM may be of particular importance in fracture analysis, which is governed by LEFM and EPFM. The two cases are considered here using **EPFBE** program and the results are compared to those obtained by **PLAST** [31].

7.2.1 LEFM Example

Considering a square plate, with a central crack, subjected to a uniform applied traction on the opposite ends of the plate (Figure 7.1). This produces a Mode I type of crack growth. The crack is assumed to be 10 units long, with a plate width of 20 units.

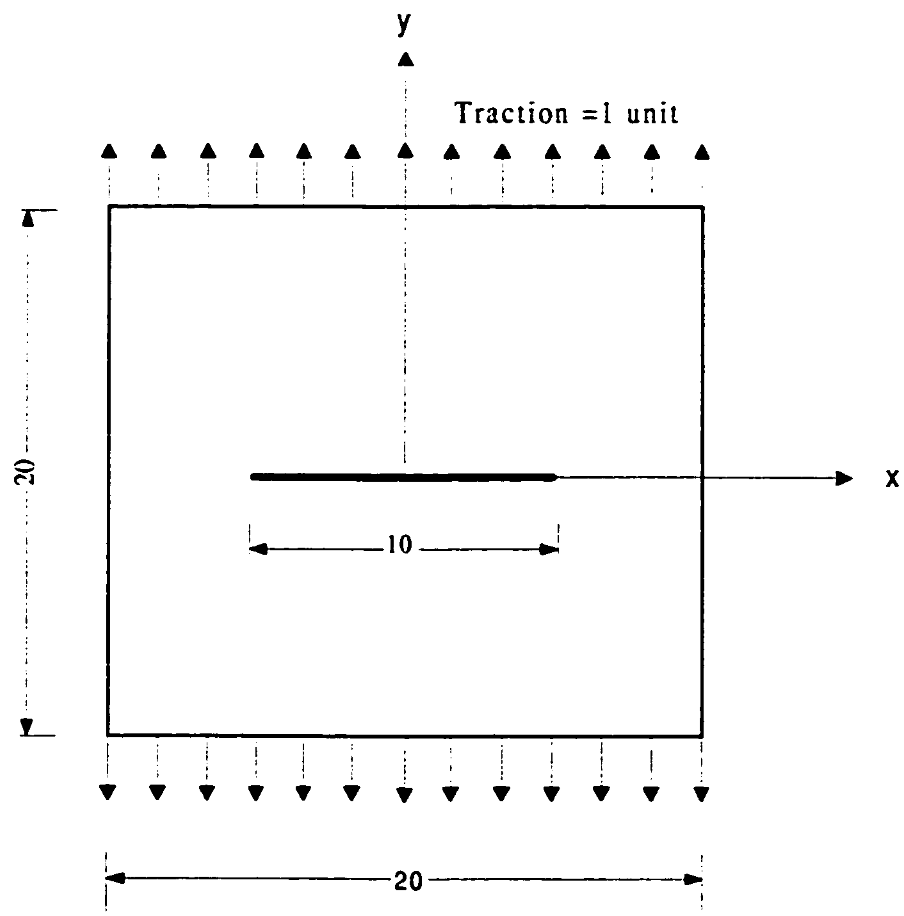

Figure 7.1: Plate with a Central Crack (LEFM Example)

Young's modulus is assumed to be $0.3\text{x}10^5$ units and a Poisson's ratio $\nu = 0.3$. A uniform traction of 1 unit is applied at the opposite ends of the plate. Due to the symmetrical nature of the problem, only a quarter of the plate is modeled. For the FEM/BEM the problem is modeled using 42 non-uniform linear boundary elements and 30 linear finite quadrilateral elements. The same problem is solved using the FEM with 682 linear quadrilateral elements. The FEM and FEM/BEM discretizations are shown in Figure 7.2.

The stress intensity factors at the tip of the crack using the FEM/BEM and FEM are shown in Table 7.1. The coupled FEM/BEM gives a stress intensity factor that is only 1.9% different than the analytical solution [60], while the FEM gives an error of 5.9%. The difference in CPU time recorded for both methods is insignificant and therefore a comparison is not given here.

7.2.2 EPFM Example

The geometry and loading assumed in this example is shown in Figure 7.3. Von Mises yield criterion is assumed, and the material properties employed are as follows: Young's modulus $E = 2.06\text{x}10^5$ units, Poisson's ratio $\nu = 0.3$, tensile yield stress $\sigma_y = 480$ units, and the tangent modulus for plasticity $H' = 2.06\text{x}10^3$ units. Due to symmetry, only one quarter of the plate is modeled. The FEM and coupled FEM/BEM analysis are performed with the discretization shown in Figure 7.4.

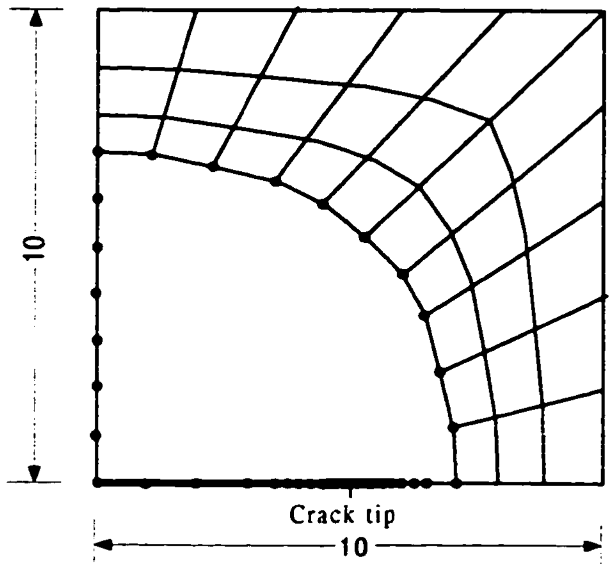

(a) FEM/BEM

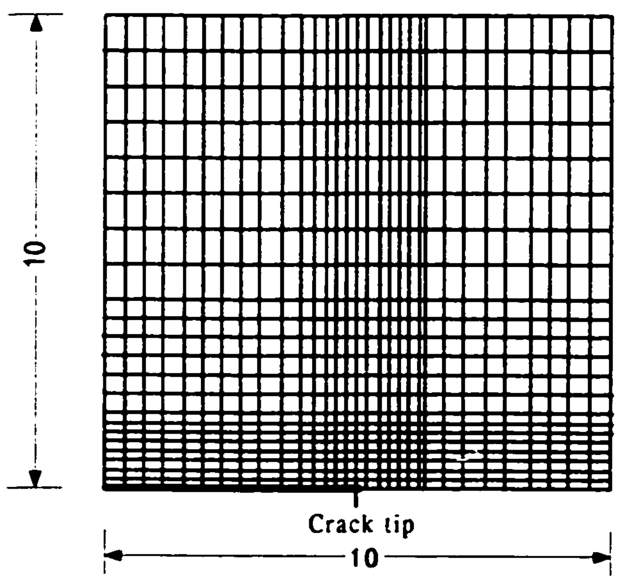

(b) FEM

Figure 7.2: FEM/BEM and FEM Discretization for LEFM Example

Table 7.1: Stress Intensity Factors for the Cracked Plate

Method	Stress Intensity Factor	% Error
Exact	4.71	-
FEM	4.28	5.9
FEM/BEM	4.62	1.9

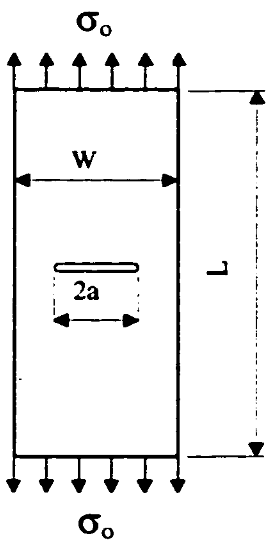

Von Mises yield Criterion
Plane Strain
E = 2.06 H 10^5 units
ν = 0.3
σ_y = 480 units
H/ = 2.06 H 10^3 units
W = 40 units
L = 100 units
2a = 20 units

Figure 7.3: Geometry and Loading Condition for EPFM Example

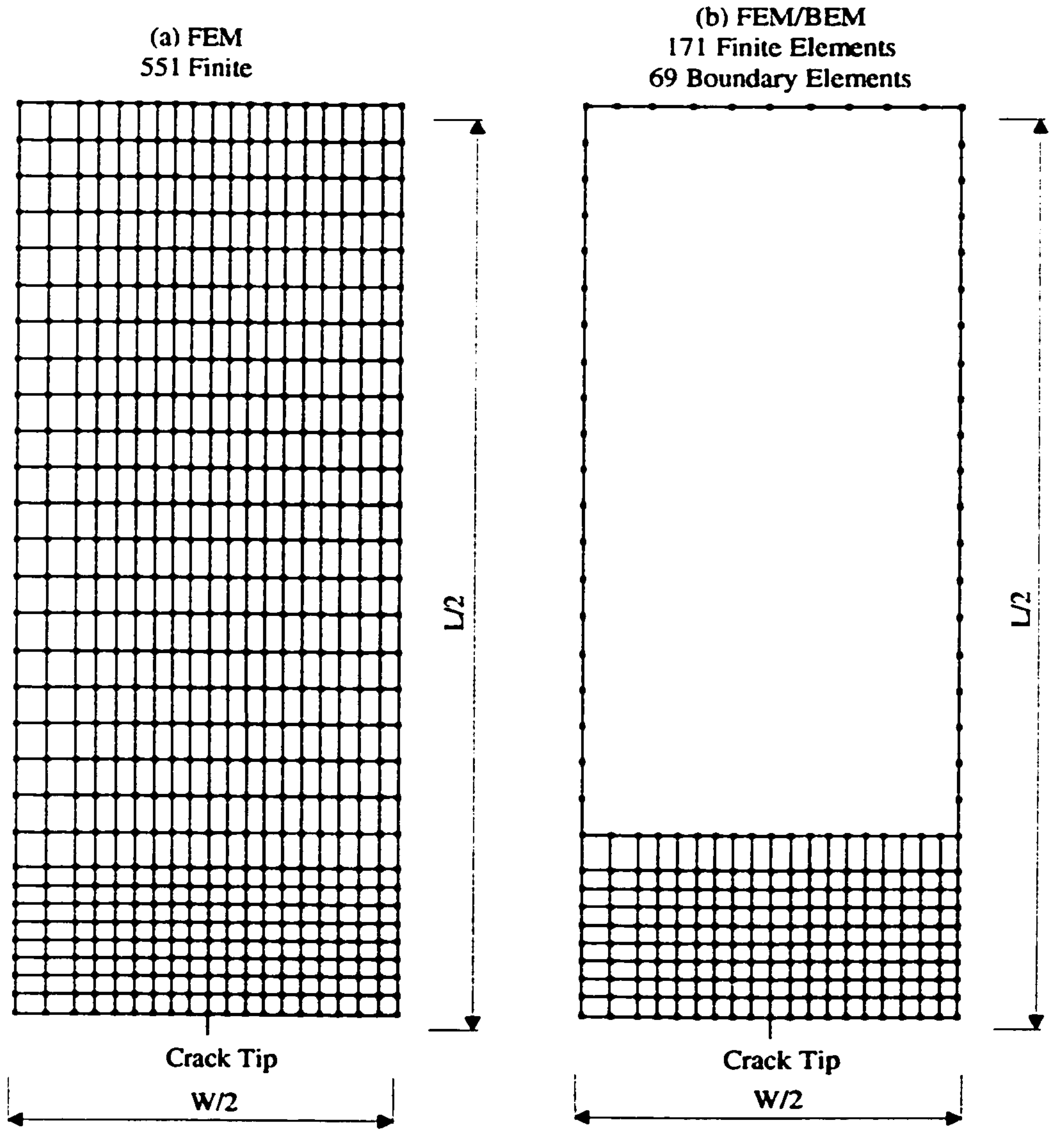

Figure 7.4: Discretization for EPFM Example

Table 7.2 shows the computed remote stress σ_o vs. load-point displacement δ_o normalized to the plate width (W). It also shows the results obtained in a previous investigation [69], using the FEM and conventional FEM/BEM coupling method. The calculated yield zones are also shown in Figure 7.5. The results in Table 7.2 and Figure 7.5 indicate close agreement between the FEM and coupled FEM/BEM solutions. Furthermore, the FEM and FEM/BEM solutions agree very well with those obtained in reference [69]. Table 7.3 shows the CPU time required for analysis with the FEM and coupled FEM/BEM. The table shows a less CPU time when the analysis is performed using the FEM. The difference in CPU time increases as load increases.

7.3 TUNNEL PROBLEM

As an application for elasto-plastic infinite and semi-infinite problems the analysis of deep and shallow tunnels is considered in this section. Both cases are investigated using **OVEPFBE** program. The results are compared to those obtained by **PLAST** [31].

7.2.1 Deep Tunnel

The problem considered here is the excavation of a circular tunnel in a geological medium. The tunnel is deeply inserted in a surrounding medium, which is governed by the true Drucker-Prager yield criterion without any hardening effect. The plane strain condition is assumed to prevail. The radius of the tunnel R is taken as 100 units. The material properties employed are as follows: Young's modulus

Table 7.2: Remote Stress vs. Normalized Load-Point-Displacement for EPFM Example

σ_o (units)	δ_o/W		
	FEM	FEM/BEM	Ref. [69]
100	0.065×10^{-2}	0.065×10^{-2}	0.07×10^{-2}
150	0.098×10^{-2}	0.096×10^{-2}	0.10×10^{-2}
200	0.131×10^{-2}	0.130×10^{-2}	0.13×10^{-2}
226	0.149×10^{-2}	0.146×10^{-2}	0.14×10^{-2}
250	0.166×10^{-2}	0.162×10^{-2}	0.16×10^{-2}
284	0.194×10^{-2}	0.192×10^{-2}	0.19×10^{-2}

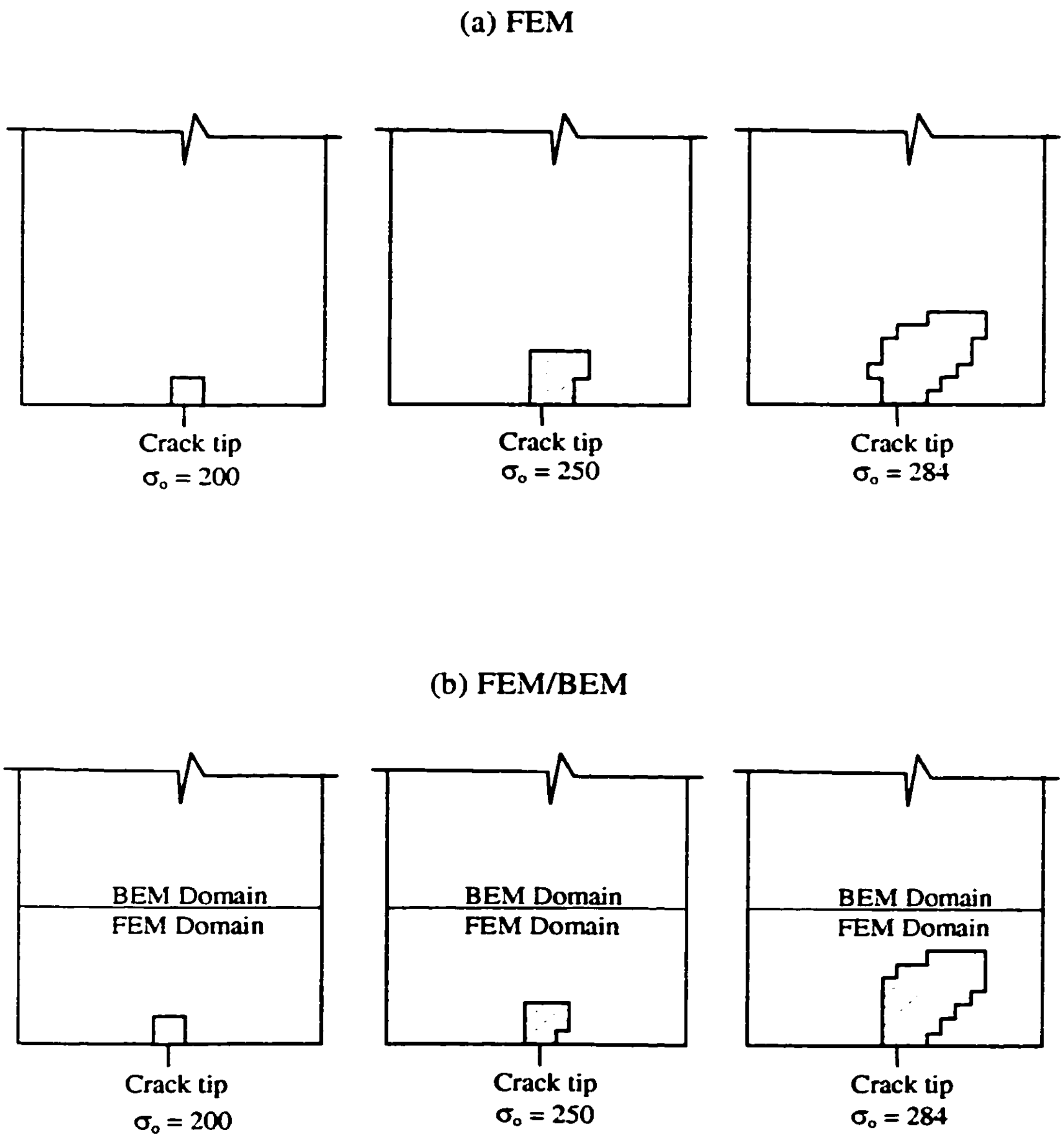

Figure 7.5: Yielded Zones for EPFM Example

Table 7.3: CPU Time for EPFM Example

	CPU time (Sec.)	
σ_o	FEM	FEM/BEM
100	3	5
150	4	5
200	4	8
226	5	8
250	5	8
284	6	11

$E = 2.1x10^4$ units, Poisson's ratio $\nu = 0.18$, cohesion $c = 10$ units, and angle of internal friction $\phi = 41^o$. The stress condition in the geological medium is assumed to be hydrostatic. The equivalent nodal loads on the excavated surface are calculated and then applied in the opposite directions to simulate the excavation of the tunnel.

First, the excavation of the tunnel is analyzed with the BEM and the FEM using **PLAST** [31]. For the FEM analysis, the infinite domain is truncated at 4.3, 8.7 and 15 R. The problem is then analyzed with the FEM/BEM using **OVEPFBE** program. Figure 7.6 shows the discretization with the BEM, FEM and FEM/BEM.

The investigation of this problem can be divided into three parts as follows:

1. Elastic analysis.

2. Effect of non-homogeneity of the surrounding media.

3. Elasto-plastic stress analysis.

7.3.1.1 Elastic Analysis

The purpose of this analysis is to compare the results of the BEM, FEM and coupled FEM/BEM to the available exact solution [72]. The hydrostatic stress is taken to be 10 units. Table 7.4 shows the number of elements and CPU time required for the analysis with BEM, FEM and FEM/BEM. The difference in the CPU time required for the analysis by all methods is negligible.

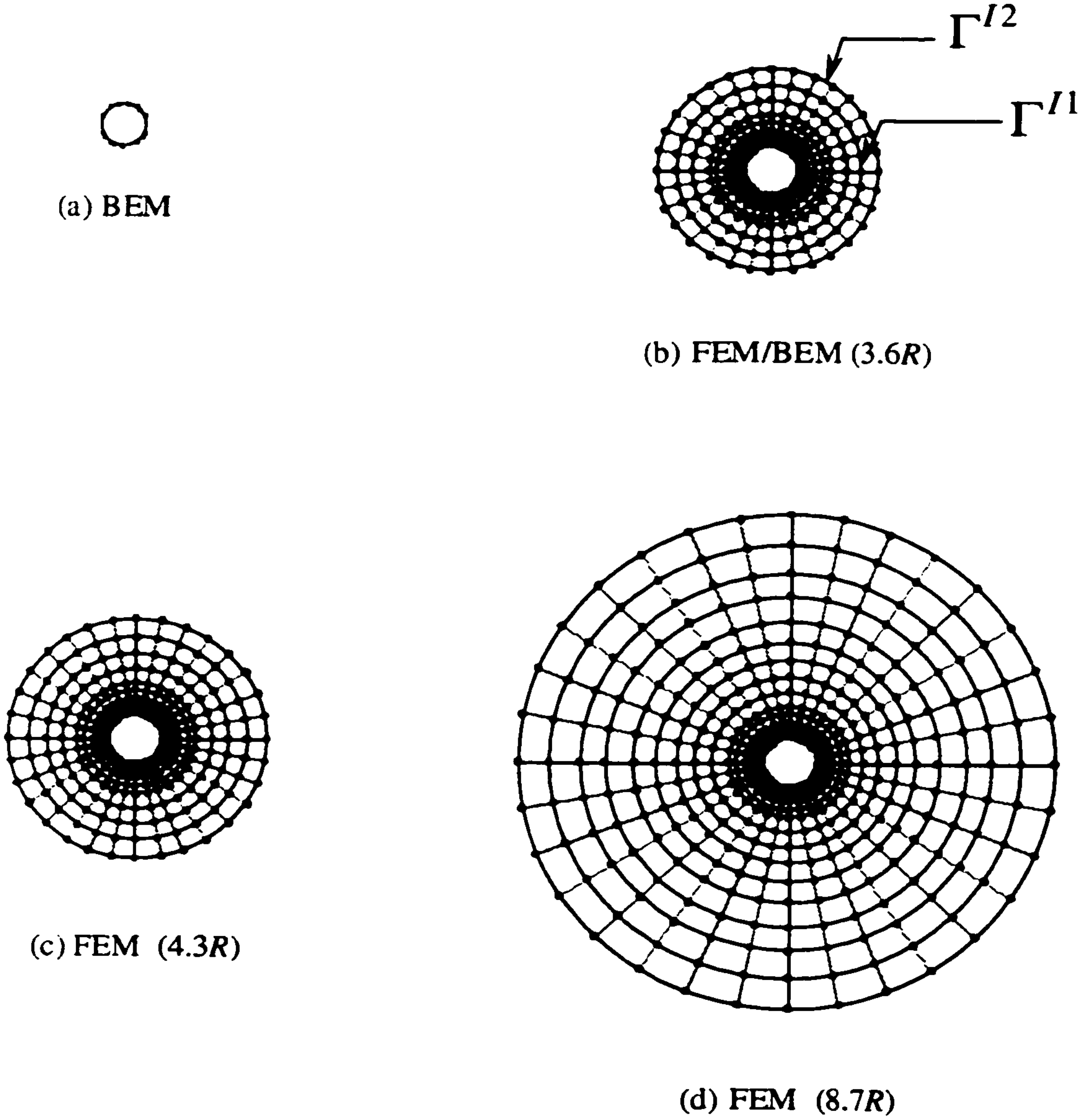

Figure 7.6: FEM and FEM/BEM Discretization for Deep Tunnel

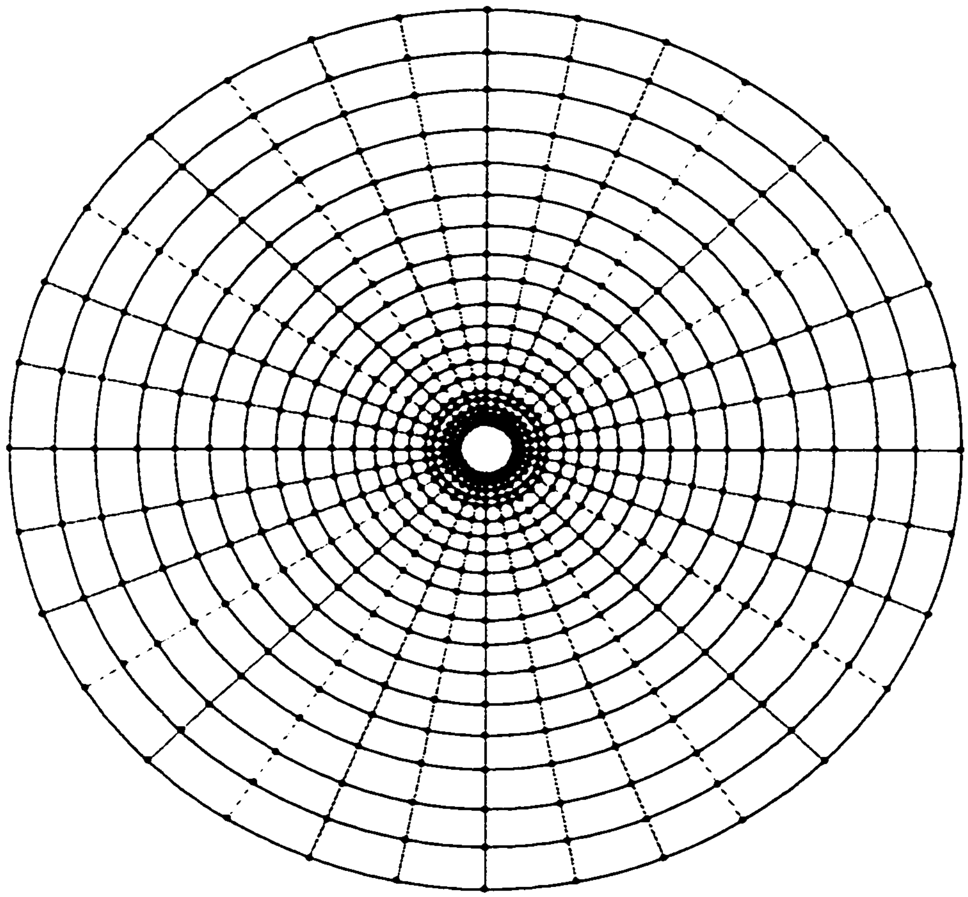

(e) FEM (15R)

Figure 7.6: Continued

Table 7.4: Number of Elements and CPU Time for Elastic Analysis of Deep Tunnel

Method	Number of Finite Elements	Number of Boundary Elements	CPU Time (Sec.)
FEM (4.3 R)	288	-	2
FEM (8.7 R)	448	-	3
FEM (15 R)	608	-	4
BEM	-	32	2
FEM/BEM	256	32	3

Figure 7.7 and 7.8, respectively, show the radial displacements (u_r) and radial stresses (σ_r) by the BEM, FEM and FEM/BEM as compared to the closed form solution. For the FEM, It is observed that better accuracy is achieved as the extent of boundary distance increases. The BEM and FEM/BEM solutions give higher accuracy compared to the FEM. Table 7.5 shows the displacement at the excavated surface of the tunnel (u_R) and the percentage error compared to the exact solution.

The results clearly show the advantage of using the FEM/BEM in terms of accuracy. Another advantage, which cannot be seen from these results, is the incredible reduction of data preparation required for the FEM/BEM analysis as compared to the FEM.

7.3.1.2 Effect of Non-homogeneity of the Surrounding Soil

One of the major advantages of using FEM/BEM for the analysis of tunnel problems is that the non-homogeneity of the surrounding geological medium can be easily taken into consideration. Consider the case in which the change in material properties near the tunnel is due to excavation. This can be handled by employing finite elements in that region. Also as indicated earlier the input data are less, and the infinity condition is rigorously fulfilled. To evaluate the efficiency of the use of the FEM/BEM over FEM in such cases, the example given in Section 7.3.1.1 is reinvestigated. Beyond the distance of 250 units, i.e., $2.5R$, the constant value of

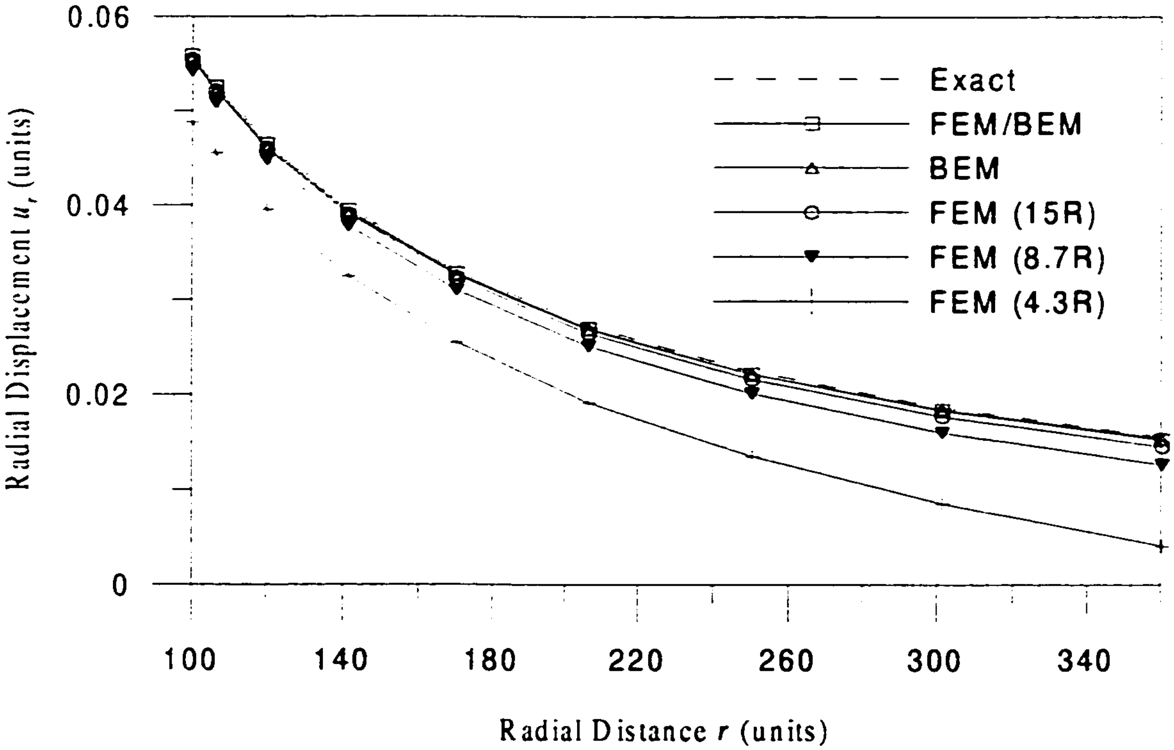

Figure 7.7: Radial Displacements for Elastic Analysis of Deep Tunnel

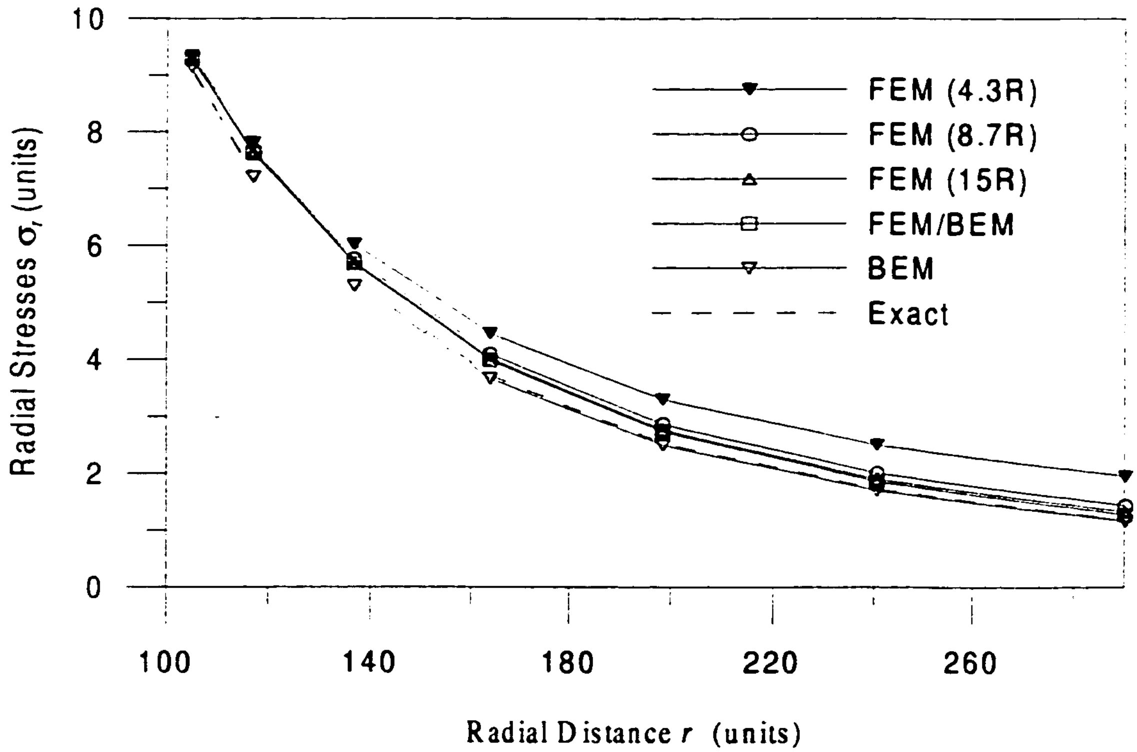

Figure 7.8: Radial Stresses for Elastic Analysis of Deep Tunnel

Table 7.5: Displacement at the Excavated Surface of Deep Tunnel

Method	u_R/R	% Error
Exact	0.0562×10^{-2}	-
FEM (4.3 R)	0.0488×10^{-2}	13.17
FEM (8.7 R)	0.0542×10^{-2}	3.56
FEM (15 R)	0.0554×10^{-2}	1.42
BEM	0.0557×10^{-2}	0.88
FEM/BEM	0.0559×10^{-2}	0.54

Young's modulus (E_2) is kept equal to $2.1\text{x}10^4$ units. In the remaining region close to the tunnel, the Young's modulus (E_1) is varied as 1, 1/2, 1/4 and 1/10 times the value of E_2.

The displacements at the excavated surface of the tunnel are shown in Table 7.6. The cases for which $E_1/E_2 > 1$ are also investigated and the results are shown in Table 7.7. The Young's modulus (E_1) is varied as 2 and 4 times the value of E_2. The results in Table 7.6 and 7.7 indicate that for different values of E_1/E_2, the FEM converges to the FEM/BEM solution as the extent of boundary distance for the FEM increases.

7.3.1.3 Elasto-Plastic Stress Analysis

The elasto-plastic analysis is used to study the excavation of the tunnel. The excavation is simulated in a single stage. The hydrostatic stress is taken as 25 units. Again the problem is analyzed with the FEM and FEM/BEM using the discretization shown in Figure 7.6. The radial displacements (u_r) determined by both methods are shown in Figure 7.9. Again it is observed that the FEM converges to the FEM/BEM solution as the extent of boundary distance for the FEM increases. The yielded zones determined by all methods are identical and are obtained as 70 units from the boundary of the tunnel.

Table 7.6: Displacements at the Excavated Surface of the Deep Tunnel for $E_1/E_2 \leq 1$

Method	u_R/R			
	$E_1/E_2 = 1$	$E_1/E_2 = 0.5$	$E_1/E_2 = 0.25$	$E_1/E_2 = 0.1$
FEM (4.3 R)	0.0488×10^{-2}	0.0886×10^{-2}	0.1655×10^{-2}	0.3931×10^{-2}
FEM (8.7 R)	0.0542×10^{-2}	0.0969×10^{-2}	0.1762×10^{-2}	0.4058×10^{-2}
FEM (15 R)	0.0554×10^{-2}	0.0990×10^{-2}	0.1791×10^{-2}	0.4096×10^{-2}
FEM/BEM	0.0559×10^{-2}	0.0998×10^{-2}	0.1798×10^{-2}	0.4109×10^{-2}

Table 7.7: Displacements at the Excavated Surface of the Deep Tunnel for $E_1/E_2 \geq 1$

Method	u_R/R		
	$E_1/E_2 = 1$	$E_1/E_2 = 2$	$E_1/E_2 = 4$
FEM (4.3 R)	0.0488×10^{-2}	0.0273×10^{-2}	0.0152×10^{-2}
FEM (8.7 R)	0.0542×10^{-2}	0.00302×10^{-2}	0.0164×10^{-2}
FEM (15 R)	0.0554×10^{-2}	0.0307×10^{-2}	0.0166×10^{-2}
FEM/BEM	0.0559×10^{-2}	0.0309×10^{-2}	0.0166×10^{-2}

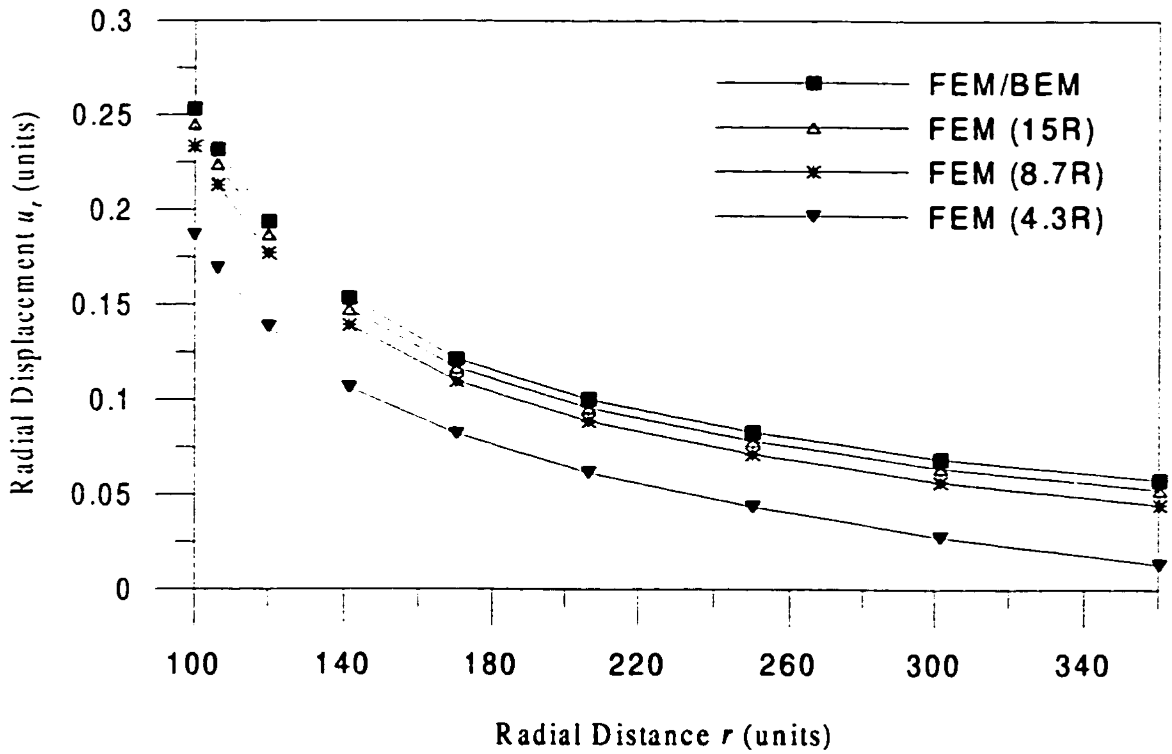

Figure 7.9: Radial Displacements for Elasto-Plastic Analysis of Deep Tunnel

Table 7.8 gives a comparison between the FEM and FEM/BEM in terms of the computation time required for convergence. The CPU time is least for the FEM with a boundary distance of $4.3R$. The FEM solution with boundary truncated at $15R$, has the same level of accuracy as that by FEM/BEM, but it requires more CPU time.

7.3.2 Shallow Tunnel

The Example considered here is the excavation of a circular shallow tunnel in a geological medium. The surrounding geological medium rock is governed by the true Drucker-Prager yield criterion without any hardening effect. The plane strain condition is assumed to prevail. The geometry and material properties are shown in Figure 7.10. The radius of the tunnel (R) and the depth from the center of the tunnel to the ground surface (d) are taken as 1 and 5 units, respectively. The material properties employed are as follows: Young's modulus $E = 210$ units, Poisson's ratio $\nu = 0.18$, cohesion $c = 10$ units, and angle of internal friction $\phi = 41^\circ$.

7.3.2.1 Elastic Analysis

It is well known that the BEM is best suited for linear elastic infinite and semi-infinite problems. The purpose of the elastic analysis is to compare the FEM/BEM to the FEM and BEM in terms of accuracy. The stress condition in the geological medium is assumed to be hydrostatic and the stress is taken to be 10 units. The problem is

Table 7.8: Comparison of CPU Time for Elasto-Plastic Analysis of Deep Tunnel

Method	FEM (4.3 R)	FEM (8.7 R)	FEM(15 R)	FEM/BEM
CPU-time (Sec.)	4	5	8	5

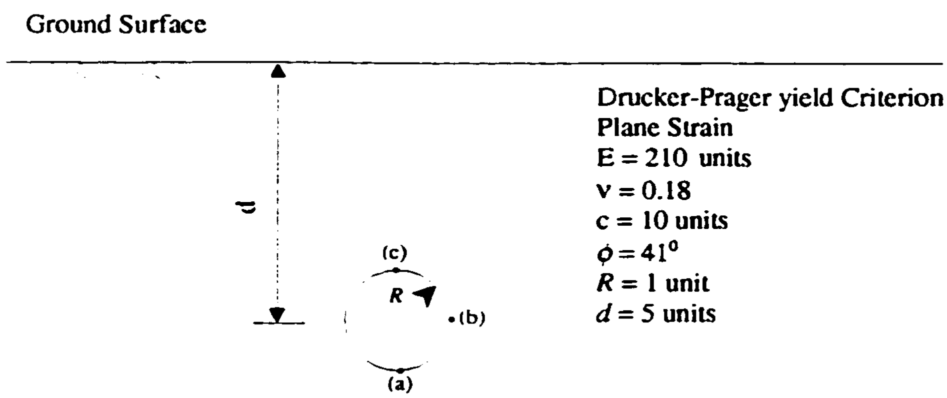

Point (a): Invert
Point (b): Springline
Point (c): Crown

Figure 7.10: Geometry and Material Properties of the Shallow Tunnel

analyzed with the BEM, FEM and FEM/BEM with the discretization shown in Figure 7.11.

Table 7.9 shows the number of elements and CPU time required for the analysis with different methods. Table 7.10 shows the vertical displacements (u) and horizontal displacements (v) by the BEM, FEM and FEM/BEM at points (a) invert, (b) springline, and (c) crown. Due to the non-uniqueness of displacements in 2-D analysis (17), the vertical displacements are given with reference to the corresponding displacement of the invert (u_a). It is observed that the FEM converges to the BEM solution as the extent of boundary distance for the FEM increases. The BEM and FEM/BEM solutions are in close agreement.

7.3.2.2 Elasto-Plastic Stress Analysis

The elasto-plastic analysis is used to study the excavation of the tunnel. The hydrostatic stress is taken as 25 units. The problem is analyzed with the FEM and FEM/BEM using the discretization shown in Figure 7.11. Table 7.11 shows the displacements for both methods. As the extent of boundary distance for the FEM increases, the FEM converges to the FEM/BEM solution.

Table 7.12 gives a comparison between the FEM and FEM/BEM in terms of CPU time. The CPU time is highest for the FEM/BEM. However, with the use of the FEM/BEM, one can gain an incredible reduction of data preparation as compared

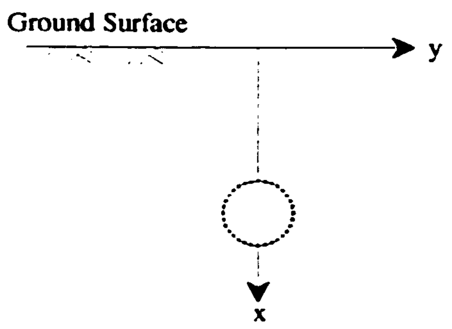

(a) BEM

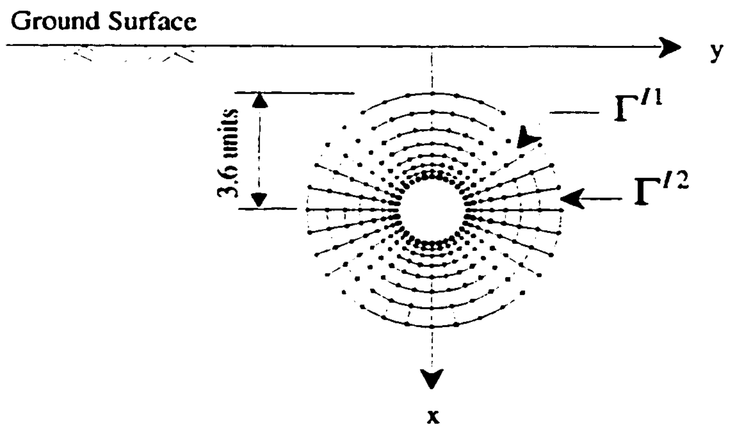

(b) FEM/BEM

Figure 7.11: Discretization of the Shallow Tunnel

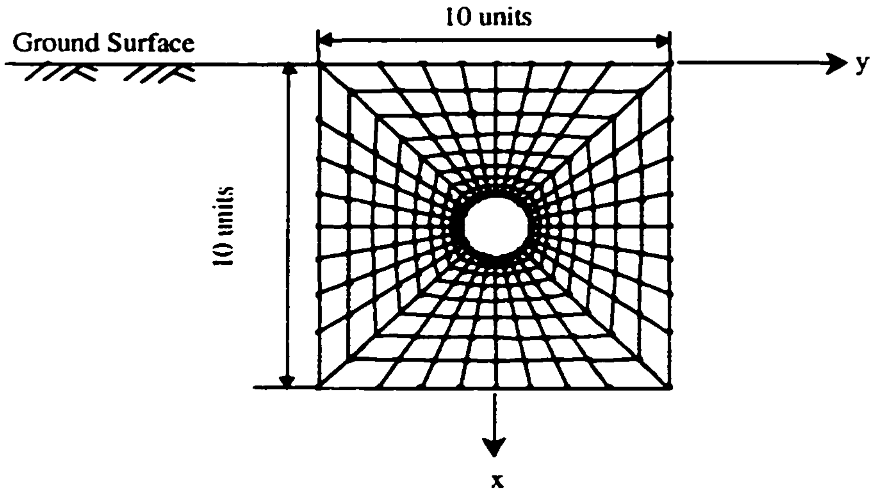

(c) FEM (1)

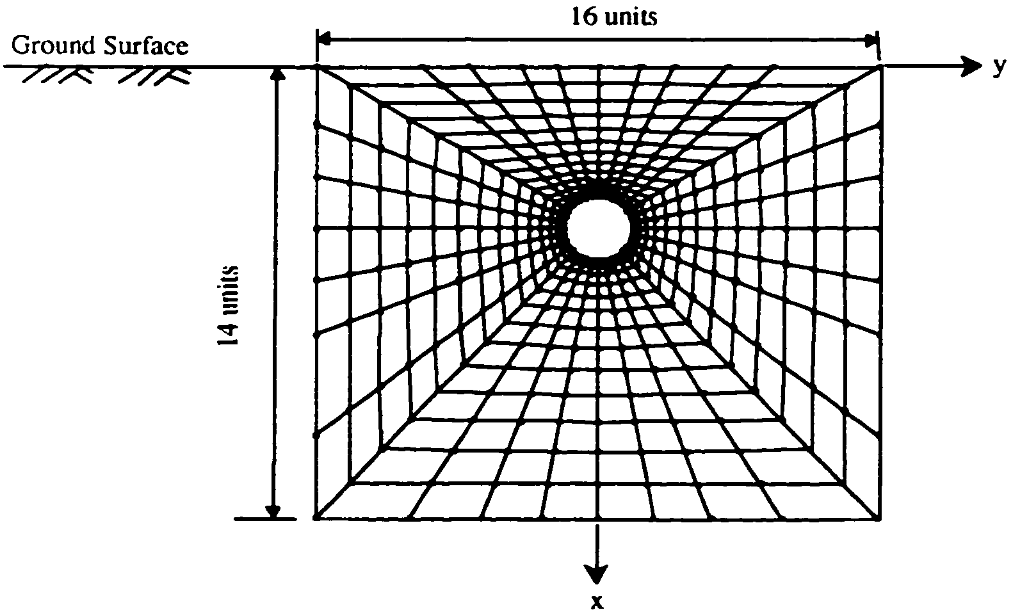

(d) FEM (2)

Figure 7.11: Continued

Table 7.9: Number of Elements and CPU Time for Elastic Analysis of Shallow Tunnel

Method	Number of Finite Elements	Number of Boundary Elements	CPU-time (Sec.)
BEM	-	32	2
FEM (1)	288	-	2
FEM (2)	448	-	3
FEM/BEM	256	32	5

Table 7.10: Displacements at the excavated Surface of the Shallow Tunnel (Elastic Analysis)

Method	Node (a) (Invert)		Node (b) (Springline)		Node (c) (Crown)	
	$u-u_a$	v	$u-u_a$	v	$u-u_a$	v
FEM (1)	0	0	0.0617	0.0509	0.1246	0
FEM (2)	0	0	0.0599	0.0527	0.1209	0
BEM	0	0	0.0587	0.0557	0.1189	0
FEM/BEM	0	0	0.0587	0.0569	0.1197	0

Table 7.11: Displacements at the Excavated Surface of the Shallow Tunnel (Elasto-Plastic Analysis)

Method	Node (a) (Invert)		Node (b) (Springline)		Node (c) (Crown)	
	$u-u_a$	v	$u-u_a$	v	$u-u_a$	v
FEM (1)	0	0	0.1899	0.16	0.3836	0
FEM (2)	0	0	0.1865	0.1675	0.3752	0
FEM/BEM	0	0	0.1833	0.1804	0.3746	0

Table 7.12: Comparison of CPU Time for Elasto-Plastic Analysis of Shallow Tunnel

Method	FEM (1)	FEM (2)	FEM/BEM
CPU-time (Sec.)	3	5	8

with the FEM and avoid the convergence analysis required for the FEM due to the truncation of the infinite domain.

7.4 SUMMARY

The examples discussed in the preceding sections cover a variety of practical applications, where the FEM/BEM may be most efficient. As detailed above, the results obtained are encouraging in most cases. For the elastic problems considered, the FEM solution is not as accurate as the coupled FEM/BEM. For the elasto-plastic problems, the FEM/BEM seems to give more accurate results than the FEM, which is confirmed by the convergence of the FEM solution to FEM/BEM solution. The difference in CPU time is insignificant in most cases. The coupled FEM/BEM has an important advantage which can not be seen from the results; that is the incredible reduction of data preparation as compared to the FEM, especially with problems characterized with infinite and semi-infinite domains.

CHAPTER 8

SUMMARY, CONCLUSIONS AND RECOMMENDATIONS FOR FUTURE RESEARCH

8.1 SUMMARY

In certain cases, it may be beneficial to couple the FEM and the BEM in the analysis. The iterative domain decomposition coupling methods offer such alternative. The concepts behind the iterative coupling methods have physical meaning, and are easy to comprehend. In this study, the convergence of the Sequential Dirichlet-Neumann iterative coupling method is investigated and the factors involved in the convergence are identified. The study also extends the Sequential Dirichlet-Neumann method to elasto-plasticity.

A major contribution of this study is the development of a new iterative domain decomposition coupling method. The new overlapping method introduces a common region that is modeled by the FEM and BEM. The method is capable of handling cases where the natural boundary conditions are specified on the entire external boundary of the FEM or BEM sub-domains. Such cases cannot be handled using the existing iterative non-overlapping coupling methods. The overlapping iterative

coupling method is most suited for problems involving infinite or semi-infinite regions. The method is also extended to elasto-plasticity.

Practical applications involving fracture mechanics problems and the analysis of deep and shallow tunnels are given.

8.2 CONCLUSIONS

Several conclusions can be drawn from the presented analysis. They are summarized in the following points:

1. The convergence analysis of the Sequential Dirichlet-Neumann iterative coupling method provides an interval from which the relaxation parameter has to be chosen. The choice of this parameter is essential to guarantee the convergence of the iterative method.

2. Several factors control the convergence of the Sequential Dirichlet-Neumann iterative coupling method. These include the mesh density on the FEM/BEM interface, specified type of boundary conditions and the geometrical and material properties of the FEM and BEM sub-domains.

3. One of the strong points of the iterative methods is that the initial guess of the degrees of freedom on the interface is not involved in the conditions for convergence. Furthermore, the initial guess has an insignificant effect on the

speed of convergence, at least for all cases considered. Therefore, it is reasonable to start with values of zeros at the interface for the initial displacements/potentials, which seems convenient as well as appropriate from the physical realization.

4. The new overlapping iterative coupling method is very efficient in solving problems where the natural boundary conditions are specified on the entire external boundary of the FEM or BEM sub-domains. The method is best suited for problems involving infinite or semi-infinite regions.

5. Unlike the existing iterative methods, the new overlapping method has the advantage of avoiding the computation of the transformation matrix relating BEM interfacial tractions to FEM forces.

6. The new overlapping method provides a wider range for the applicable range of the parameter α, as compared to the Sequential Dirichlet-Neumann iterative coupling method.

7. The extension of the Sequential Dirichlet-Neumann and the new overlapping iterative coupling methods to elasto-plasticity gives the best solution for all the practical applications considered. The iterative FEM/BEM seems to give more accurate results than the FEM, which is confirmed by the convergence of FEM solution to coupled FEM/BEM solution.

8. In many cases, although the FEM yields less CPU time than the coupled FEM/BEM, its solution is not as accurate as the coupled FEM/BEM. However, the coupled FEM/BEM has an important advantage that cannot be seen from the results; that is the incredible reduction of data preparation as compared to the FEM. Moreover, the method avoids the need for convergence analysis as required by the FEM, especially with problems characterized by infinite or semi-infinite regions.

8.3 RECOMMENDATIONS FOR FUTURE RESEARCH

Although this study aimed at developing an efficient coupled FEM/BEM method, future work can be conducted to cover the following:

1. An integration of EPFBE and OVEPFBE programs, with an automatic mesh-generation, and pre- and post-processing routines, is desirable in order to reduce the amount of effort in problem input and output.

2. The extension of the iterative methods to 3-D problems is encouraged. The advantage of the reduction of the input data is expected to be more appreciable, especially with cases involving infinite/semi-infinite domains.

3. It is useful to implement the new overlapping method for parallel processing. It is possible to do this on a big supercomputer or smaller super-stations placed in parallel with each other.

4. Other useful applications of the new overlapping coupling method can be considered. These may include solid-fluid interaction, soil-structure interaction as well as other problems involving infinite/semi-infinite domains.

REFRENCES

1. Hrenikoff, A., "Solution of Problems in Elasticity by the Framework Method," *Transactions of the ASME, Journal of Applied Mechanics*, Vol. 8, 1941, pp. 169-175.

2. Courant, R., "Variational Methods for the Solution of Problems of Equilibrium and Vibration," *Bulletin of the American Mathematical Society*, Vol. 49, 1943, pp. 1-43.

3. Argyris, J. H. and Kelsey, S., *Energy Theorems and Structural Analysis*, Butterworth Scientific Publications, London, 1960.

4. Turner, M., Clough, R.W., Martin H. H. And Topp, L., "Stiffness and Deflection Analysis of Complex Structures," *Journal of Aeronautical Science*, Vol. 23, 1956, pp. 805-823.

5. Muskhelishvilli, N. I., *Some Basic Problems of the Mathematical Theory of Elasticity*, Noordhoff, Groningen, 1953.

6. Mikhlin, S. G., *Integral Equations*, Pergamon, New York, 1957.

7. Smirnov, V. J., *Integral Equations and Partial Differential Equations*, In A Course in Higher Mathematics, Vol. IV, Addison-Wesley, London, 1964.

8. Kupradze, O. D., *Potential Methods in the Theory of Elasticity*, Daniel Davey & Co., New York, 1965.

9. Kellog, O. D., *Foundation of Potential Theory*, Dover, New York, 1953.

10. Jaswon, M. A., "Integral Equation Methods in Potential Theory," *Int. Proc. Roy. Soc. Ser. A 275*, 1963, pp. 23-32.

11. Symm, G. T., "Integral Equation Methods in Potential Theory," *I, Proc. Roy. Soc. Ser. A 275*, 1963, pp. 33-46.

12. Massonet, C. E., "Numerical Use of Integral Procedures," *In Stress Analysis*, O. C. Zienkiewicz and G. S. Holister (eds.), Wiley, London, 1966.

13. Rizzo, R. J., "An Integral Equation Approach to Boundary Value Problems of Classical Elastostatics," *Q. Appl. Math.*, Vol. 25, 1967, pp. 83-95.

14. Cruse, T. A. and Rizzo, F. J., "A Direct Formulation and Numerical Solution of the General Transient Elasto-Dynamic Problem," *J. Math. Anal. Appl.*, Vol. 22, 1968, pp. 244-259.

15. Brebbia, C. A., *The Boundary Element Method for Engineers*, Pentech Press, London, Halstead Press, New York, 1978.

16. Banerjee, P. K. and Butterfield, R., *Boundary Element Method in Engineering Science*, McGraw-Hill, New York, 1981.

17. Brebbia, C. A., Telles, J. C. F. and Wrobel, L. C., *Boundary Element Techniques - Theory and Applications in Engineering*, Springer-Verlag, Berlin, 1984.

18. Hartmann, F., *Introduction to Boundary Elements*, Springer-Verlag, Berlin, 1987.

19. Brebbia, C. A. and Dominguez, J., *Boundary Elements - An Introductory Course*, CMP, Southampton, 1992.

20. Beer, G. and Watson, J. O., *Introduction to Finite and Boundary Element Methods for Engineers*, John Wiley & Sons, Chichester, UK, 1992.

21. Banerjee, P. K., *Boundary Element Method in Engineering*, McGraw-Hill, New York, 1994.

22. Love, A. E. H., *A Treatise on the Mathematical Theory of Elasticity*, Dover, New York, 1944.

23. Melan, E., "Der Spannungszustand der Durcheine Einzelkraft in Innern Beanspruchten Halbscheibe," *Z. Argew. Mech.*, Vol. 12, 1932, pp. 343-346.

24. Telles, J. C. F. and Brebbia, C. A., "Boundary Element Solution for Half-Plane Problems," *International Journal of Solids & Structures*, Vol. 17, No. 12, 1981, pp. 1149-1158.

25. Wang, Ching-bo and Liu Xing-yeh, "Boundary Element Method for Semi-Infinite Region Problems, *13th World Conference on the Boundary Element Method, BEM 13*, Tokyo, Japan, September, 1986, pp. 237-246.

26. Chuhan, Z. and Chongmin, S., "Boundary Element Technique in Infinite and Semi-Infinite Plane Domain," *Proceedings of the international Conference on Boundary Elements*, Beijing, China, October, 1986, pp. 551-558.

27. Huang, Y. Y. and Hubei, W., "A Direct Method for Deriving Fundamental Solution Of Half-Plane Problem," *Proceedings of the international Conference on Boundary Elements*, Beijing, China, October, 1986, pp. 665-672.

28. Beer, G. and Watson, J. O., "Infinite Boundary Elements," *International Journal for Numerical Methods in Engineering*, Vol. 28, 1989, pp. 1233-1247.

29. Hartmann, F., "Computing the C-Matrix in Non-Smooth Boundary Points," in *New Developments in Boundary Element Methods*, Brebbia, C. A. Ed., CML Southampton, 1983, pp. 367-379.

30. Hunter, P. and Pullan, A., FEM/BEM Notes, Department of Engineering Science, the University of Auckland, New Zealand, December, 1998.

31. Owen, D. R. J. and Hinton, E., Finite Elements in Plasticity: Theory and Practice, Pineridge Press, Swansea, U.K., 1980.

32. Aliabadi, M. H., Cartwright, D. J., Nachring, D. W. and Daney, W. A., "Stress Intensity Factor Weight Functions for Cracks at Holes and Half Plane," *Proceedings of the 11th International Conference on the Boundary Element Methods*, Vol. 1, Springer-Verlag, Berlin, 1989, pp. 83-89.

33. Stok, B. and Bukovec, B., "Stress and Stress Intensity Factor Analysis in Cracked Elastic Bars under Torsion by the Boundary Element Method," *Proceedings of the 11th International Conference on the Boundary Element Methods*, Vol. 1, Springer-Verlag, Berlin, 1989, pp. 111-122.

34. Zienkiewicz, O. C., Kelly D. W. and Bettes P., "The Coupling of the Finite Element Method and Boundary Solution Procedures," *International Journal for Numerical Methods in Engineering*, Vol. 11, 1977, pp. 355-375.

35. Atluri, S. N. and Grannel, J. J., Boundary Element Methods (BEM) and Combination of BEM-FEM, *Report No. GIT-ESM-SA-78-16 of the Center for the Advancement of Computational Mechanics*, Georgia Institute of Technology, Atlanta, 1978.

36. Brebbia, C. A. and Georgion, P., "Combination of Boundary and Finite Elements in Elastostatics," *Appl. Math. Model.* Vol. 3, 1979, pp. 212-220.

37. Beer, G. and Meek, J. L., "The Coupling of Boundary and Finite Element Methods for Infinite Domain Problems in Elasticity," In *Boundary Element Methods*, C. A. Brebbia (ed.), Springer, Berlin, 1981, pp. 575-591.

38. Swoboda, G., Mertz, W. and Beer, G., "Rheological Analysis of Tunnel Excavations by means of Coupled Finite Element (FEM)-Boundary Element (BEM) Analysis," *International Journal for Numerical and Analytical Methods in Geomechanics*, Vol. 11, 1987, pp. 115-129.

39. Kohno, K., Tsunda, T., Seto, H. and Tanaka, M., "Hybrid Stress Analysis of Boundary and Finite Elements by Super-Element Method," In *Advances in Boundary Elements, Vol. 3, Stress Analysis*, C. A. Brebbia and J. J. Conor (eds.), Springer, Berlin, 1989, pp. 27-38.

40. Li, H. B., Han, G. M., Mang, h. A. and Torzicky, P., "A New Method for the Coupling of Finite Element and Boundary Element Discretized Subdomains of Elastic Bodies," *Computer Methods in Applied Mechanics and Engineering*, Vol. 54, 1986, pp. 161-185.

41. Mang, H. A., Torzicky, P. and Chen, Z. Y., "On the Mechanical Inconsistency of Symmetrization of Unsymmetric Coupling Matrices for FEBEM Discretization of Solids," *Computational Mechanics*, Vol. 4, 1989, pp. 301-308.

42. Leung, K. L., Zavareh, P. B. and Beskos, D. E., "2-D Elastostatic Analysis by a Symmetric BEM/FEM Scheme," *Engineering Analysis with Boundary Elements*, Vol. 15, 1995, pp. 67-78.

43. Vallabhan, C. V. G., Sivakumar, J. and Radhakrishnam, N., "Application of Boundary Element Method for Soil-Structure Interaction Problems," In *Boundary Elements VI*, 1986, pp. 27-39.

44. Chen, A. S., Hofsletter, G., Li, Z. K., Mang, H. A. and Torzicky, P., "Coupling of FE- and BE- Discretizations for 3D-Stress Analysis of Tunnels in Layered Anisotropic Rock, In *Discretization Methods in Structural Mechanics*, Springer, Berlin, 1989, pp. 427-436.

45. Varadarjan, A., Sharma, K. G. and Singh, R. B., "Some Aspects of Coupled FEBEM Analysis of Underground Openings," *International Journal for Numerical and Analytical Methods in Geomechanics*, Vol. 9, 1985, pp. 557-571.

46. Wearing, J. L. and Burstow, M. C., "Elasto-Plastic Analysis Using a Coupled Boundary Element Finite Element Technique," *Engineering Analysis with Boundary Elements*, Vol. 14, 1994, pp. 39-49.

47. Kim, M. K., Lim, Y. M., Rhee, J. W. and Cho, W. Y., "Dynamic Analysis of Underground Structures in Multi-Layered Half Planes by FE-BE Method," Eleventh Asian Regional Conference on Soil Mechanics and Geotechnical Engineering, Balkema, 1999, pp. 511-514.

48. Tullberg, O. and Bolteus, L., "A Critical Study of Different Boundary Element Stiffness Matrices,' In *Boundary Element Methods in Engineering*, C. A. Brebbia (ed.), Springer, Berlin, 1982, pp. 621-635.

49. Reissner, E., "On a Variational Theorem in Elasticity," *Journal of Mathematical Physics*, 1950, Vol. 29, pp. 90-95.

50. Washizu, K., Variational Methods in Elasticity and Plasticity, Third Edition, Pergamon Press, Oxford, 1982.

51. Schnack, E., "Macro-elements with BEM," In *Computational Engineering with Boundary Elements, Vol. 2, Solid and Computational Problems*, Cheng, C. A. Brebbia and S. Grilli (eds.), Computational Mechanics Publications, Southampton, 1990, pp. 301-316.

52. Polizotto, C. and Zito, M., "A Variational Approach to Boundary Element Methods," In *Applied Mechanics*, M. Tanaka and T. A. Cruse (eds.), Pergamon Press, Oxford, 1989, pp.13-24.

53. Sirtori, S., Maier, G., Novati, G. and Miccoli, S., "A Galerkin Symmetric Boundary Element Method in Elasticity: Formulation and Implementation," *International Journal for Numerical Methods in Engineering*, Vol. 35, 1992, pp. 255-282.

54. Dumont, N. A., "The Hybrid Boundary Element Method in Elastostatics: Overview of the Theory and Examples," In *Boundary Elements X*, C. A. Brebbia et al. (eds.), Computational Mechanics, Southampton, 1988, pp. 43-57.

55. Felippa, C. A., "A Parametric Representation of Symmetric Boundary Finite Elements," In *Advances in BEM in Japan and USA*, M. Tanaka, C. A. Brebbia and R. Shaw (eds.), Computational Mechanics Publications, Southampton, 1990, pp. 365-378.

56. Defigueiredo, T. G. B., *A New Boundary Element Formulation in Engineering*, Springer, Berlin, 1991.

57. Brebbia, C. A. and Defigueiredo, T. G. B., "A New Boundary Element Formulation and its Application in Engineering," *Boundary Element Technology*, Vol. 6, Computational Mechanics Publications, Southampton, 1991, pp. 295-308.

58. Kelly, D. W., Mustoe, G. and Zienkiewicz, O. C., "Coupling Boundary Element Methods with other Numerical Methods," *Developments in Boundary Element Methods*, Vol. 1, Chap. 10, Applied Science, London, 1979.

59. Zarco, M. A., "Solution of Soil-Structure Interaction Problems by Coupled Boundary Element-Finite Element Methods," Ph.D. Dissertation, Oklahoma State University, 1993.

60. Ganguly, S., "Symmetric Coupling of Galerkin Boundary Elements with Finite Elements," Ph.D. Dissertation, Clarkson University, 1997.

61. Gerstle, W. H., Prasad, N. N. V. and Xie, M., "Solution Method for Coupled Elastostatic BEM and FEM Domains," *Seventh International Conference on Boundary Element Technology*, Computational Mechanics Publications, Southampton, 1992, pp. 213-226.

62. Perera, R., Ruiz, A. and Alarcon, E., "FEM-BEM Coupling Procedure through the Stelkov-Poincare Operator," *Boundary Element XV*, Computational Mechanics Publications, Southampton, 1993, pp. 621-632.

63. Kamiya, N., Iwase, H. and Kita, E., "Parallel Computing for the Combination Method of BEM and FEM," *Engnng Anal. Bound. Elem.* **18**, pp. 221-229, 1997.

64. Kamiya, N., Iwase, H., "BEM and FEM Combination Parallel Analysis Using Conjugate Gradient and Condensation," *Engnng Anal. Bound. Elem.* **20**, pp. 319-326, 1997.

65. Lin, Chin-Ching, Lawton, E. C., Caliendo, J. A. and Anderson, L. R., "An Iterative Finite Element-Boundary Element Algorithm," *Computers & Structures*, Vol. 39, No. 5, 1996, pp. 899-909.

66. Feng, Y. T. and Owen, D. R. J., "Iterative Solution of Coupled FE/BE Discretization for Plate-Foundation Interaction Problems," *International Journal for Numerical Methods in Engineering*, Vol. 39, 1996, pp. 1889-1901.

67. Stoer, J. and Bulirsch, R., Introduction to Numerical Analysis, Springer-Verlag, 1980.

68. Rekach, V. G., Manual of the Theory of Elasticity, Pro/Am Music Resources, New York, 1979.

69. Kishimoto, K., Yamaguchi, I., Tachihara, M., Aoki, S. and Sakata, M., "Elastic-Plastic Fracture Mechanics Analysis by Combination of Boundary and Finite Element Methods," 5th *World Conference on the Boundary Element Method*, Hirohima, Japan, November, 1983, pp. 975-984.

70. Kui, Qi and Zailu, J. "The Elasto-Plastic Analysis of BEM and FEM in Structures Composed of Thin Plates," *Proceedings of the 2nd China-Japan Symposium on Boundary Element Methods*, Beijing, China, October, 1988, pp. 393-400.

71. Wearing, J. L. and Burstow, M. C., "Elasto-Plastic Analysis Using a Coupled Boundary Element Finite Element Technique," *Engineering Analysis with Boundary Elements*, Vol. 14, 1994, pp. 39-49.

72. Boresi, A. P., Sidebottom, O. M., Seely, F. B. and Smith, J. O., *Advanced Mechanics of Materials*, 5th ed., John Wiley & Sons, 1993.

73. Clough, R. W., "The Finite Element Method in Plane Stress Analysis," *Proceedings*, American Society of Civil Engineers, 2nd Conference on Electronic Computation, Pitsburgh, Pa., 1960, pp. 345-378.

74. Zienkiewicz, O. C. and Taylor, R. L., *The Finite Element Method*, McGraw Hill, UK, Fourth Edition, 1991.

VITA

Wael Mohamed Elleithy was born in July 15th, 1967. He received his primary, intermediate and secondary education in Alexandria, Egypt. In 1985, he joined the Faculty of Engineering, Alexandria University where he received his B.Sc. in civil engineering in 1990. He joined KFUPM in 1993, where he received his M.Sc. in civil engineering in 1995. Since 1995 he has been working as a lecturer in the civil engineering department at KFUPM and, at the same time, working towards his Ph.D.